AN ASSESSMENT OF POLYMERIC MATERIALS AND SURFACE TREATED STEELS AS CAVITATION EROSION RESISTANT MATERIALS

by

A. Barletta

A thesis submitted to the Faculty of Engineering, University of Cape Town in fulfilment of the degree of Master of Science in Applied Science.

Department of Metallurgy and Materials Science,
University of Cape Town.

March 1983

ERRATA

The following changes are to be made in the thesis by A. Barletta entitled:

"AN ASSESSMENT OF POLYMERIC MATERIALS AND SURFACE TREATED STEELS AS CAVITATION EROSION RESISTANT MATERIALS"

1. Page 120
   FIG. 5.49 Should read - En24 boronised .....

2. Page 120
   FIG. 5.50 Should read - En1A boronised for 5½ hours at 390°C. Note difference in saw tooth geometry when contrasted to boronised En24.

3. Page 123
   FIG. 5.52 "boronised" should read carburising.

ACKNOWLEDGEMENTS

I would like to thank the following for assistance with this project:

Professor A. Ball for his help and guidance throughout the course of the project

Ms Gay Perez for her assistance with the drills

Mr Nick Dreze, Mr Andy Rapley and Mr Reginald Hendricks from the workshop

Mr Bernard Greeves for his photographic work

Ms Penny Ellis who typed the manuscript, and Ms Elinor Diamond and Ms Helgard Böhm for assisting with the graphs

Robert Noël and Graham Schaffer for their efforts in proof reading this manuscript

Adi Paterson for his invaluable advice on polymers

Finally, I would like to thank the Chamber of Mines of South Africa, in particular Dr John Heathcock, for their financial support and direction during the project.

SYNOPSIS

The object of the research described in this thesis was to optimise the choice of materials used for vital components of hydraulic machinery. Frequently these components are damaged by a process known as cavitation erosion and the operation and efficiency of machines are seriously impaired.

Nineteen different polymers which have potential for use in hydraulic components have been eroded by liquid cavitation, employing the stationary specimen system. An attempt has been made to correlate the extent of erosion with the mechanical and chemical properties of the polymers. Modes of erosion of different materials were studied by scanning electron microscopy and a strong correlation was found between these modes and the resistance to erosion. Heterogenous polymers (mixture of two homogenous components), together with the polyamides and polyethylenes, showed the highest erosion resistances.

The effect of prior immersion (3 weeks at 70°C) in either a dilute or concentrated form of hydraulic fluid has been investigated for both polyacetal and ultra high molecular weight polyethylene samples in order to simulate service conditions. The polyacetal samples showed improved erosion resistance relative to the samples stored in air or water (3 weeks at 70°C). In contrast, the ultra high molecular weight polyethylene samples failed in a catastrophic manner by solvent stress cracking.

In general, it has been found that the erosion of polymers depends on no single mechanical or chemical property, but on a complex combination of properties. These include resilience, Shore hardness, elongation to fracture and glass transition temperature.

In addition to the studies of polymers, the erosion performance of a range of industrially coated and surface treated metals has been investigated. Erosion resistance has been measured relative to an uncoated substrate. Numerous techniques such as scanning electron microscopy, X-ray diffraction, micro-hardness measurements, optical microscopy and elemental analysis were used to describe and categorise performances.

Samples of steel which had been coated with electroless nickel and then heat treated at 400°C for three hours showed the optimum erosion resistance of all the coated systems tested. However, the case hardened materials, such as carburised and nitrided steels, demonstrated superior erosion resistance to the coated materials. Boronised specimens, which have a definite interface between surface treated layer and substrate, showed inferior erosion resistance.

The research on surface treated and coated materials has shown that it is important that any surface layer must have a good elastic match with the base material and a continuous diffusion type interface is preferable. Any isolated defects can render the surface susceptible to catastrophic erosion.

GLOSSARY

Comparison of En numbers and equivalent values in BS 970

En Number	New Number	Type
1A	220 M07	Low carbon
3	070 M20	Low carbon
24	817 M40	1½ Ni Cr Mo
36A	655 M13	3¼ Ni Cr
41B	905 M39	1½ Cr Al Mo

CONTENTS

CHAPTER TWO : EXPERIMENTAL APPARATUS AND TECHNIQUES 23

GENERAL INTRODUCTION

One of the most troublesome problems encountered in the use of hydraulic turbines has been pitting or erosion caused by cavitation (1).

The Mining Technology Laboratory of the Chamber of Mines Research Organisation of South Africa has focussed its attentions during the last ten years on the mechanisation of mining methods in order to improve operative efficiency of the gold mining industry (2). The high rock strength together with the narrow stoping width (typically 1 metre) necessitated the use of efficient power transmission systems, of which hydraulic power proved to be the most satisfactory. The use of mineral oils as the hydraulic fluid was unsatisfactory in terms of economy, safety and pollution of ore. Although used in other mining industries, it was not applicable to the mining of gold. Fire-resistant fluids have been used for a number of years in the coal mining industry (3). However, the problems of increased cavitation erosion and the fact that these fluids may not be as effective as mineral oils in providing lubrication and corrosion protection, prompted the development of numerous research programs (3, 4, 5).

Considerable effort has been expended over the past four decades to determine the factors controlling the erosion rate, in order to permit the selection of appropriate materials. It has generally been recognised that the erosion resistance of a particular system depends on a multitude of inter-related parameters. Parameters such as erosive stress, adhesive strength and properties of the coating and substrate are of importance when considering laminar bonded materials (6).

The work done by Heathcock (5) was directed toward an understanding of the role that microstructure plays in determining erosion resistance. It provided a guide for the selection of existing materials and showed the way towards the development of more erosion resistant materials.

The emphasis in the present work has been on further developing an understanding of what determines material performance and a study of the erosion behaviour of special materials such as polymers and surface treated and coated low alloy steels. Certain materials within these classes have previously shown promise as cavitation erosion resistant materials, but insufficient work has been done on a meaningful range.

This thesis is aimed at filling these gaps in the knowledge and establishing the industrial potential of these types of materials.

CHAPTER 1 : CAVITATION DYNAMICS

1.1 CAVITATION - GENERAL

Cavitation, ~~as defined by~~ Preece (7), is the name given to the repeated growth and collapse of cavities in a fluid resulting from local pressure fluctuations. The formation of these cavities which are largely filled with vapour occurs when the instantaneous pressure decreases to such an extent that the nucleus bubbles cannot remain stable (8). In a flowing liquid, or fluids subject to cyclic pressure pulses, these cavities collapse upon reaching a region of pressure higher than its vapour pressure. These collapses generate large hydrodynamic stresses which can result in deformation and erosion of boundary material.

1.1.1 Cavitation nucleii

Experimental values obtained (vapour pressure to about 280 atm) for the tensile strength of water vary dramatically from the theoretical estimates (500 to 10,000 atm) (8). The reason suggested is that the liquid contains microscopic gas or vapour bubbles which act as nucleii for the growth of cavities at small values of tension (9). Harvey et al (cited in ref. 9) demonstrated that if the nucleii are removed by pre-pressurisation the liquid can withstand relatively large tensions. In order for these nucleii to exist they must be stabilised or they dissolve as a result of the pressure differential across their walls (9).

Two main mechanisms of bubble stabilization have been proposed:

1. Harvey (cited ref. 9) suggests that gas is trapped in crevices on hydrophobic surfaces; whereas

2. Fox and Herzfelt (cited ref. 8) suggest the bubble is stabilized by a rigid organic skin.

Unstable cavity growth occurs when the nucleus is subject to a reduction in pressure below a critical value and this topic has been adequately documented by numerous workers (5, 7, 8, 10). Once this vapour cavity has formed its subsequent collapse can be highly dynamic and the possibility of material damage is ever present (10).

1.1.2 Bubble collapse

High pressures ($\sim 10^3$MPa) are produced during the collapse of a single cavity and Hickling and Plesset (cited ref. 7) noted that the bubble can only damage a solid if it collapses no further than half its initial radius from the surface. It has been shown theoretically (11, 12) and experimentally (13, 14) that if a cavity collapses near a boundary, it becomes involuted and a high velocity jet of liquid is produced.

Brunton (15) calculated the velocity of this jet to be about 500m/s and as such would produce a shock pressure of ∿500 MPa or twice the value if the bubble is attached to the surface. The collapsed bubble radiates a compression wave and behind this wave the bubble expands resulting in a possible fracture of restricting boundaries.

Thus single bubble collapse may produce damage by one of three mechanisms:

1. jetting
2. compression shocks
3. expansion within restricting boundaries

Brunton (16) postulated the predominant mechanism to be the repeated collapse of large individual fixed bubbles on the eroding surface.

The concerted collapse theory (17) was introduced to explain the long slip lines (>1cm in length, when the maximum bubble diameter observed was only 90 μm with jets < 1/10 this value) and through-the-thickness hardening observed in 3mm thick samples. Vyas and Preece (18) suggested that the collapse of the first bubble would trigger the others, producing a stress pulse (300 - 1200MN/m^2) of sufficient magnitude to deform most metals and account for the through-thickness hardening discussed above. Hansson et al (19) have shown that in flow erosion, cavitation is mainly by individual cavities, whereas in ultrasonic systems concerted collapse predominates.

1.1.3 Material response to cavitation

Vyas and Preece (18) showed that although macroscopic deformation occurs only at the surface of a 5mm thick nickel sheet, an increase in dislocation density, microhardness and residual stress occurs throughout the bulk. Numerous studies have been undertaken on the damage produced in metals prior to any detectable mass loss (incubation period). Plesset et al (20) using X-ray diffraction observed in the case of nickel and brass plastic deformation after very short periods of exposure to cavitation (2 sec) without any optical changes or weight loss. The depth of deformation was determined by chemically removing surface layers till a 'sharpening' of the diffraction pattern occurred. Hansson et al (19) and Erdmann-Jesnitzer and Louis (21) studied microscopic changes which occurred during the incubation period by the use of scanning electron microscopy. Settler et al (22) examined microsections of the upper surface layer and also performed microhardness observations concluding that plastic deformation is not always observed and damage development does not depend on crystal grain boundaries. A detailed study has been made by Preece et al (23) of the deformation and mechanisms of material loss in FCC, BCC and HCP materials. Four distinct modes of material removal have been proposed by Heathcock (5):

(a) Ductile tearing in nickel and cobalt alloys, austenite stainless steels and low carbon steels.

(b) Brittle transgranular and intergranular failure as in ferritic stainless steels.

(c) Fibrous tearing in resilient polymers such as nylon and polyacetal copolymer.

(d) 'Plastic flow' like deformation of polytetraflouro-ethylene.

Thus an understanding of the relationship between material properties and erosion performance is vital in the prediction of material responses to cavitation.

1.1.4 Prediction of material performance

Many investigators over the past thirty years have attempted to obtain a correlation between some bulk mechanical property(s) and erosion resistance. Early investigations carried out by Mousson (24) indicated that erosion performance was not directly related to hardness, but the result of a number of inter-relating mechanical properties. Thiruvengadam (25) used the strain energy to fracture, as defined under the area of the conventional stress-strain curve, in predicting erosion performance. Ultimate resilience, expressed as ½(tensile strength)^2/elastic modulus, was shown by Hobbs (26) to correlate well (unlike the proof resilience and work to fracture). No precise correlations applicable to tensile strength, yield strength, engineering strain energy, true strain energy, hardness, reduction in area and elastic modulus could be found by Garcia and Hammitt (27). However, a simple damage predicting equation related primarily to ultimate resilience proved the best correlation, assuming that no plastic deformation occurs. Thus, the ultimate resilience was by far the most successful single material property by which to gauge erosion resistance.

Hirotsu (28) also found a rough correlation between ultimate resilience and erosion performance. Wood et al (29) concluded that damage resistance is related to a combination of mechanical properties and phase structure. Using a least mean square fit regression analysis, a correlating equation containing both a strength and ductility factor, was developed.

Rao (30) showed the product of ultimate resilience and Brinell Hardness to have the best correlation to the erosion resistance.

At present no single parameter can be used by an engineer in gauging the life expectancy or performance of materials in erosive environments. The reason for this is that most material tests are quasi-static, unlike the dynamic situation encountered in cavitation (31). Thus the response to cavitation is more dependent on micro-deformation modes and strain rate sensitivity than most conventional mechanical properties (23).

1.1.5 Influence of water based emulsions on erosion performance

A limited amount of work has been conducted on the influence of water based emulsions on the erosion performance of polymers. Heathcock (5) observed that oil-in-water emulsions generally suppress cavitation by forming a thin oil film on the metal surface and that the increased dissolved air content associated with emulsions damped the damage capacity of bubble collapse.

1.2 CAVITATION EROSION OF POLYMERS

Structural materials in contact with cavitating fluids have generally been metallic and consequently little study has been made of the cavitation erosion of non-metallic materials (7). Most research on the cavitation erosion of polymeric materials has focussed on coatings or overlays (32, 33).

1.2.1 Prediction of erosion performance

Lichtman et al (34) examined bulk polymeric materials and noted the elongation to fracture of plastics to be significant in determining their erosion resistance. For example, excellent erosion resistance was found in nylon 66 which has a reported elongation to fracture of 300 per cent. Thiruvengadam (25) explained this in terms of the strain energy concept where higher elongation suggests a higher strain energy and hence lower intensity of damage.

However, Hammitt et al (35) found a trend of increasing erosion resistance with increasing hardness for a small group of elastomers in both impact and cavitation tests. He pointed out that this correlation probably applies only to the limited group of materials tested and is not applicable in general.

1.2.2 Influence of physical properties

The erosion resistance of polymeric materials depends on mechanical properties which are likewise dependent on chemical compositions. The relationship between mechanical and chemical phenomena has been extensively examined by Mears (36) and Brydson (37). However, little is known of the influence of these parameters on erosion resistance.

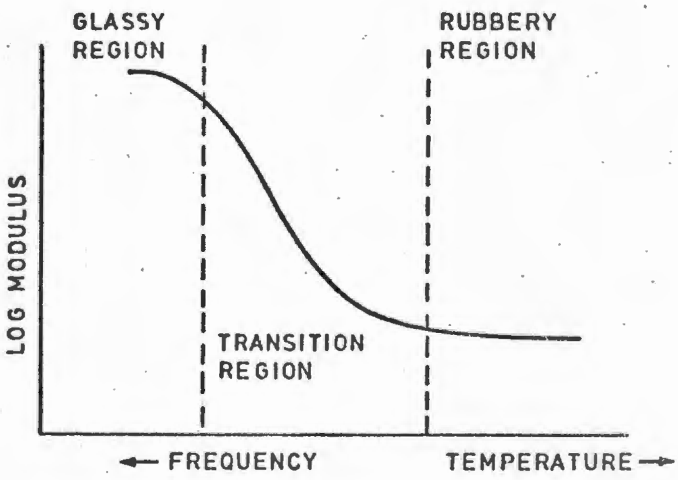

FIG. 1.1 Variation of elastic modulus with temperature and frequency for a typical polymer (ref. 38)

Chatten and Thiruvengadam (39) noted that the frequency of the cavitation stress pulse has more significance for erosion of viscoelastic materials than for metals. Consulting Fig. 1.1 it will be noted that an increase in temperature at constant frequency, or a decrease in frequency at constant temperature, lowers the elastic modulus from a glassy to rubbery region. Because of the high frequencies associated with cavitation (20kHz) one must select a material with a low Tg (Glass Transition Temperature) in order to avoid brittle fracture. Peak damping occurs at frequencies or temperatures which lie within the transition region and these polymers would possibly provide optimum erosion resistance (38).

If the time between successive stress pulses is less than the relaxation time of the elastomer, then it behaves in a brittle manner; however, at low frequencies the cavitation energy transmitted into the material is partly released elastically and partly dissipated as heat between stress pulses. In some instances the behaviour of plastics, under cyclic loading may lead to failure by melting as a result of high mechanical hysteresis and low thermal conductivity (40).

1.2.3 Characterisation of erosion damage

Although the majority of the research on fracture mechanisms in polymers has concentrated on samples damaged by drop impact erosion (41, 42), a similarity between droplet impact and cavitation has been reported in various materials by Engle (42). Scanning electron micrographs of the eroded surface displaying various modes of erosion have been presented by Engle (42) and Heathcock (5). It has been noted that hard 'glassy' polycarbonate, which is characterised by a high glass transition Temperature and low elongation to fracture, fails in a brittle manner; whereas failure of 'soft' polymers and elastomers occurred in either a 'tearing' manner or in a mixture of both brittle and tearing modes. There is a limited amount of literature available on vibratory cavitation of bulk polymers suggesting that further investigation is necessary.

1.3 CAVITATION EROSION OF COATINGS AND SURFACE TREATMENTS

1.3.1 Polymeric coatings

Many of the investigations of cavitation erosion of coatings have concentrated on polymeric or elastomeric overlays (32 - 34, 43, 44).

Lichtman (32) used a rotating disc apparatus in the determination of the erosion performance of cured and sheet elastomeric materials. The relationship between erosion performance and mechanical properties such as tensile strength, ultimate elongation, hardness, tear strength and rebound resilience were investigated. Both dynamic (high speed fluid flow conditions) and static (peel tests) adhesion tests were carried out according to ASTM (D-429-62) method B and ASTM (1002-64) respectively. No clearly defined trends relating erosion performance to mechanical properties were observed. It was realised, however, that both methods of coating application and geometric design (ie. 'edge protection') are of importance.

In addition, both high frequency and high velocity flow apparatus have been used (33, 44) in the determination of erosion performance. The intensity of erosion produced by these apparatus is significantly higher than that of the rotating disc device and once again no precise correlations between erosion performance and mechanical properties were observed.

Kallas (43), using a rotating disc device observed a broad correlation between erosion resistance and mechanical properties, although no precise correlations existed. It has generally been recognised that phenomena such as adhesion failure, tearing and substrate-coating mismatch need be understood in order to optimise erosion performances of coated systems. Thus an elementary wave propagation model was developed by Thiruvengadam and Hochrein (45) in order to study the complex nature of viscoelastic coating removal due to cavitation.

The importance of a coherent substrate was demonstrated when a coating that performed for 32 hours lasted only 3 hours when used on an incorrect substrate. This occurs as a result of wave reflections because of the impedence mismatch between coating and substrate.

In contrast with the extensive research conducted on polymeric coatings, the erosion performance of metallic coatings remains relatively unresearched.

1.3.2 Metallic coatings and surface treated materials

One of the earliest works performed on surface treated materials was by Mousson (24). He noted the depth of case hardening to be important in the determination of erosion resistance. Further, the ability of a material or coating to deform plastically appears to be an important factor in determing erosion performance (34). A large volume of information is available on coatings (application techniques, chemical and mechanical properties) and this will be fully reviewed in Chapter 3. A vacuum whirling arm spin rig was used by Tuitt (46) in order to relate particle impact erosion performance with the mechanical properties of numerous nickel coatings. In addition, the erosion performance of numerous nickel, titanium, aluminium and chromium alloys used in compressor systems, has been investigated. No precise correlation was found between erosion performance and properties of tensile strength, ductility, proof stress, specific gravity and internal stress. Although previous in-service experience suggested that a high compressive stress within the coating was desirable for erosion resistance, no correlation between the two variables was found in vitro. A correlation between erosion performance and elastic modulus, over the range of 50 to 210 x 10^3 MPa, was determined for both coated materials and compressor alloys (46). King (47), used cadmium coatings for accelerated erosion measurements to predict the performance of harder materials used in hydromachinery. Variations in coating thickness were measured with a beta-back scatter instrument which was relatively unaffected by variation in surface roughness, unlike magnetic, ultrasonic and eddy current techniques. The following points arose from this development work:

1. Erosion rate decreases as coating thickness decreases. King (47) explained this by suggesting that the substrate absorbs a greater degree of the incident energy pulse as the coating thickness decreases.

2. The variability of results was attributed to the inconsistancy of coating application from one batch to another. This is in agreement with Heathcock et al (48) where it was pointed out that these variations in results complicated the interpretation.

Heathcock (48) tested a range of coated and surface treated materials such as Tufftrided steel and hard chrome and electroless nickel coatings on steel. Some of the more important findings are:

1. The erosion performance of electroless nickel coated En24 samples which have received a post application heat treatment improves as shown in Fig. 1.2.

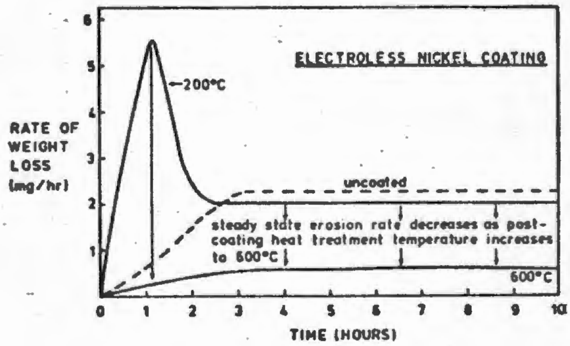

FIG. 1.2 The effect of post-coating heat treatment on the erosion resistance of electroless nickel coated En24 (Q & T 600°C) (ref. 48).

2. Varying the base metal hardness failed to produce any conclusive trends for electroless nickel coated steel.

3. Hard chrome coatings generally offer little improvement to erosion resistance, whereas Tufftriding results in a threefold improvement in performance.

In tribological applications large shear forces can act on the coating, and adhesion failure can occur by mechanical or thermal fatigue (49).
The adhesive strength is therefore of great practical importance and a theoretical appreciation of the coating behaviour under dynamic load situations, is vital.

1.3.3 Theoretical considerations of coating damage

1.3.3.1 Model for coating systems

There are many similarities between the damage caused by liquid impingement attack and that caused by cavitation (42). This is because the imploding bubbles result in the formation of a highly accelerated flow of liquid and the following arguments developed by Rieger and Boche (6) are applicable to both forms of erosion.

The impact pressure of a drop of water striking a surface with velocity v is expressed by the following equation:

$$\sigma_{pl} = \frac{\rho_w C_w \rho_l C_l}{\rho_w C_w + \rho_l C_l} \times V \qquad (1)$$

where ρ_w and C_w are the density and sonic velocity of the water, and ρ_l and C_l are the density and sonic velocity in the surface layer. The above equation can be expressed in the form of:

$$\sigma_{pl} = \frac{\rho_w C_w V}{[1 + \rho_w C_w / \rho_l C_l]}$$

and is attributed to de Haller (50) and based upon the conservation of momentum equations.

In a two-layer bonded system differences in mechanical properties result in the incident pressure wave σ_{p1} being broken up into:

1. a reflected wave, σ_{p1r}

2. a transmitted, wave, σ_{p2}, which penetrates the underlayer.

$$\sigma_{p2} = \sigma_{p1} + \sigma_{p1r} \quad (2)$$

When considering an elastic regime, equation (1) can be modified as follows:

$$\sigma_{p1r} = \frac{\rho_2 C_2 - \rho_1 C_1}{\rho_1 C_1 + \rho_2 C_2} \times V \quad (3)$$

$$\sigma_{p2} = \frac{2\rho_w C_w \rho_1 C_1 \rho_2 C_2}{(\rho_w C_w + \rho_1 C_1)(\rho_1 C_1 + \rho_2 C_2)} \times V \quad (4)$$

It will be noted from the above equation that the magnitude of the propagated wave is dependent on the physical properties of the individual layers. This is of importance when considering coatings of different modulus and density as displayed in Figs. 1.3 and 1.4.

FIG. 1.3 Water impact on a solid coated with a thin elastomeric layer (ref. 51).

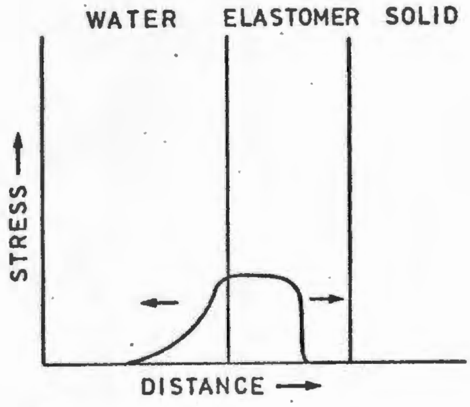

Fig. 1.3a Stress distribution before the stress pulse reaches the solid surface (arrows indicate propagation direction).

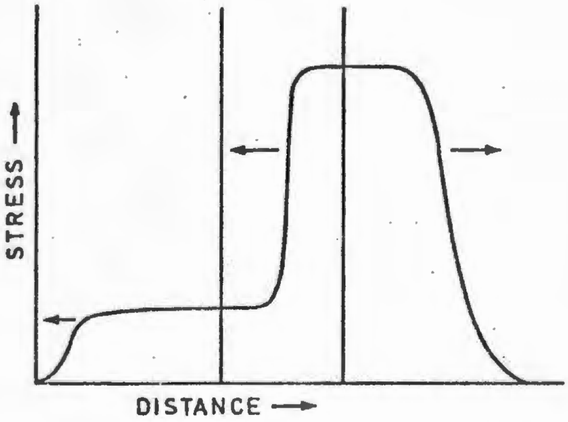

Fig. 1.3b Stress distribution shortly after stress wave impinges on the solid/elastomeric interface.

FIG. 1.4 Water impact on a solid coated with a thin, hard coating (ref. 51).

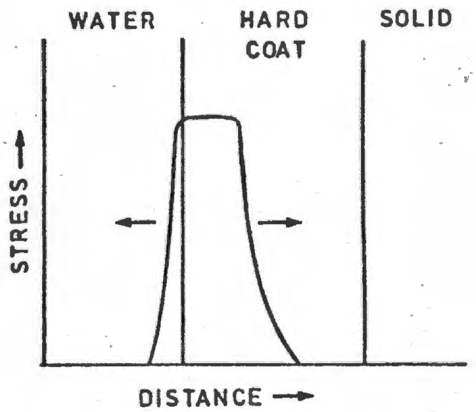

Fig. 1.4a Stress distribution before stress reaches the coating - solid interface (arrows indicate propagation direction).

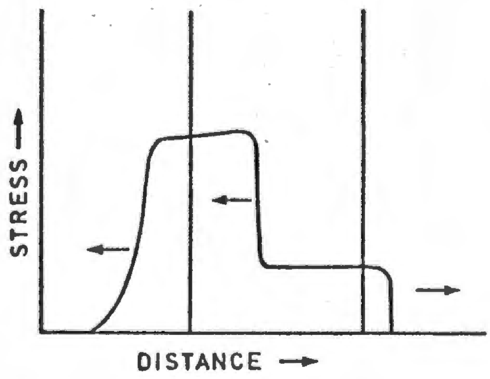

Fig. 1.4b Stress distribution shortly after the stress wave impinges on the coating solid interface.

From Fig. 1.3 it is evident that the initial stress pulse experienced by the elastomer is low. However, upon reaching the interface an intensified pulse is reflected and transmitted into the bulk. Conversely, the initial stress pulse experienced by the hard metallic coat is high, in view of the high bulk modulus (Fig. 1.4). So, upon reaching an interface of lower modulus a low level stress pulse is reflected back into the coat as well as transmitted into the bulk. The impact of the shock wave places the surface of the coating in compression (6), and this is compensated for by a horizontal expansion of the coating. The mismatch in horizontal expansions between coating and substrate sets up a shear stress at the interface, given below by equation (5). A full derivation of this shear stress equation is found in Appendix 1.1.

$$\sigma_s = \tfrac{1}{2}\,\frac{d(\nu_1E_2 - \nu_2E_1)G_1G_2\sigma_{p2}}{E_1E_2\left[\ell_{x1}G_2\left(1 - \frac{\sigma_{p2}}{E_1}\right) + \ell_{x2}G_1\left(1 - \frac{\sigma_{p2}}{E_2}\right)\right]} \qquad (5)$$

where: $\nu_1\nu_2$ = poissons ratio

E_1E_2 = moduli of elasticity

G_1G_2 = moduli of shear of surface and supporting layer

$\ell_{x1}\ell_{x2}$ = thickness of surface and supporting layer respectively

d = diameter of drop

σ_{p2} = is given by equation (4)

Depending on the magnitude of this shear stress two different forms of coating removal can occur:

(a) Erosion of the coating without layer separation. This occurs if the shear stress is less than the adhesive strength; or

(b) If the shear stress exceeds the adhesive strength, then separation of the surface layer from the substrate occurs. An example of each case is shown in Fig. 5.14 and Fig. 5.15 (Chapter 5).

1.3.3.2 Dependence of layer thickness

Equation (5) shows that the shear stress at the interface decreases as coating thickness increases. Accordingly, work done by Schmitt (52) on polyurethanes showed an increase in erosion resistance with coating thickness. However, a contrasting trend has been reported by King (47) where the erosion resistance decreases as the coating thickness increases, for pure cadmium.

CHAPTER 2 : EXPERIMENTAL APPARATUS AND TECHNIQUES

A number of techniques have been developed in order to simulate conditions associated with cavitation erosion. The most common are the rotating disc, venturi and vibratory cavitation devices (7, 9). The rotating disc device produces cavitation similar in intensity to vibratory devices. However, the rotary device has the disadvantage that large volumes of fluid are required and that flow patterns are complex when compared with venturi systems. The venturi system, though providing good simulation of in-service conditions, produces cavitation of low intensity and requires large volumes of fluid. In contrast, the vibratory cavitation test is the simplest and most commonly used. Its major disadvantage is that results cannot be used to predict damage rates in flow machinery. However, this technique produces a high intensity cavitation which requires little laboratory space and its popularity as lead to its standardisation (ASTM G32-72) for determining the cavitation erosion resistance of a wide range of materials.

2.1 VIBRATORY CAVITATION EQUIPMENT

A vibratory cavitation equipment was constructed by Heathcock (5) in accordance with ASTM G32-72. A stationary specimen mount, adopted by Preece (17), was used in order to avoid longitudinal stresses. These stresses can cause fatigue failure of the test specimen and make the testing of low strength ceramics and brittle polymers impossible. The apparatus as shown in Fig. 2.1 consists of a piezoelectric transducer which vibrates at a frequency of approximatley 20 kHz.

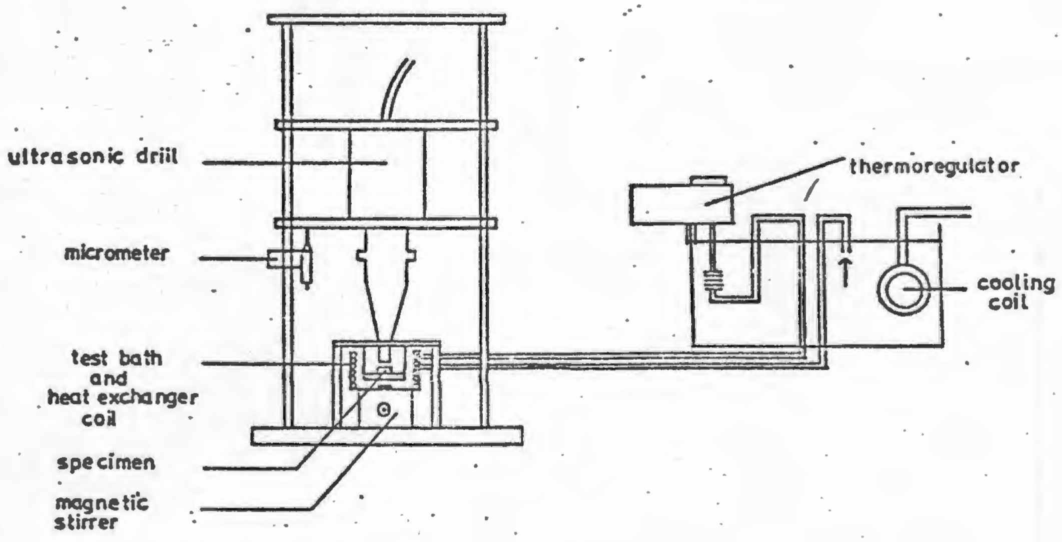

FIG 2.1 The Vibratory Cavitation Erosion Test Apparatus (cited in ref. 5)

An exponential velocity transformer or 'horn' amplifies the oscillations produced by the piezoelectric transducer by a factor of approximatley 3,5. The amplitute is determined optically by measuring the vertical expansion of a horizontal machining mark on the drill tip when the drill is operating. The size of this extended point is measured against a calibrated graticule and adjusted to give the correct amplitude, with a precision of approximately 3 µm.

2.2 SPECIMEN PREPARATION

2.2.1 Polymeric materials

Polymeric specimens were machined into discs of 14mm diameter x 3mm. These discs were mounted on a brass block and ground on 1000 grit SiC paper, prior to polishing with 1 μm diamond paste. An automatic polishing machine was used and the polishing time was approximatley 24 hours. Specimens were 'annealed' at 80°C prior to testing in order to relieve the internal stresses generated by polishing.

2.2.2 Coatings and surface treated materials

All specimens (14mm diameter x 3mm) were industrially coated or surface treated. The different techniques, their characteristics and uses will be discussed in Chapter 3. The substrates were polished to a 1μm surface finish prior to treatment and specimens were eroded employing standard test procedures discussed in section 2.3.

2.3 TYPICAL TEST PROCEDURE

(i) The distilled water in the test bath and the drill tip at the end of the drill horn are replaced before each new specimen is tested. The tip is made from a titanium alloy (Ti 318A) chosen for its good acoustic properties, high erosion resistance and low density.

(ii) The vibratory equipment is warmed up for one hour prior to testing in order to allow the horn to expand until equilibrium temperature is reached. The temperature in the test bath is maintained at 25°C by the circulation of regulated water through a heat exchange coil.

(iii) A polished disc specimen which has been notched and weighed is inserted into an insulated specimen holder keyed for orientation.

(iv) After reaching running temperature a specimen is inserted and a separation distance of 0,35mm between specimen and drill tip is set using the micrometer.

(v) The duration of a test run is one hour after which the specimen is removed, ultrasonically cleaned, washed in alcohol, dried and weighed on a chemical balance accurate of 0,1mg. Specimens are tested for periods ranging between five and twenty hours depending on the response of the material to cavitation.

2.3.1 Special test procedures

A. Water absorption - Polymers

In the case of polymeric materials, weight losses were recorded after each hour and corrected for the water absorbed by using an identical control specimen immersed in water. This method gives an indication of the 'true weight loss' after each hour. However, it may be imprecise since the control specimen is not subject to the stresses associated with cavitation and the water uptake may be influenced by cavitational stresses.

B. Influence of dilute and concentrate forms of high water based fluids (HWBF's) on polyacetal and ultra high molecular weight polyethylene (UHMWPE)

Twenty-four polyacetal samples (14mm diameter x 3mm) were polished and weighed. Ten of these samples were immersed in five different HWBF's (ie. 2 samples in each fluid). Ten of these samples were immersed in five different derivitives (5% HWBF/95% H_2O) and two immersed in water and two kept in air. All samples were held for 3 weeks in their particular environments, at 70°C. After 3 weeks samples were reweighed and cavitated at 25°C in distilled water employing standard cavitation procedures discussed in section 2.3. Results are presented in Figs. 4.15 and 4.16 (see Chapter 4).

2.4 EXPERIMENTAL TECHNIQUES - POLYMERS

2.4.1 Tensile tests

Tensile tests were carried out in accordance with ASTM D-638 using a strain rate of 0,188 per minute. All tensile specimens (Type IV in ASTM standard) were machined in such a way as to make the tensile axis parallel to the direction of extrusion and strained to fracture using a Hounsfield Tensometer. The ultimate tensile strength (UTS) and percentage elongation to fracture ($\%E_f$) were subsequently calculated. Results of these tests are shown in Table 4.1 (see Chapter 4). These results were compared with the manufacturer's specifications (Appendix 2.1) and discrepancies existed in some instances. Repeat tests were performed which confirmed reproducibility of results.

2.4.2 Resilience measurements

Another property of polymeric materials considered was the resilience number (Rn) which is directly related to material hardness. A Shore Scheleroscope was used to determine resilience number. A 'hammer' falls under gravity from a fixed height onto the test specimen, and the resulting rebound is recorded and this provides a measure of a material's ability to absorb and reflect the energy of impact. Flat 14mm diameter x 3mm thick specimens which had been annealed for 1 hour prior to testing were used for resilience tests and results are shown in Table 4.1 (see Chap. 4).

2.4.3 Hardness measurements

The indentation hardness of polymeric materials was tested by means of a Durometer. Type A is used for measuring the softer materials such as elastomers and Type D for the harder materials. The indentation hardness is inversely related to the penetration and is dependent on the elastic modulus and viscoelastic behaviour of the material. This method is used primarily for control purposes and there is no simple relationship between indentation hardness, as determined by this method, and any fundamental property of the material tested. Results of these tests are shown in Table 4.1 (see Chapt. 4).

2.4.4 Determination of glass transition temperature (Tg) by differential scanning calorimetry

A polymer may be amorphous or crystalline or a combination of both of these. The Tg is a function of segmental thermal motions in the amorphous regions of the polymer. Below the Tg an amorphous polymer can be said to have the characteristics of a 'glass' while above Tg it becomes 'rubbery'. This is due to the onset of molecular motions of short chain segments which do not occur below Tg. Differential thermal analysis was performed using differential scanning calorimetry (DSC) which records the differential heat flow dH/dt, required to maintain a constant temperature T, in both a sample and an appropriate inert reference material placed in a furnace. From this, one can calculate the enthalpy change for a change of state in the sample.

A number of important physical changes in a polymer may be measured by DSC. These include the glass transition temperature (Tg), the crystallisation temperature (Tc), the melting temperature (Tm), and the degredation temperature (Td). A typical DSC trace is shown in Fig. 2.2 together with definitions of the Tc, Tm and Td. After a period of time T, an increase in heat capacity occurs at Tg due to the onset of these additional molecular motions and this shows up as an endothermic response with a shift in the base line.

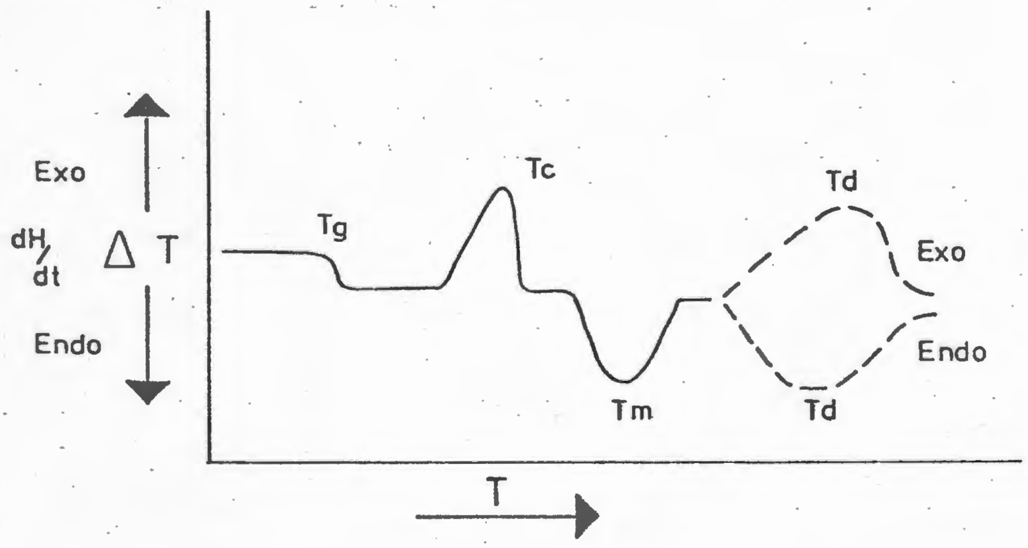

FIG. 2.2 Typical DSC trace for a polymer showing:
1) Tg 2) Tc 3) Tm 4) Td

Melt temperature (Tm): The melt temperature can be defined as the temperature at which solid and liquid phases are in equilibrium, and as these are affected slightly by pressure they are usually referred to normal pressure (760mm).

Crystallisation temperature (Tm): At the crystallisation temperature molecules or segments of molecules move relative to one another and arrange themselves in a regular manner on the crystal lattice; unlike the transition to the glassy state, which corresponds to an instantaneous 'freezing in' of the amorphous structure.

Degredation temperature (Td): The degredation temperature can be defined as that temperature at which chain breakdown occurs.

2.4.5 Scanning electron microscopy

Scanning electron micrographs (Figs. 4.5 - 4.13) of eroded surfaces have been taken in order to gain information relating to the mode of failure. The eroded surfaces were coated with gold-palladium and examined at magnifications varying between 100x and 3000x.

2.5 EXPERIMENTAL TECHNIQUES - COATED AND SURFACE TREATED MATERIALS

2.5.1 X-ray diffraction (XRD)

Most materials have some degree of crystallinity and hence show some symmetry and regularity. This can be made visible by x-ray diffraction or diffractometry. Electroless nickel coatings which are given a 200°C post application heat treatment (PHT) are totally amorphous. However, above 200°C (PHT) a nickel phosphide (Ni_3P) phase begins to crystallise out. The varying degrees of crystallinity at various PHT's (200 - 600°C) was studied using this technique. The crystallographic structures of Boronised En24 was also investigated and the following set of standard conditions employed in all cases:

Radiation = CuK_α
40kV 20mA
1° slits (convergence and receiving)
Scan 4° 20/min
Chart = 4cm/min
Time Const = 1 sec
All XRD work was performed after erosion and typical results are shown in Figs. 5.8 to 5.12.

2.5.2 Optical

After eroding the specimen, it was vertically cross-sectioned, hot mounted in bakelite, polished with 1μm diamond paste, and then etched in a 5% Nital solution. Optical micrographs of the sectioned discs and of eroded surfaces, at hourly intervals of exposure to cavitation, were taken in order to facilitate an understanding of the mechanisms of material removal.

2.5.3 Scanning electron microscopy and elemental analysis

In addition to scanning electron microscopy, discussed earlier in section 2.45, a spot analysis technique was employed to investigate the possibility of interdiffusion for an electroless nickel sample which received a 600°C PHT (3 hrs). A Kevex micro X-7000 energy dispersive multichannel analytical spectrometer was used.

2.5.4 Microhardness Measurements

A diamond pyramid microhardness test was used to obtain hardness measurements of various surface treated materials which had been sectioned and mounted after erosion.
A load of 20 Pond was used in all cases and the microhardness calculated from the following formula:

$$MH = 1854{,}4\ P/d^2 \quad kp/mm^2$$

where P = load in Pond
d = diagonal measured in microns

CHAPTER 3: OVERVIEW OF COATED AND SURFACE TREATED LOW ALLOY STEELS

3.1 INTRODUCTION

The erosion performance of a number of coated and surface treated materials have been investigated. All surface modifications and overlay coating treatments were performed by commercial organisations. En24 was, in general, used as the standard base metal and its surface was polished with 1μm diamond paste prior to treatment.

3.2 SURFACE MODIFICATIONS

The principal types of surface treatments are shown in Table 3.1, and taken from the article by Wells (53). Of these, the erosion performance of only nitrided and boronised samples have been determined. The processes, general characteristics and uses are discussed in sections 3.2.1 and 3.2.2. In addition, carburized steels, which were previously tested by Yamey (54) showed excellent erosion resistance and the process and results are discussed in this thesis.

TABLE 3.1 TREATMENTS INVOLVING SURFACE MODIFICATION (cited in ref. 53)

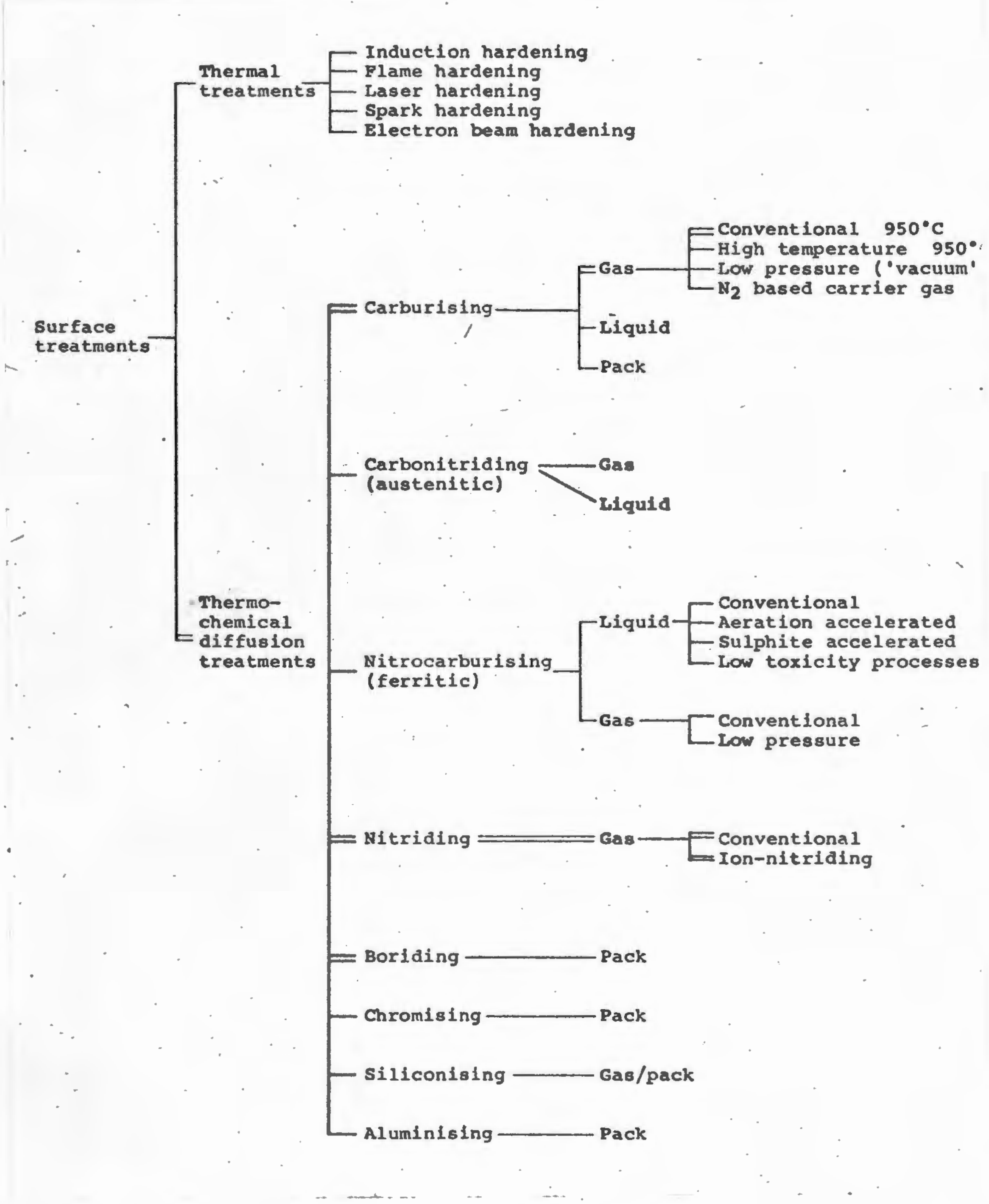

Double lines represent surface treatments tested

3.2.1 Boronising

A. *Process*

Boronising temperature : 930°C

Medium : The boronising medium can be either gas, liquid or solid (pack), with the latter being most favoured. In the pack process the powder consists of boron carbide with an activator (KBF_4) and a dilutent (SiC).

En24 and En1A discs, 14mm diameter x 3mm were boronised for periods ranging between 1 and 12 hours. The industrially reported case depths (74) for varying periods of boronisation are given in Table 3.2, below.

TABLE 3.2: INDUSTRIALLY REPORTED CASE DEPTHS FOR VARYING PERIODS OF BORONISATION

	Case depth (mm)	Time (hours)
En 24	0,05	1
	0,10	2
	0,15	4
	0,20	5½
En 1A	0,1	2
	0,2	5½
	0,3	7
	0,4	10
	0,5	12

B. *Characteristics*

Boronisation is a surface diffusion process analagous to carburizing or nitriding. High hardness (1000 - 2000VHN) is attained directly due to the formation of borides at the process temperature : 900°C (unlike carburizing, which requires quenching) (55). The formation of these alloy borides places the surface layers in compression because of their associated higher volume fraction.

The Fe-B equilibrium diagram is shown in Fig. 3.1 below. It is notable that two intermettalic phases exist, namely FeB and Fe_2B. At low boron potentials the Fe_2B phase predominates, whereas at high boron potentials a dual phase exists consisting of both Fe_2B and an undesirable β-rich phase, FeB. The harder FeB phase should be avoided because of its associated brittleness (56).

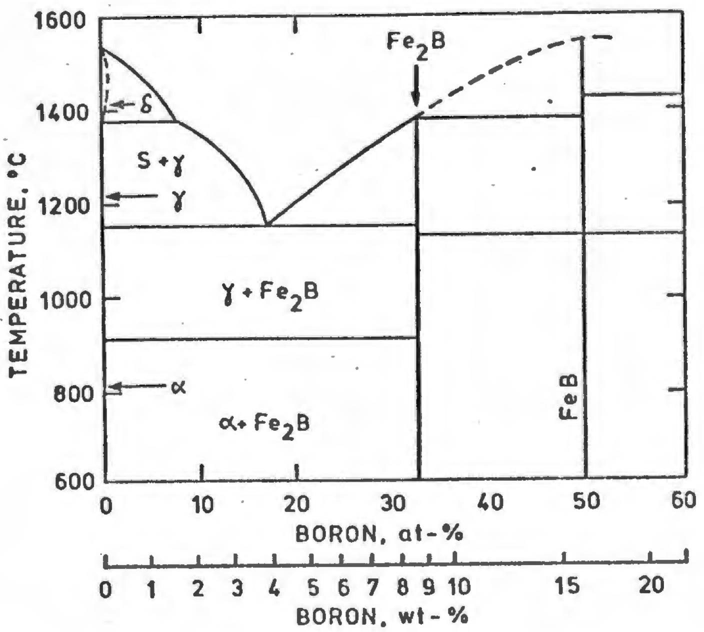

FIG. 3.1 Iron-boron system according to M. Hanson in 'Constitution of binary alloys', 1958, New York, Toronto, London, (McGraw-Hill). (Ref. 56)

The structure of the boride/metal interface has been extensively investigated by numerous researchers (55,56,57,58,59). In general the boronised layer can have either a jagged or linear interface. The dentate structure is common to low carbon steels, whereas a linear interface is common to high alloy steels, (55). The latter can cause failure by spalling, whereas the saw tooth interface shows excellent adhesion to the substrate and spalling is not observed even under the most severe working stresses.

Upon cooling from 900°C a residual compressive strain develops in the Fe_2B layer and the substrate is placed in tension. This arises from a mismatch in thermal expansion coefficients between boride layer and substrate. However, the saw tooth geometry of the boride layer minimises the interfacial stresses by distributing the residual stress over a greater area (55).

TABLE 3.3 PROPERTIES OF IRON NITRIDE AND IRON-BORIDE LAYERS ON UNALLOYED STEELS. (Ref. 60)

Phases of the compound layer	Structure	Hardness (HV 0,2)	Decrease in hardness	Thickness (μm)	Roughness R_z (μm)
Fe_xN Fe_4N	hex. cub.	500	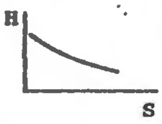	20	3 after mech. treatment: 1
Fe_2B FeB	tetr. rhomb.	1500	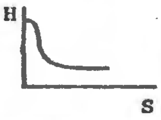	800	3 after mech. treatment: 1

Unlike nitriding or carburizing where hardness falls off gradually with depth, a steep gradient exists for boronised samples, (60). This is reflected in the hardness profiles shown in Table 3.3. However, boronising produces extremely large case depths when compared to nitriding.

C. *Uses*

To improve wear resistance of polishing jigs, wire drawing dies and also the corrosion resistance of mild steel components.

3.2.2 Nitriding

A. *Process*

Gas Nitriding En41B (Q & T 600°C) discs were gas nitrided for 60 hours and the process was performed according to the following specifications: The discs were purged for 1 hour in N_2 and then placed in a furnace set at 510°C, in a N_2 atmosphere. When the charge reached 510°C the N_2 flow was reduced and NH_3 added to give a percentage dissociation between 25 and 35%. The discs were held at temperature for 60 hours and the NH_3 flow adjusted to give the required percentage of dissociation. At the end of the cycle the NH_3 flow was reduced, the N_2 increased and the discs removed and placed in a cooling pit (61).

Ion Nitriding En41B (Q & T 600°C) discs were ion nitrided for 72 hours. These specimens were pre-heated for 6-8 hours at 470°C. The components were then placed in an evacuated chamber and set at a negative potential of 1000V. A mixture of nitrogen and hydrogen was then introduced until a pressure of 0,1 to 10mbar was reached. This causes a plasma discharge which uniformly heats the component causing the surface reactions to take place. After the 72 hours of exposure the specimens were cooled under vacuum for 8 hours. The required case depth of 0,4 to 0,5mm was achieved after 72 hours of nitriding.

B. *Characteristics*

The steels suitable for nitriding are specified in BS 970 Part 2 (62). In general they are steels which contain alloying elements that form stable nitrides such as aluminium, chromium, molybdenum, vanadium, tungsten. Nitriding causes the surface precipitation of alloy nitrides which places the upper layers in compression because of the restrictions of the underlying bulk. This improves the fatigue strength. Hardness of the surface layer is a function of the alloy content.

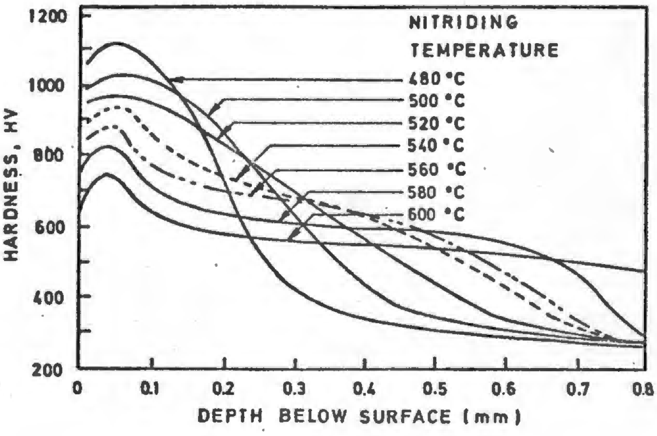

FIG. 3.2 Effect of nitriding temperature on hardness and depth of nitriding of BS 905M39 (En41B), after a period 60 hrs (Thelning 1975). (cited in Ref. 62)

From Fig. 3.2 it is noted that increasing the nitriding temperature results in a reduction in surface hardness although the case depth increases. A 'white layer' which is a mixture of Fe_4N (gamma nitride) and Fe_2N (epsilon nitride) is formed if the nitrogen potential is too high. This layer must be avoided as it is brittle and can initiate fatigue of the alloy nitride layer.

C. *Uses*

A typical use is the nitriding of gears in order to improve their fatigue and wear characteristics. This technique is used because component distortion is avoided in view of the low application temperature (500°C).

3.2.3 Carburizing

A. *Process*

The surface hardening effects produced by carburizing have been extensively reviewed by Child (62). Briefly, the aim of the process is to diffuse carbon into the surface of a steel when heated into the austenite phase (ie. 850°C). The component is then quenched and the desired hardness achieved depending on the carbon content of the surface layer. After heat treatment components are generally tempered, at 150 - 200°C, in order to remove residual stresses from the case.

B. *Characteristics*

The application temperatures, case depths and surface hardnesses produced by this process are summarised in Table 3.4, together with the properties of numerous other case hardening techniques.

TABLE 3.4 PROPERTIES OF SOME COMMON THERMOCHEMICAL TREATMENTS
(cited in Ref. 53)

Process	Medium			Temperatures	Case depth	Surface hardness HV
	Solid	Liquid	Gas			
Boronising (or boriding)	*			850-1000	0,025-0,1	1000-2000
Carburising	*	*	*	850-950	0,25-4,00	700-900
Carbonitriding		*	*	750-900	0,05-0,75	600-850
Nitrocarburising		*	*	570	0,2 1,0#	500-650
Nitriding			*	500-525	0,4 - 0,6	800-1050

maximum thickness of diffusion zone

On quenching, the surface layers are placed in compression. This arises because of the volume change which occurs when transforming from a high carbon austenite to martensite. In addition this residual compressive stress arises because increased carbon content is associated with a lower martensite transformation temperature. Thus on quenching sequential transformation occurs from the core inwards. This compressive stress results in improved fatigue characteristics.

C. *Uses*

Mainly used in the automotive industry because of its versatility of application ranging from mild steel to high alloy steels.

3.3 OVERLAY COATING PROCESSES

The principal types of overlay coating processes are shown in Table 3.5, and typical coating thicknesses produced are shown in Table 3.6.

3.3.1 Chemical vapour deposition (CVD)

A. *Process*

Samples of En24 (Q & T 500°C), together with nodular cast iron and grey cast iron were coated with tungsten carbides (W_2C) for 2 hours at 500°C to give a coating of approximately 20 μm thick. All the samples were grit blasted and electroless nickel plated to a thickness of 1 µm to aid bonding between the steel and tungsten carbide. The reason for this is that it is believed that the tungsten will not adhere to iron when deposited from tungsten hexafluoride because an interfering layer of iron fluoride is formed (63).Thus coating the steel with a thin layer of nickel or copper eleminates the formation of the iron fluoride.

Similarly, samples of En24 (Q & T 600°C), nodular cast iron and grey cast iron were coated by CVD with titanium carbide (TiC). The samples were treated for 3 hours at 900°C to give a TiC coating approximately 5 µm thick. No pretreatment is necessary to obtain a good bond because interdiffusion occurs between the coating and substrate due to the high deposition temperature.

TABLE 3.5: TYPES OF OVERLAY COATINGS (cited in ref. 53)

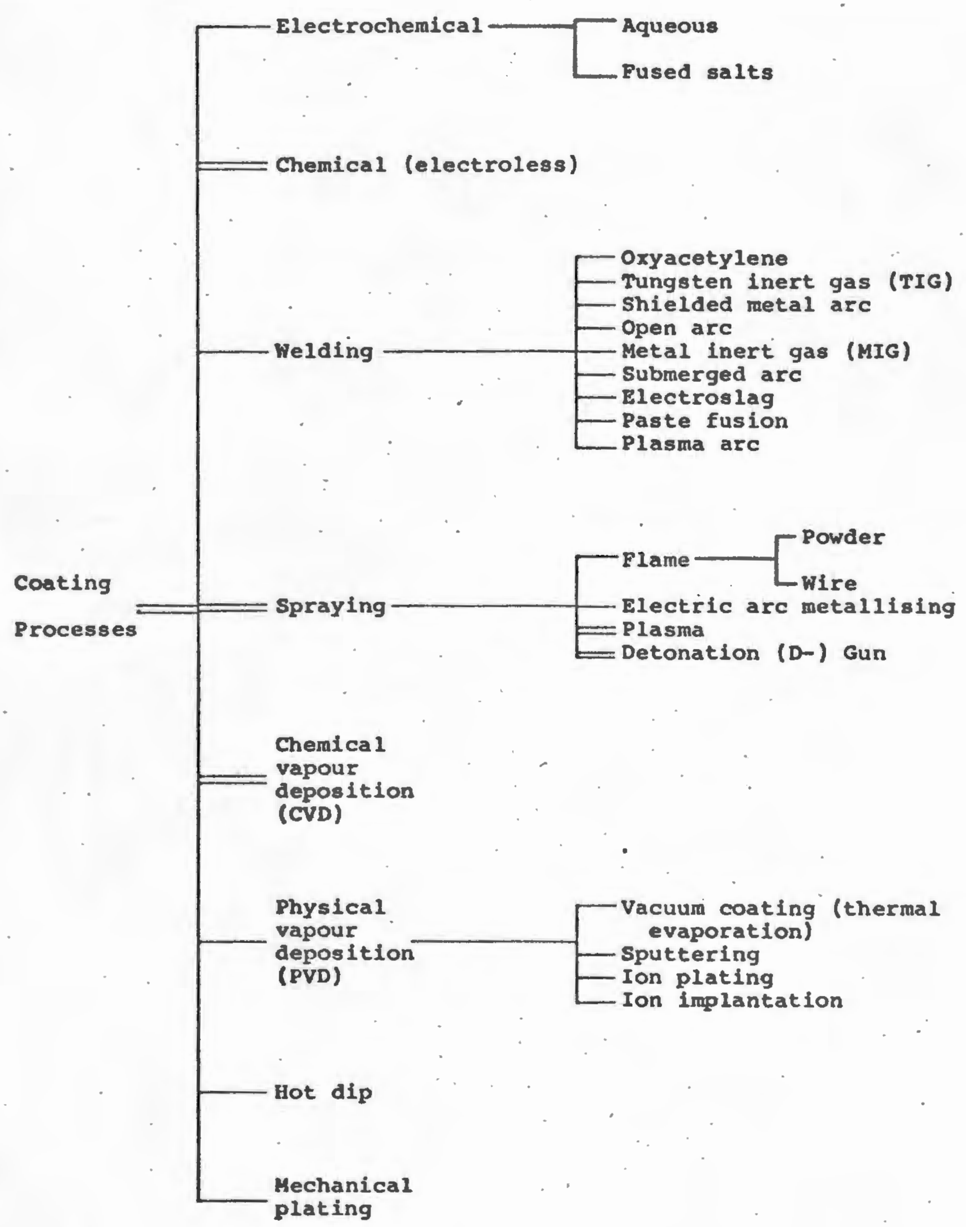

Double lines represent coatings tested.

TABLE 3.6: TYPICAL COATING THICKNESSES PRODUCED BY DIFFERENT PROCESSES
(cited in ref. 53)

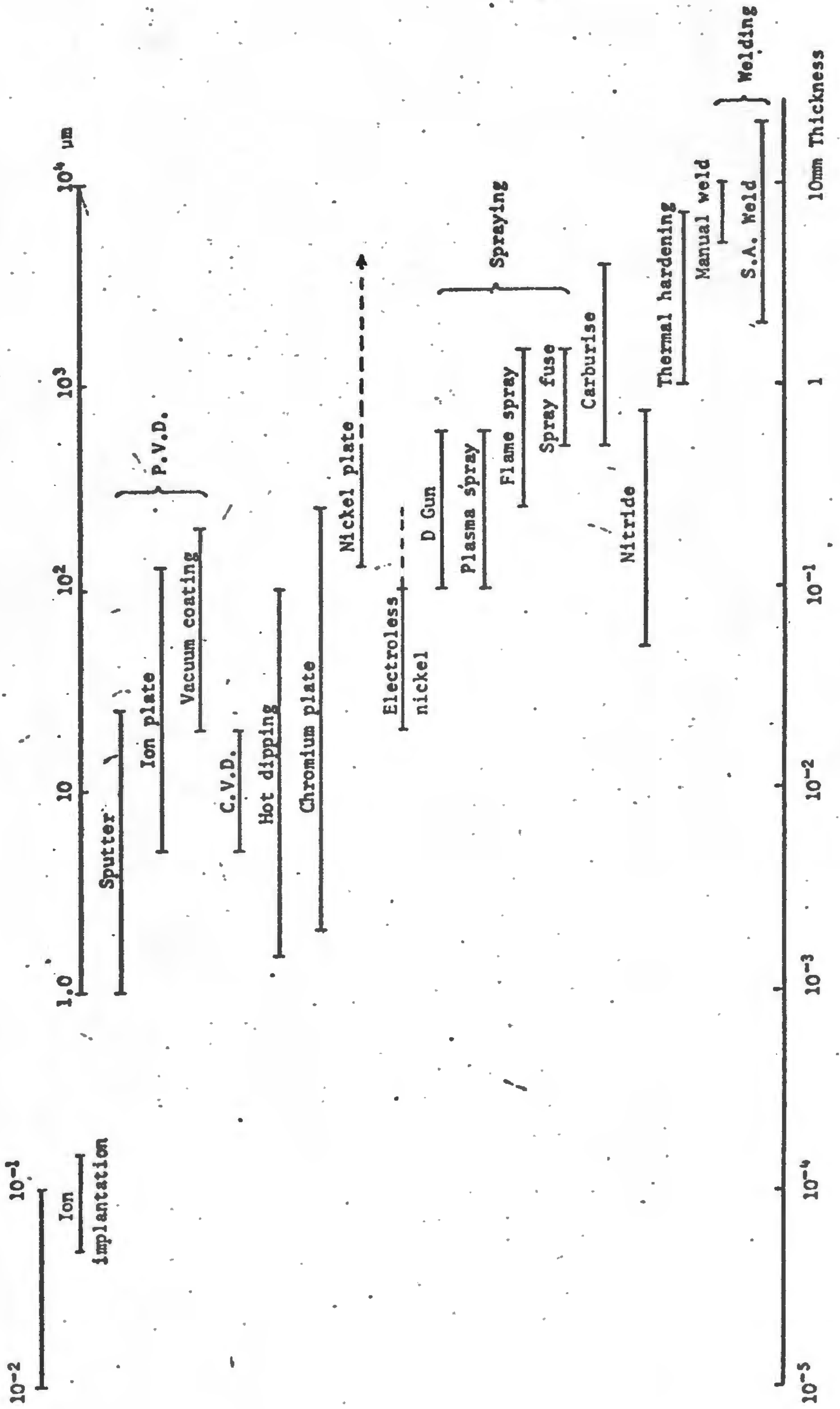

B. *Characteristics*

The subject of chemical vapour deposition has been well documented and the characteristics of these coatings have been drawn from the works of Hintermann (64, 65) and Archer (63).

Chemical vapour deposition is carried out at higher temperatures than other coating proceses and this places a limitation on the choice of substrate (ie. plastics are excluded).

The formation of the overlay is nucleation controlled and a well-ordered porous free structure is produced. As a result of competition between neighbouring growth centres and the differences in thermal expansion coefficients between the coating and substrate, residual stresses form in the overlay upon cooling. As a result these coatings are generally brittle and deform elastically at a strain of 2 percent (64).

In the case of titanium carbide a strong bond is formed because interdiffusion can occur at the high application temperatures (900°C). Conversely for depositions which occur at temperatures too low for interdiffusion, such as in the case of tungsten carbide, a strong bond can be attained by having a 'rough' substrate which aids 'mechanical keying' between coating and substrate.

C. *Uses*

1. It is important for coating of internal surfaces and complex objects.

2. The major use is in improving wear and frictional behaviour of cutting tools. Titanium carbide coatings ($\sim 5\mu m$ thick) have shown improvements in the performance of single point cutting tool tips. An important aspect of these coatings is the formation of a thin layer of TiO_2 on the surface which is inert and has no affinity for the workpiece.

3. Corrosion resistance : Dense coatings, which are free of porosity, are produced, which shield the substrate, and provide good corrosion resistance.

3.3.2 SPRAYING

3.3.2.1 Plasma sprayed Triballoy coatings

A. *Process*

Mild steel discs (14mm diameter x 3mm) were plasma spray coated with Triballoy T-100, T-400 and T-800, the compositions of which are shown in Table 3.7.

TABLE 3.7: CHEMICAL AND PHASE COMPOSITION OF TRIBALLOY (cited in Ref. 66)

DESIGNATION	CHEMICAL COMPOSITION (wt%) Co	Ni	Mo	Cr	Si	Laves phase content, vol%
T-100	55	-	35	-	10	65
T-400	62	-	28	8	2	50
T-700	-	50	32	15	3	60
T-800	52	-	28	17	3	55

The process of plasma spraying has been well documented (67-69). Briefly, specimens to be coated are mounted in an evacuated chamber and the alloy powders are injected into a plasma jet, melted and sprayed onto the substrate at velocities ranging between 100 and 400 ms^{-1}.

B. *Characteristics*

Triballoy is a trade name of E I du Pont de Nemours & Co (66). It consists of an intermetallic phase (Laves phase) dispersed in a softer matrix of nickel or cobalt. This intermetallic phase has a hardness of approximately 1100 VPN compared with the bulk hardness of 950 VPN. In metal spraying adhesion is generally achieved by a 'mechanical keying' action rather than by interdiffusion so an as-machined surface is desirable for bonding.

C. *Uses*

Parts can be fabricated by casting, hard facing, powder metallurgy and plasma spraying. The major uses are in:

Valve bearings and valve seat inserts
Thrust bearings
Mechanical seals
Wear inserts in Textile machinery
Coated magnetic tape heads

The wear behaviour of this intermetallic material has been documented by Cameron (66).

3.3.2.2 D-Gun carbide coated En3

A. *Process*

The principal of the detonation (D)-gun technique is that powder is inserted into an explosive oxygen-acetylene mixture and deposited at high velocities. This detonation occurs several times per second and the coating is applied in layers onto the substrate, which lies 5-10cm from the open end of the gun (53). Four samples of En3 were D-gun carbide coated. Two of the samples were polymerically sealed and two unsealed. When used in gaseous environments these coatings are polymerically sealed, due to their high porosity.

B. *Characteristics*

The characteristics of the D-Gun carbide coated En3 samples are summarised in Table 3.8, below. These coatings are extremely dense and have the greatest adhesive strength of any of the sprayed coats.

TABLE 3.8: CHARACTERISTICS OF D-GUN CARBIDE COATING

Process	D-Gun
Composition weight %	25 WC + 5Ni + mixed W/Cr carbides
Hardness	VHN = 1100, R_C = 69
Porosity Average volume %	0.7
Density g/cm^3	10.1
Modulus of rupture MPa	275
Modulus of elasticity GPa	55
Coefficient of thermal expansion 10^{-6}/°C	8.3
Maximum operating temp. (oxidising atm.)	760°C

C. *Uses*

High speed cutting tools.

3.3.3 Electroless nickel

A. *Process*

Discs of En24 (Q & T 600°C) were coated with electroless nickel to thicknesses ranging from 10μm to 100μm. These samples were then given a post plating heat treatment of 300°C for 10-12 hours. In addition, these En24 samples (Q & T 600°C) were coated with 25 μm of electroless nickel and then given post coating heat treatments ranging from 200°C to 600°C for 3 hours.

The coating procedure used was as follows (70):

1) Pre Treatment - Acid clean
Alkali clean
Nickel strike

2) Electroless nickel bath

(a) 85°C
(b) 10-11% phosphorous
(c) pH - 4.7
(d) 5μm filtration
(e) air agitation
(f) 1 hourly replenishment

3) Post plating treatment

Heat treated at 300°C for 10-12 hours.

B. *Characteristics*

Typical properties of electroless nickel are summarised in Table 3.9, given below. A plot of hardness as a function of post heat treating temperature is also given (Fig. 3.3).

TABLE 3.9: TYPICAL PROPERTIES OF FUNCTIONAL ELECTROLESS NICKEL DEPOSITS (cited in ref. 71)

Material	: 10 to 11% phosphorous dissolved in nickel
Structure	: Amorphous, no crystal or phase structure, laminations or segregation
Density	: 7.75 g/cm^3
Melting point	: 890°C
Magnetic coercity	: Non-magnetic
Tensile strength	: Greater than 700 MPa
Ductility	: 4 to 6% elongation
Modulus of elasticity	: 17 to 19 x 10^4 MPa
Adhesion strength	: 300 to 400 MPa
Hardness	: 480 to 500 VHN$_{100}$ as deposited; heat treatable to 1000-1100 VHN$_{100}$
Corrosion resistance	: Resists attack by most organic and inorganic environments

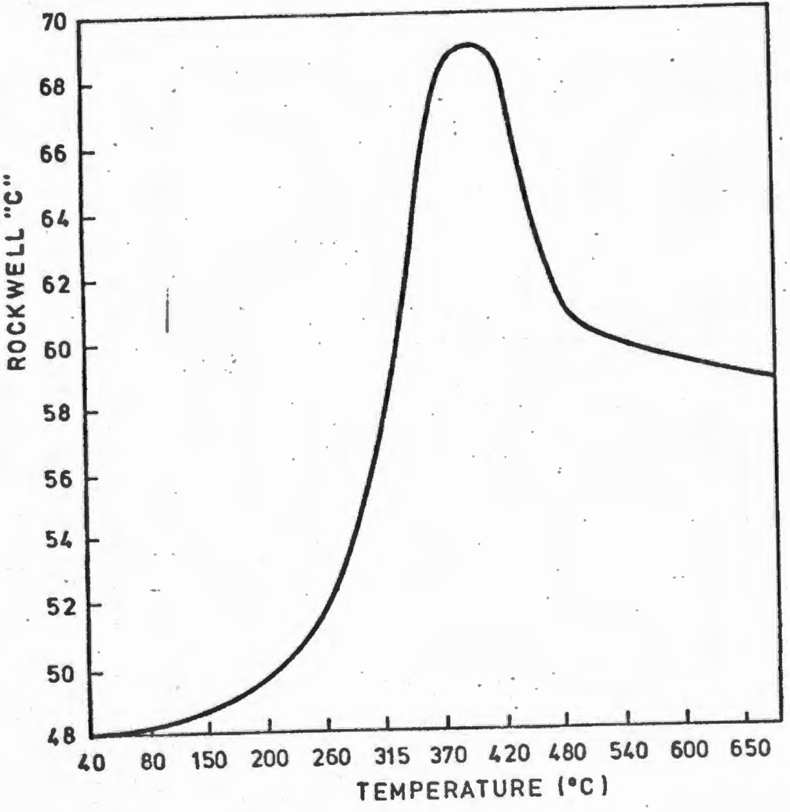

FIG. 3.3 Effect of heat treating upon hardness properties of electroless nickel (cited in ref. 71)

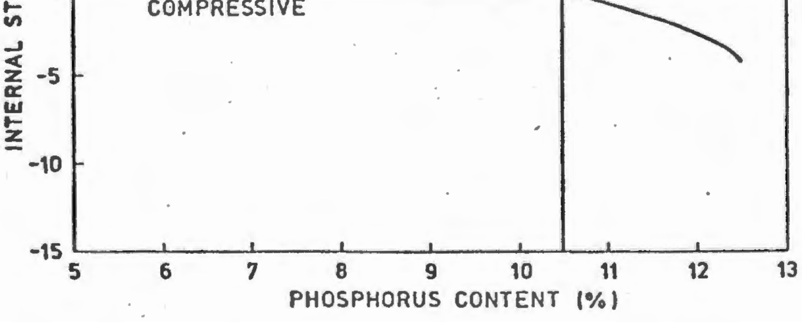

FIG. 3.4 Effect of phosphorous content on the internal stress of electroless nickel deposits on steel (cited in ref. 71)

Some important features of electroless nickel coating are discussed below

1. From Fig. 3.4 it will be noted that the phosphourous content has an effect on the internal stresses present in the deposit.

2. An increase in hardness of electroless nickel above 200°C (Fig. 3.3) is due primarily to the formation of nickel phosphide particles (Ni_3P). Peak hardness is reached at 400°C but above this temperature a drop in hardness occurs due to recrystallisation and grain growth of the nickel phosphide.

3. The structural transformations which occur above 200°C have been researched by Parker (72). A 5μm Ni-Fe diffusion layer has been observed after 4 hours of heat treating the applied coating at 621°C.

C. *Uses*

Used to coat rollers in the printing industry because of extremely smooth surface finishes required.

CHAPTER 4 : RESULTS OF BULK POLYMERIC MATERIALS

4.1 GENERAL RESULTS

The results of all the erosion tests conducted by the University of Cape Town's cavitation research program are presented in Appendix 4.1. A Pascal program was written to rank the materials performances in terms of their five hour cumulative volume loss (5hr CVL). Numerous other parameters were used to gauge the erosion performance of the polymers and surface treated materials. These include cumulative weight loss (CWL) and rate of weight and volume loss over periods ranging between five and forty hours. Other parameters of importance are the incubation period (t_o), the volume loss in the steady state zone ($\dot{E}$) and the time to reach maximum erosion rate (t_{max}). Heathcock (5) defined the incubation time as that time when the slope of the erosion curve deviates from the average slope of the low erosion rate period. Repeat tests were performed on the majority of surface treated materials and the percentage experimental error ± $\bar{\bar{\delta}}$ calculated using the following formula:

$$\bar{\delta}\ (\%) = 1/\bar{x} \sum_{i=1}^{n} |\ \bar{x} - x_i\ | /n \ \ x100$$

where $\bar{x}$ = average CVL

x_i = CVL for 1st, 2nd ... nth test

n = no. of test conducted

The average error calculated from all of the repeat tests is 13,1percent.

The results of the coated and surface treated materials are presented by plotting the rate of volume loss against time for both treated and untreated specimens. These specimens were eroded until a steady state erosion rate was reached and compared with the erosion characteristics of the untreated substrate. Because the different coatings varied in density the rate of volume loss was plotted in order to get a comparative indication of the erosion performances. This leads to numerous difficulties as both coating and substrate can be removed simultaneously during erosion. A typical example is tungsten carbide which has a density of 17.34g/cm^3, whereas the substrate's density (say En24) is only 7.74g/cm^3. After each hour of erosion the surfaces were examined optically and the appropriate density used to calculate the rate of volume loss. The density used could be either that of the coating (if only coating is removed) or the average of coating and substrate densities if both are removed. Once all the coating has been removed the density of the substrate is used to calculate the volume loss. Although this technique has inherent errors it is a simple method to calculate the relative erosion performances of coatings with widely differing densities.

4.2 CAVITATION EROSION AND POLYMERIC PROPERTIES

The results of the cavitation tests of a large variety of polymers classified by codes in Table 4.2, are shown in Figs. 4.1, 4.2 and 4.3. Nineteen different polymers were tested under the test conditions described in section 2.3. The results of the erosion tests are summarised in the form of an envelope graph shown in Fig. 4.4 in which the polymers tested are classified into three distinct groups in accordance with their 5 hour cumulative volume loss (CVL). In the case of polyamide 66 + PE, the decline in the curve (Fig. 4.1) is a result of the eroded sample absorbing more water than the control specimen. This phenomenon is apparently due to the stresses associated with cavitation which activate this water absorption.

The results together with the mechanical properties (determined by tensile tests) and resilience measurements (obtained by Shore Schlerescope and Shore Hardness) are shown in Table 4.1. Glass transition temperatures (Tg) obtained by Differential Scanning Calorimetry, and density measurements are also shown. Some relationships exist between the properties (shown in Table 4.1) and the various groupings shown in Fig. 4.4; this will be fully discussed in Chapter 6.

4.3 SCANNING ELECTRON MICROSCOPY

Scanning electron microscopy was performed on the eroded surfaces and typical micrographs taken at three magnifications are shown in Figs. 4.5 - 4.13. For the three groups identified in Fig. 4.4 and Table 4.1, erosion mechanisms vary from fully ductile (Group I) to fully brittle (Group III). Hard glassy polymers like polyethylene terephalate (Group III) were found to erode by fracture in a brittle manner. While erosion of soft polymers, such as UHMWPE, ocurred by a tearing or ductile mode (Group I) of failure.

An intermediate erosion mechanism (Group II) is shown by only one of the 'pure' polymers, namely polyacetal, but the filled polymers which show a mixed mode of erosion can also be classified in the intermediate grouping.

4.4 DIFFERENTIAL SCANNING CALORIMETRY

The thermal analysis results are shown in Table 4.1. A few selective plots are given in Fig. 4.14 for polyvinyl chloride (PVC), polyacetal + glass fibre (GF), and polyurethane A. The values obtained correspond with values given in the Polymer Handbook (73).

TABLE 4.1: RELEVANT POLYMER PROPERTIES

Polymer	Trade Name	No.	5hr CVL[1] (mm^3)	Tg[2] (°C)	UTS[3]	$\%E_f$[4]	Shore Hardness (D)	Density g/mm^3	Resilience No.	SEMS[5]	Code	Grouping according to SEM micrograph
Polyamide 66 + PE[6]	PAS-80 X	1	*0,09	-120,140 [11]	27,34	10,00	78	1,12	70	D	□	Group I
Polyacetal + PE	PAS-LX	2	0,24	-2 to 0,-60[11]	43,69	20,75	81	1,33	66	D	□	
DS[7] UHMWPE	-	3	0,53	-	30,41	467,4	66	0,95	46	VD	○	
Polyacetal copol[10]	-	4	0,64	-	74,73	64,15	81	1,41	73	D	⊘	
UHMWPE	Solidur 10/100	5	0,85	-120 to -70	19,33	485,5	66	0,94	55	D	○	
HDPE[8]	Solidur 80/100	6	1,06	-120	25,78	1030	68	0,94	45	D	○	
Polyamide 66 + GF[9]		7	*1,09	-	86,19	35,73	83	1,38	70	-	◐	
Polyacetal	Delrin	8	2,79	-2 to 0,-60[11]	65,65	30,65	81	1,40	76	D/B	○	Group II
" + PE + GF	PAS-LGX	9	3,01	-2 to 0,-60[11]	56,50	12,71	83	1,46	69	B	◐	
Polyacetal + GF	PAS-LG	10	3,14	-2 to 0,-60[11]	49,92	15,85	85	1,59	66	B	◐	
Poly(amide-imide)	TORLON	11	*10,07	-	-	-	86	1,39	75	B	○	Group III
Polypropylene	PAS-PP	12	11,20	-27	26,52	234,0	76	0,91	60	B	○	
Polysulfone	PAS-SUL	13	21,53	175 to 190	70,22	20,70	86	1,24	83	VB	○	
Polyethylene terephatalate	PAS-POT/E	14	35,57	63 to 80	78,83	17,30	86	1,31	103	VVB	○	
Polyurethane A	Vulkollan	15	-	-53	-	-	32	1,23	52	M	○	Group IV
" B	Polycast 880	16	-	-38	-	-	21	1,20	25	M	○	
" C	Polycast 885	17	-	-40	-	-	32	1,19	45	M	○	
Polycarbonate	-	18	-	-	70,10	38,89	83	1,14	91	VVB	○	
Polyvinylidene flouride	Kynar Homopolymer	19	-	-62	44,29	59,82	78	1,77	76	M	○	

[1] - cumulative volume loss
[2] - glass transition temperature
[3] - ultimate tensile strength
[4] - percentage elongation to fracture
[5] - scanning electron microscopy
D = ductile
B = brittle
M = melt

[6] - PE = polyethylene
[7] - DS = double sintered ultra high molecular weight PE
[8] - HDPE = high density PE
[9] - GF = glass fibre
[10] - copol = polyacetal copolymer

[11] - 2nd order Tg
* - Figure approximate only - samples absorbed water during test-corrected against a control.

Description to codes given in Table 4.2, overleaf.

TABLE 4.2 : POLYMER GROUPINGS FROM SEM FRACTURE DATA

POLYMER	NO.	MELTING POINT	CODE	GROUPING ACCORDING TO SEM MICROGRAPHS
Polyamide 66 + PE	1	ca. 255	□	Group I
Polyacetal + PE	2	ca. 165	□	
DS UHMWPE	3	-	○	
Polyacetal copol	4	157	⊘	
UHMWPE	5	137	○	
HDPE	6	-	○	
Polyamide 66 + PE	7	255	◐	
Polyacetal	8	ca. 165	○	Group II
Polyacetal + PE + GF	9	ca. 165	◐	
Polyacetal + GF	10	ca. 165	◐	
Poly(amide - imide)	11	650 ± 20	○	Group III
Polypropylene	12	ca. 160	○	
Polysulfone	13	-	○	
Polyethylene terephalate	14	ca. 256	○	
PTFE[1]	33	-	○	
PTFE + 60% Bronze	34	-	△	
PTFE + 25% Carbon(C)	35	-	△	
PTFE + C + Graphite	36	-	△	
PTFE + 15% Glass	37	-	◐	
PTFE + 25% Glass	38	-	◐	

□ = Hetrogenous polymer
○ = Homogenous polymer
⊘ = Co polymer
◐ = Fibre reinforced polymer
△ = Filled polymer
1 = polytetrafluroethylene

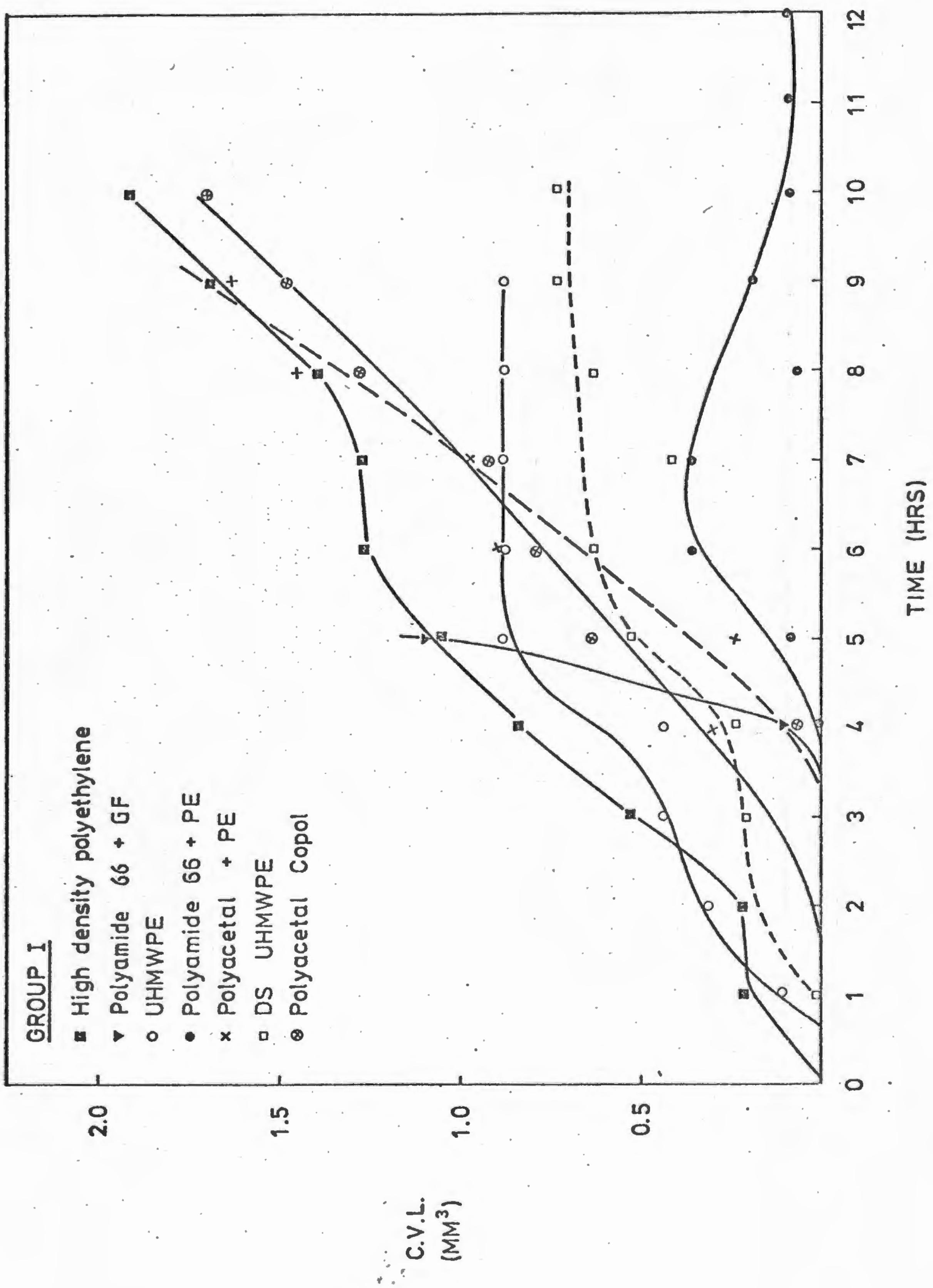

FIG. 4.1

Cumulative volume loss vs time curves for Group I polymers - ductile failure.

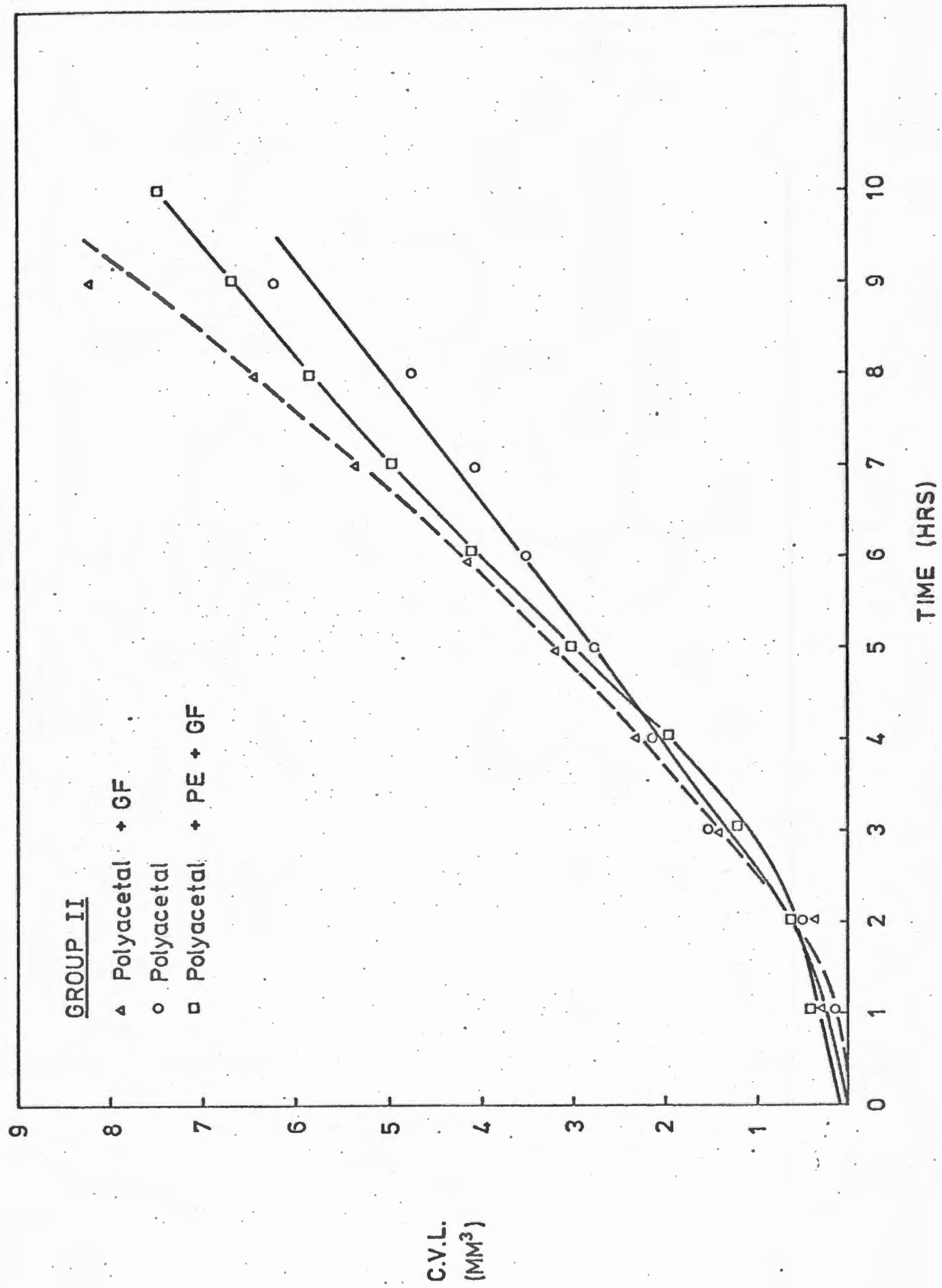

FIG. 4.2

Cumulative volume loss vs time curves for Group II polymers - intermediate mode of failure

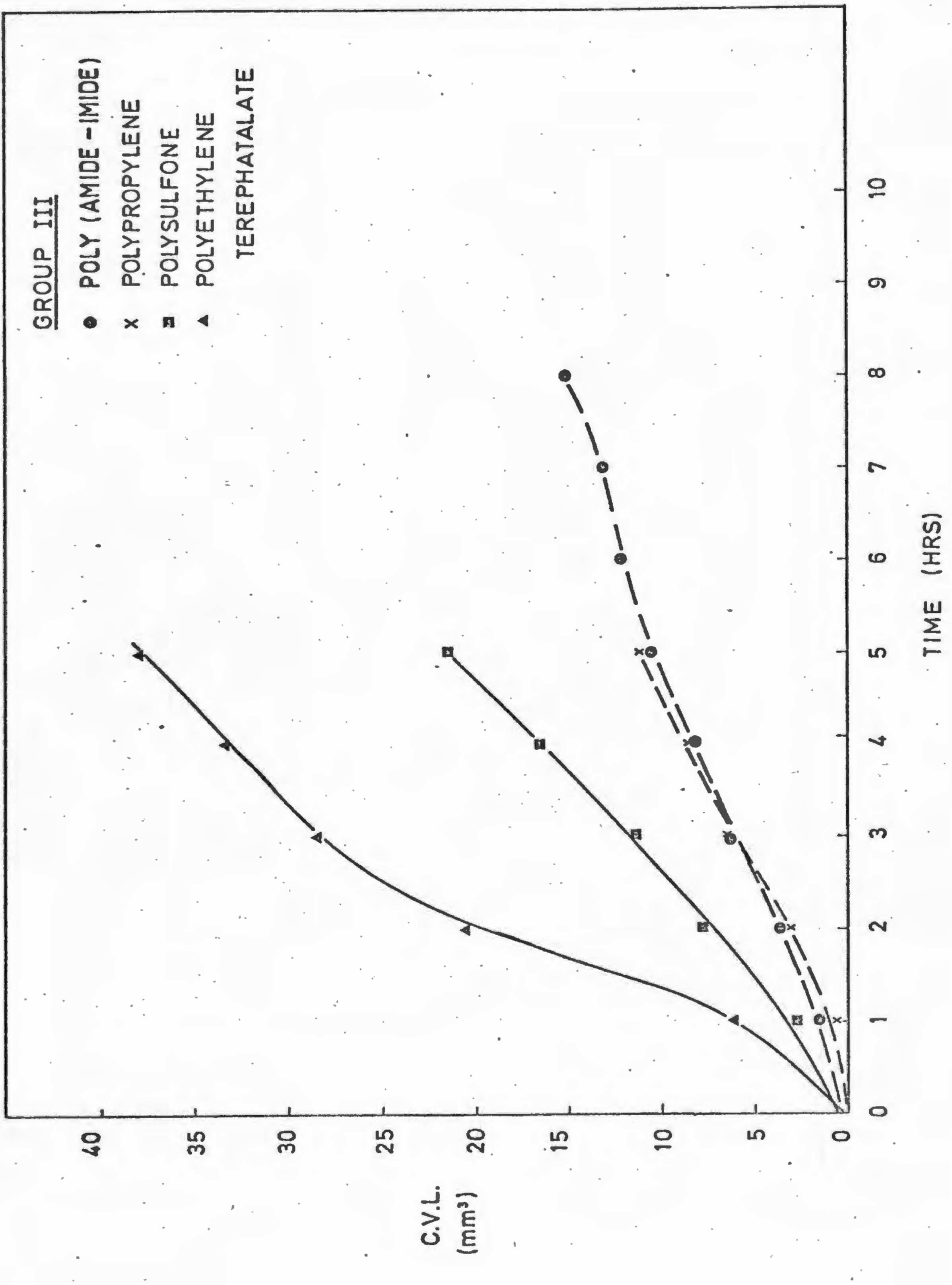

FIG. 4.3

Cumulative volume loss vs time curves for Group III polymers - brittle failure.

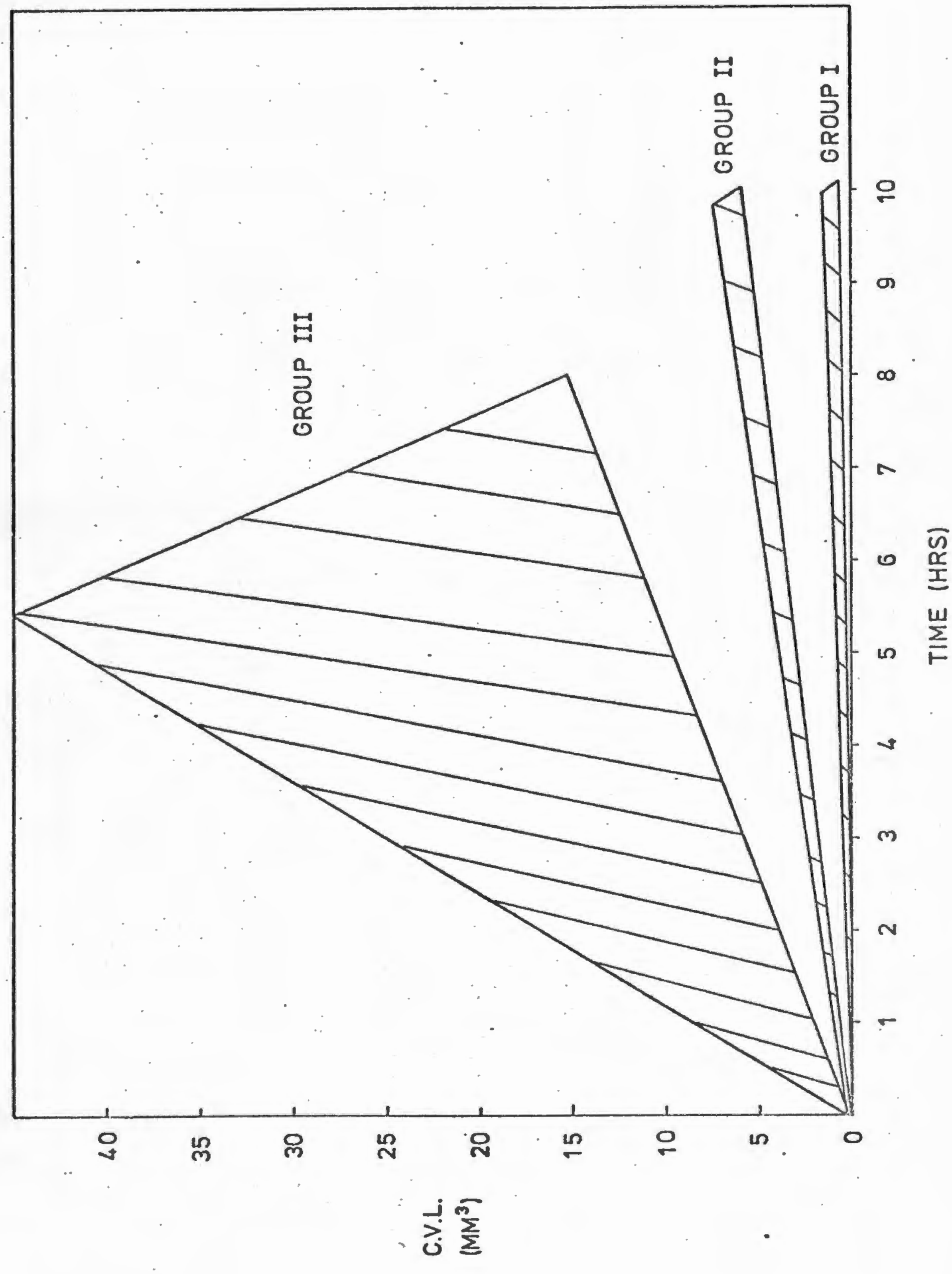

FIG. 4.4

CVL envelopes for ductile, brittle and intermediate failure modes.

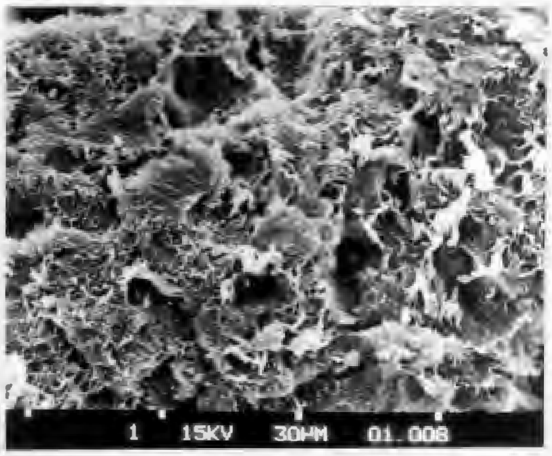

FIG. 4.5

Overview of ductile eroded surface of Polyamide 66 + PE (Group I)

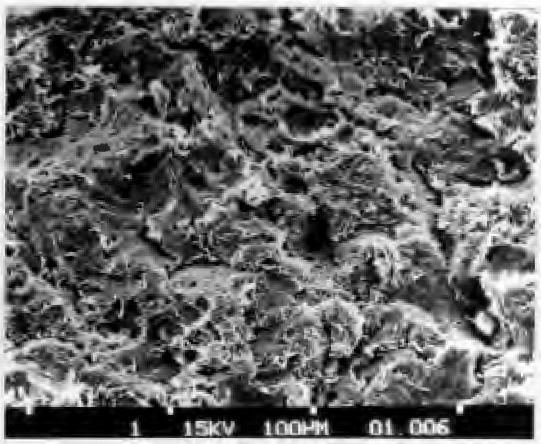

FIG. 4.6

Erosion of Polyacetal (Group II) displaying 'intermediate' mechanism of erosion.

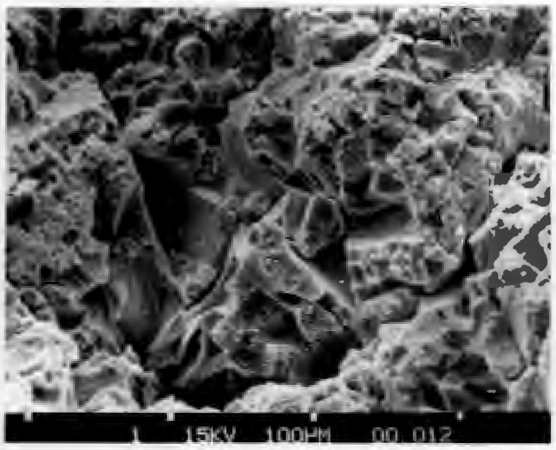

FIG. 4.7

Highly brittle mode of erosion at pit interface of Polysulfone (Group III)

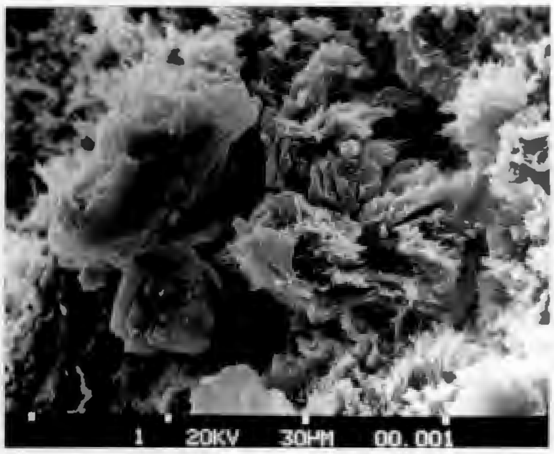

FIG. 4.8

Evidence of ductile tearing in HDPE (Group I) grains.

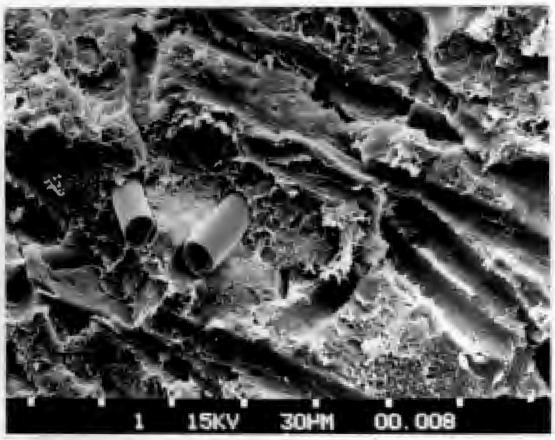

FIG. 4.9

Ductile tearing of Polyacetal matrix showing glass fibre pull-out (Group II).

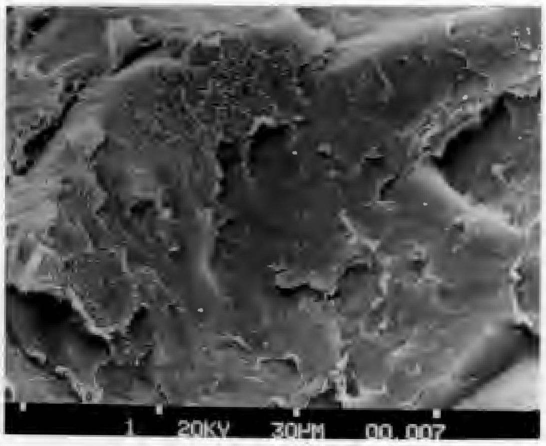

FIG. 4.10

Brittle erosion mode showing formation of cleavage steps with splinter chips in Polyethylene terephalate (Group III).

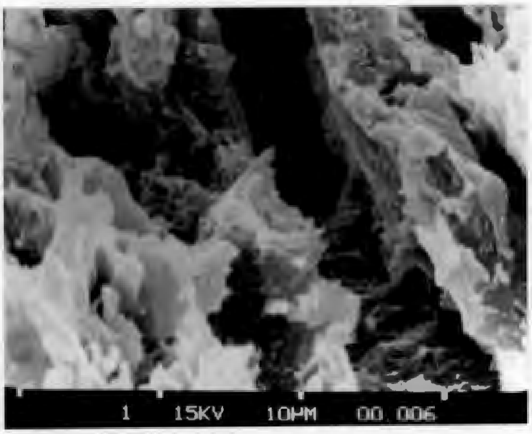

FIG. 4.11

Highly ductile cavitation pit boundary showing extensive deformation in UHMWPE (Group I).

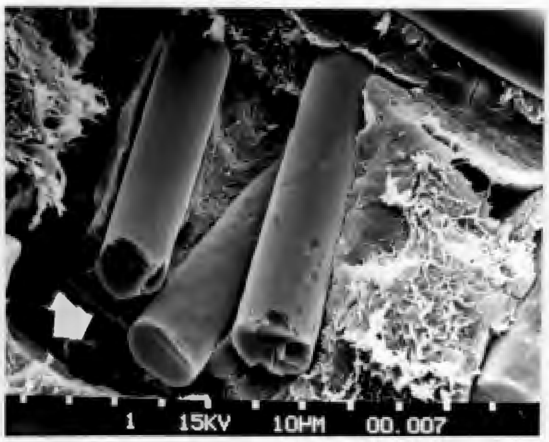

FIG. 4.12

SEM micrograph of Polyacetal + GF (Group II) displaying glass fibre-matrix interface.

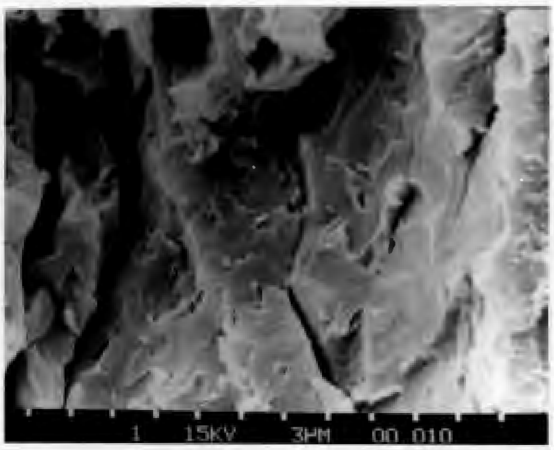

FIG. 4.13

Brittle failure of Poly(amide-imide) (Group III) displaying chip removal.

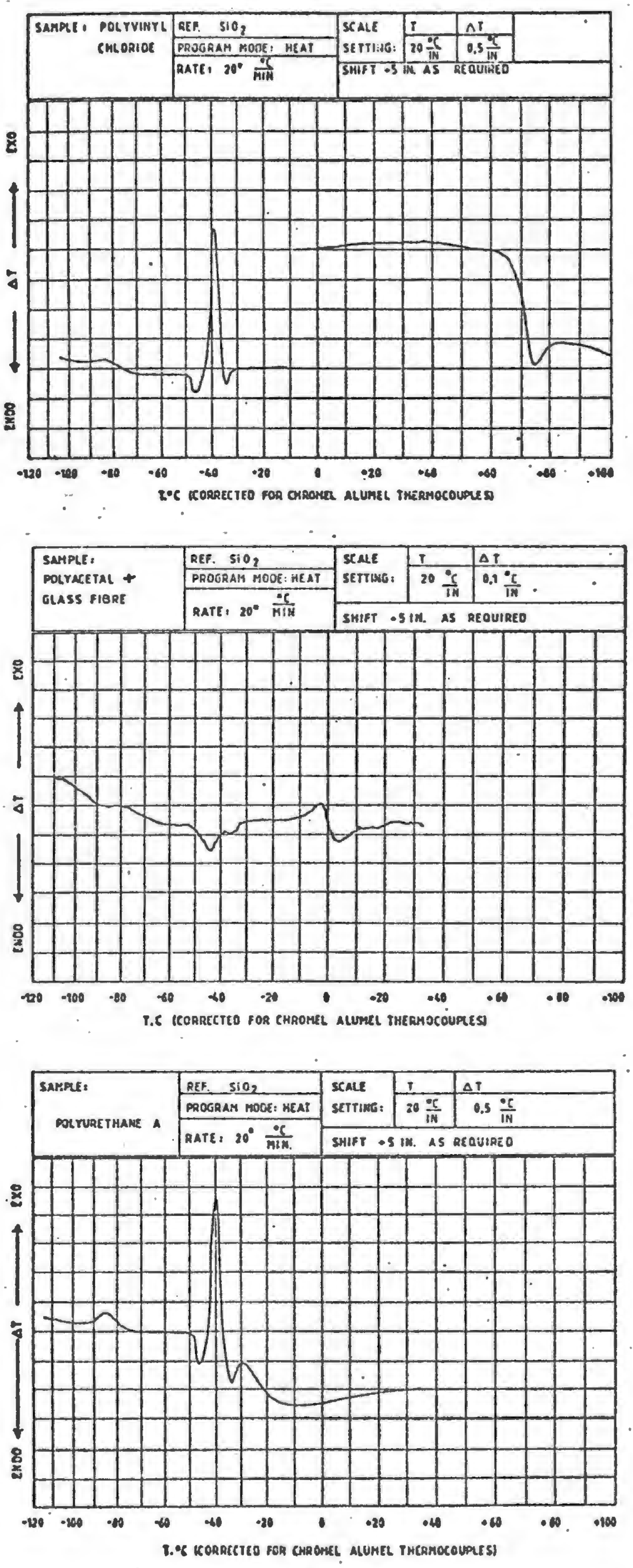

FIG. 4.14 Selective thermal analysis results (Tg) obtained by Differential Scanning Calorimetry

4.5 THE INFLUENCE OF CONCENTRATED AND DILUTE ADDITIVES ON THE EROSION PERFORMANCE

4.5.1 Determination of absorption prior to erosion

The pre-erosive treatment given to both polyacetal and UHMWPE is discussed in section 2.3.1(B). These polymers were soaked in five different concentrated additives (at 70°C for 3 weeks) which were designated the symbols A - E.

Concentrated additive A - 5% oil + emulsifyer
" " B - 23% " "
" " C - 31% " "
" " D - 90% " "
" " E - mineral based oil

They were also soaked in a 5% concentrated additive/95% water solution (5/95) and were disignated the symbols A_5, B_5, C_5, etc. These results together with that of the materials soaked only in air and water, are given in Table A and Table B in Appendix 4.1, and represented in the form of histograms which are shown in Figs. 4.15 and 4.16.

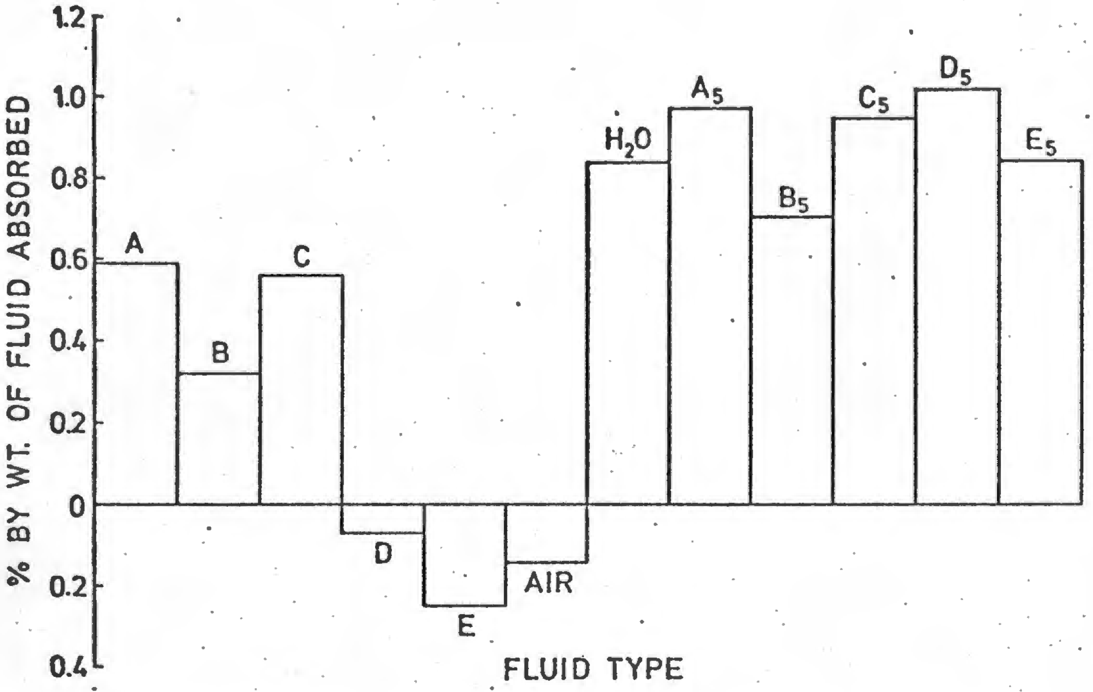

FIG. 4.15 POLYACETAL: FLUID ABSORPTION OVER A PERIOD OF 3 WEEKS AT 70°C

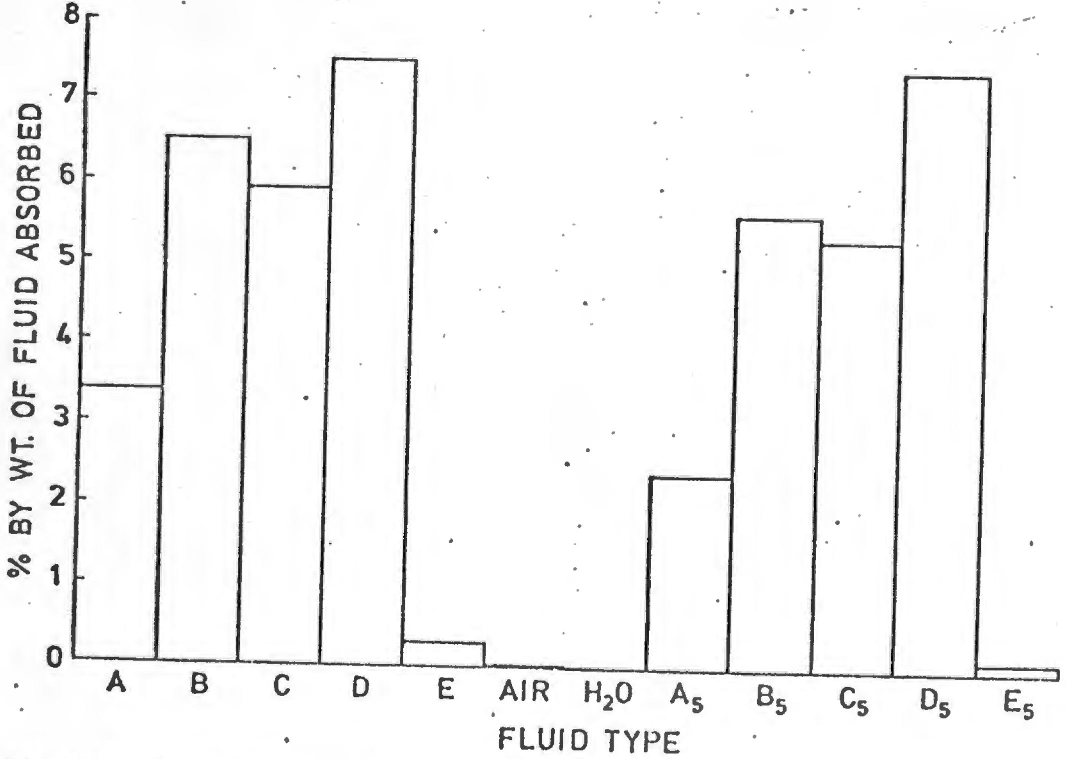

FIG. 4.16 UHMWPE: FLUID ABSORPTION OVER A PERIOD OF 3 WEEKS AT 70°C

4.5.2 Cavitation erosion tests

The erosion curves for polyacetal are given in Figs. 4.17, 4.18 and 4.19 and the 5 hour CVL for both UHMWPE and polyacetal is displayed in Table 4.3, together with losses at maximum number of hours tested. From Table 4.3 it will be noted that the polyacetal samples soaked in the concentrated additives (A - E) showed superior erosion resistance when compared with those samples kept in either air or water. In addition, the samples soaked in the dilute additives (5/95), generally showed a marginally improved erosion resistance (relative to samples stored in air and water).

Repeat tests were performed on a number of polyacetal samples and an error of 8,05% calculated.

In contrast, the UHMWPE samples which were soaked in fluids B, C and D failed 'catastrophically' when eroded. This failure was due to a 'mushrooming' effect (see Fig. 4.20) which caused the specimen to interfere with the tip of the horn.

TABLE 4.3

CUMULATIVE VOLUME LOSSES FOR POLYACETAL AND UHMWPE

Symbol	5hr CVL (mm^3)	Total CVL	Total Time Tested (hrs)
Polyacetal			
A	1,67	2,85	9
B	0,93	1,92	8
C	1,86	3,92	10
D	1,71	2,29	7
E	1,43	4,00	10
Air	2,57	2,57	5
H_2O	2,14	2,14	5
A_5	2,64	4,50	9
B_5	2,07	3,21	8
C_5	2,00	4,00	10
D_5	2,50	2,86	7
E_5	2,57	4,86	9
UHMWPE			
A	0,00	0,60	22
B	CF	-	-
C	CF	-	-
D	CF	-	-
E	0,21	0,63	10
Air	0,21	0,32	10
H_2O	0,21	0,32	10
A_5	0,32	0,85	22
B_5	CF	-	-
C_5	CF	-	-
D_5	CF	-	-
E_5	0,10	0,32	10

CF = catastrophic failure

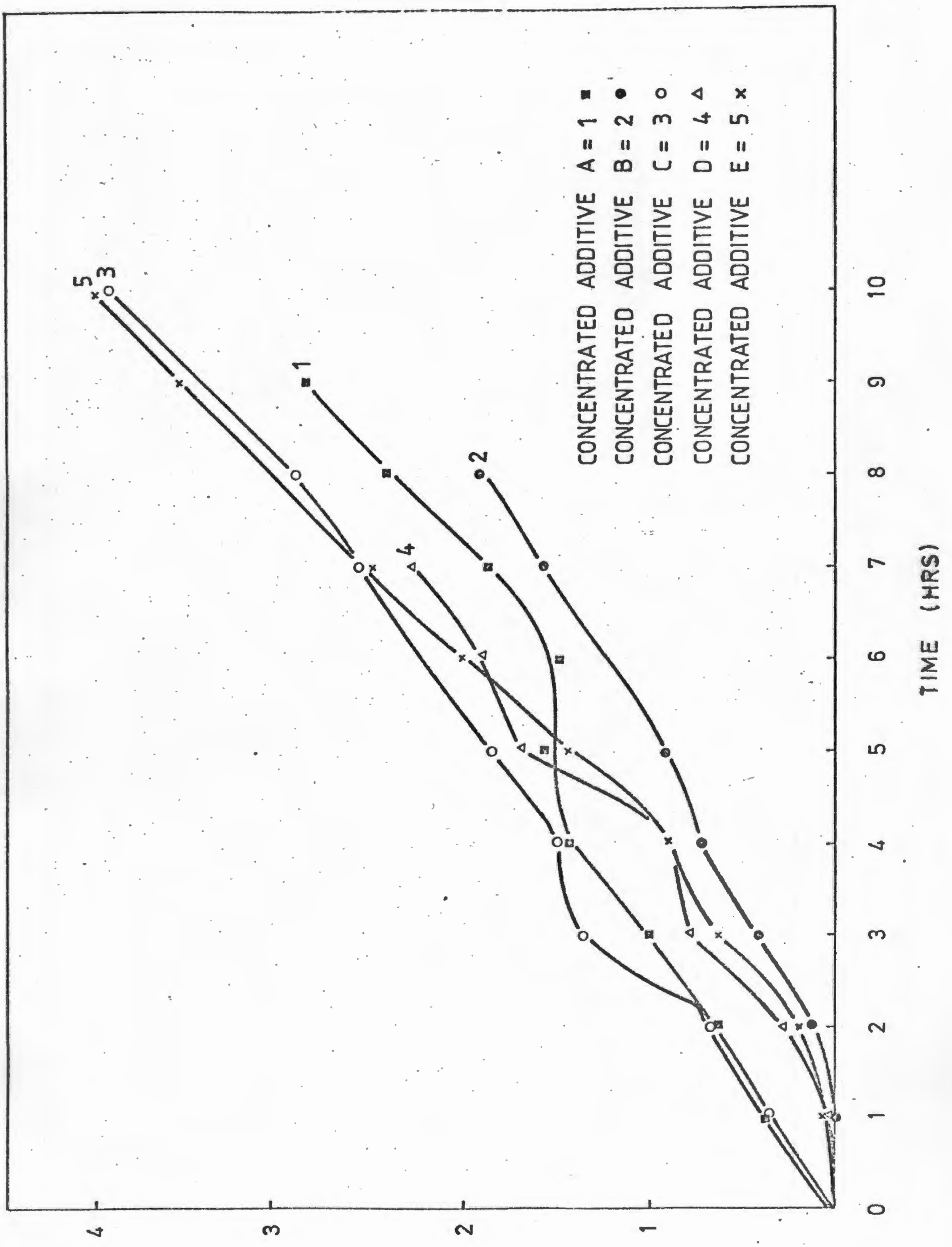

FIG. 4.17

CVL (mm^3) vs time (hrs) for polyacetal which has been previously soaked in a concentrated additive for 3 weeks at 70°C.

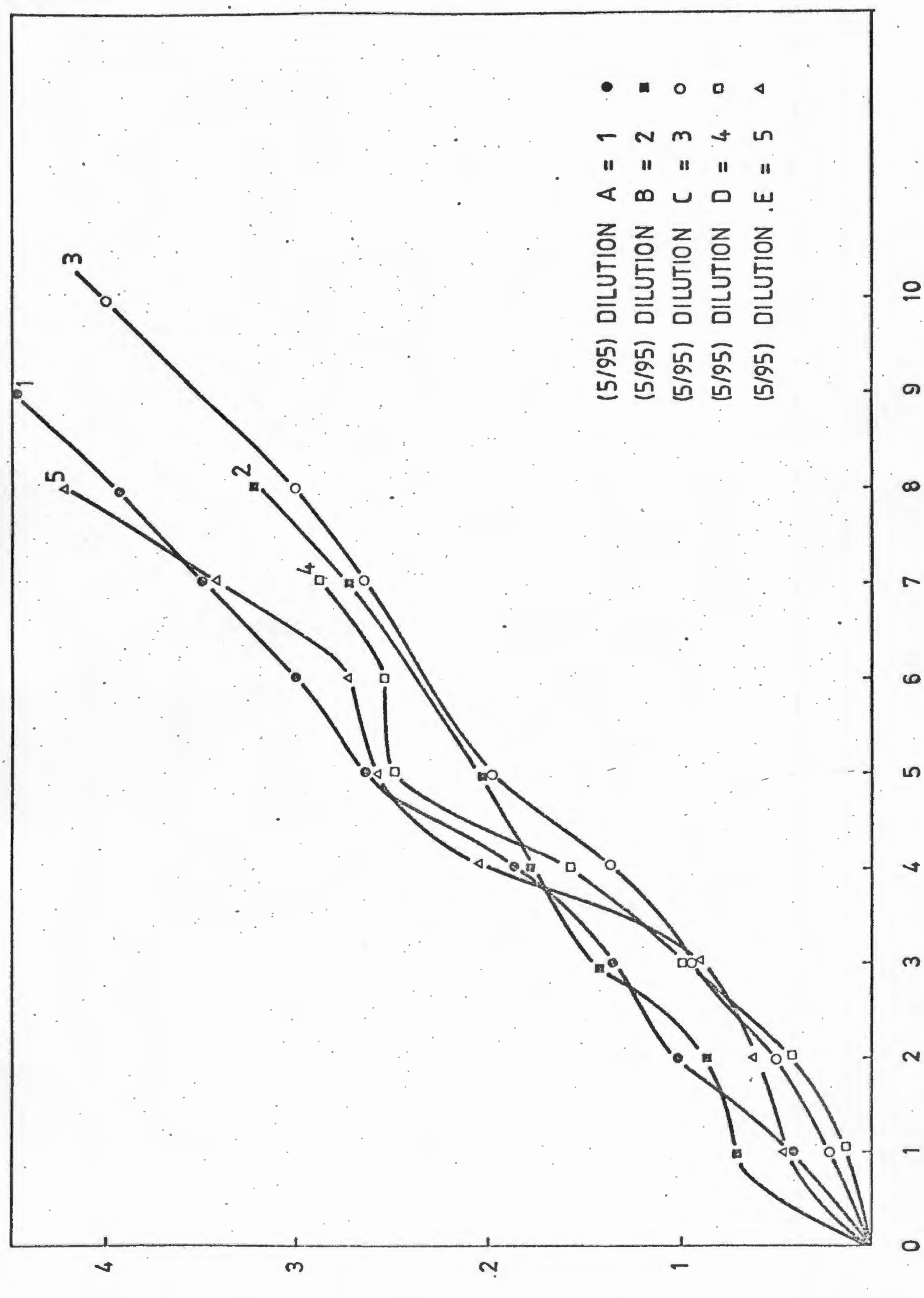

FIG. 4.18

CVL (mm^3) vs time (hrs) for polyacetal which has been soaked in (5/95) dilution for 3 weeks at 70°C.

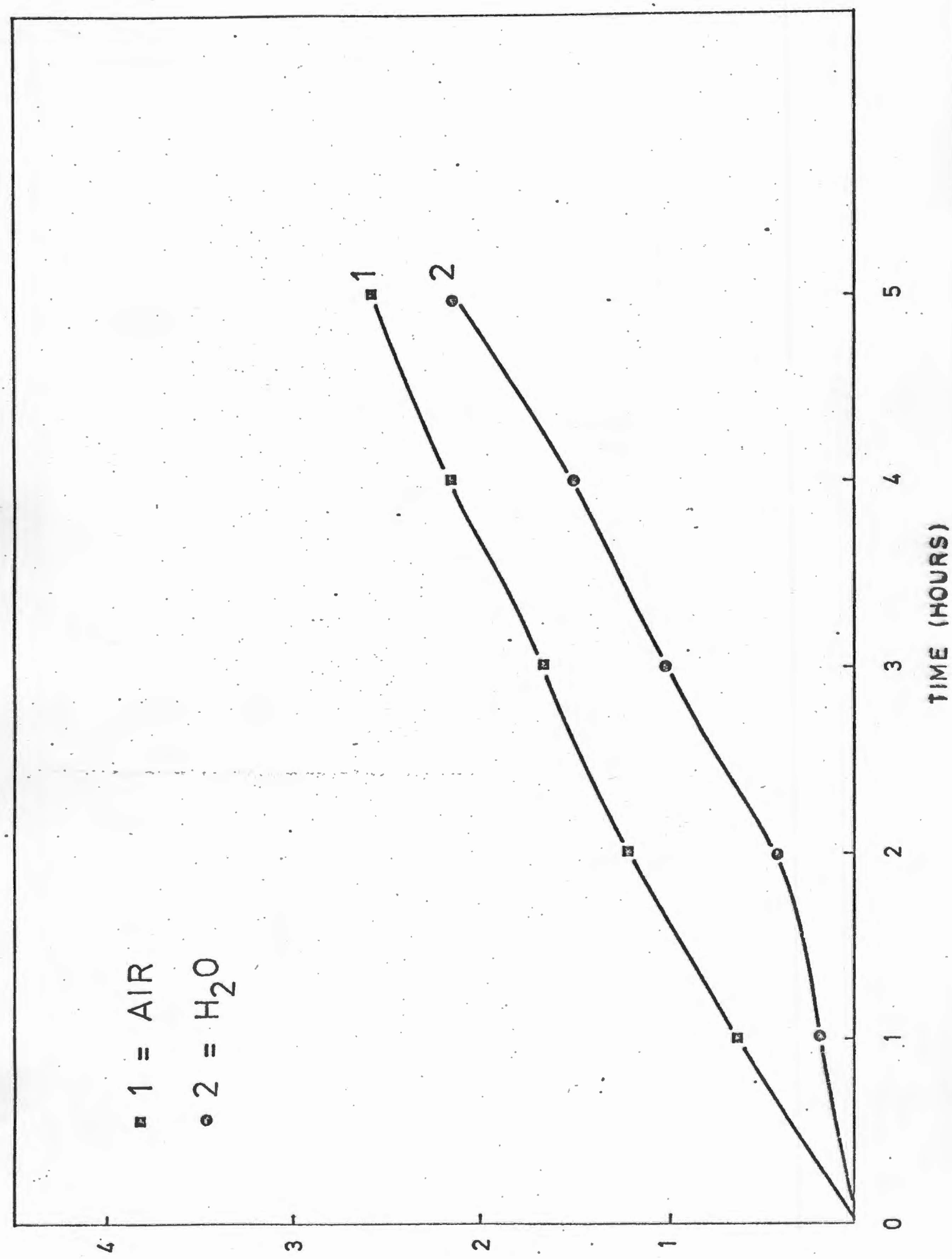

FIG. 4.19

CVL (mm^3) vs time (hrs) for polyacetal which has previously been stored in air and water at 70° C for 3 weeks.

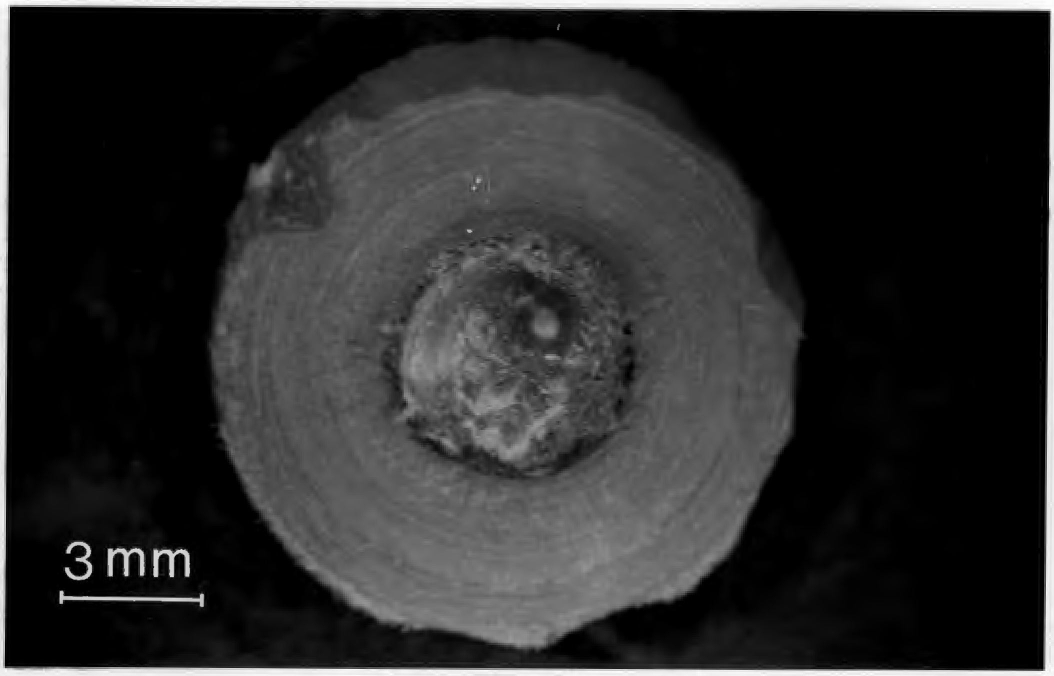

FIG. 4.20 Optical micrograph of UHMWPE eroded for 5 seconds under standard conditions. Sample had been soaked in concentrated form of fluid B for 3 weeks at 70°C prior to erosion. Note that fracture of the polymer occurs by plastic flow.

4.5.3 Scanning electron microscopy

Scanning electron microscopy has been performed on the eroded surfaces of polymers in order to ascertain if the mode of erosion altered as a result of immersion, and typical micrographs are shown in Figs. 4.21 to 4.27.

From the micrographs presented in Figs. 4.21 to 4.25 it appears that the eroded surfaces of polymers which were immersed in additives A - E (3 weeks at 70°C) showed increased ductility when contrasted with those stored in air and water for the same period of time, at 70°C.

This increased ductility, characterised by a greater proportion of free fibril ends (evident from the fracture surfaces), could account for the improved erosion resistance.

SCANNING ELECTRON MICROGRAPHS OF THE ERODED SURFACES OF POLYACETAL SOAKED IN OILS A - E (FOR 3 WEEKS AT 70°C) PRIOR TO EROSION

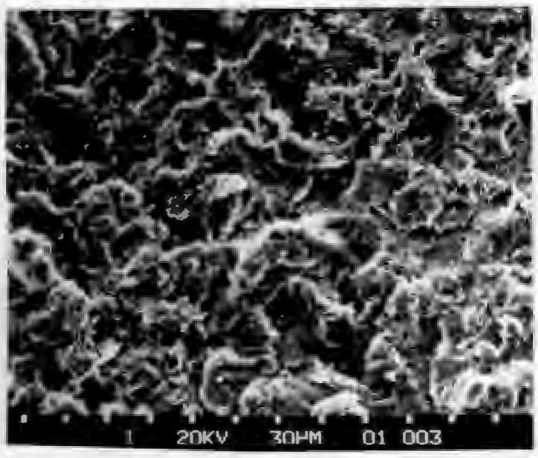

FIG. 4.21

Eroded surface of Polyacetal soaked in concentrated additive A (3 weeks at 70°C) prior to erosion.

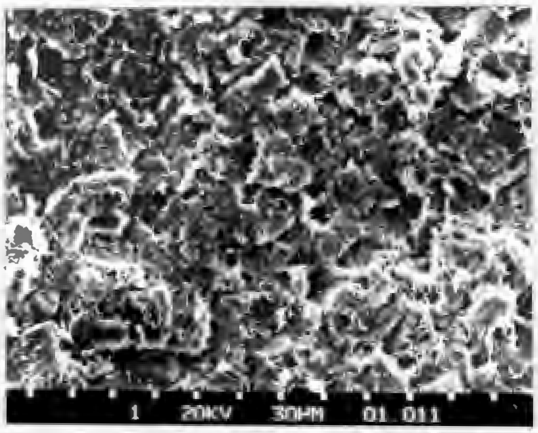

FIG. 4.22

Eroded surface of Polyacetal soaked in concentrated addtive B (3 weeks at 70°C) prior to erosion.

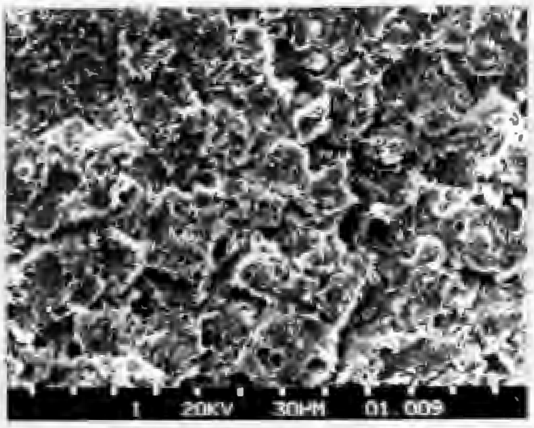

FIG. 4.23

Eroded surface of Polyacetal soaked in concentrated additive C (3 weeks at 70°C) prior to erosion.

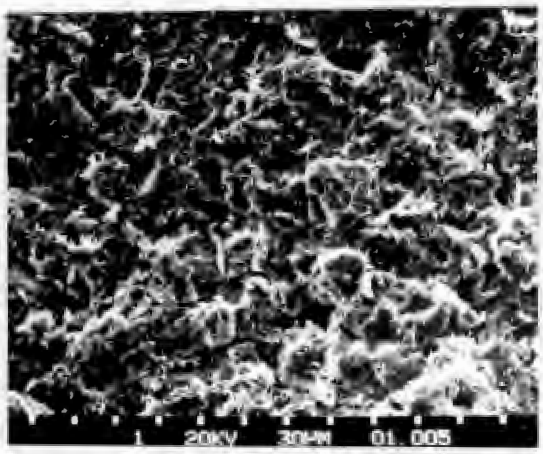

FIG. 4.24

Eroded surface of Polyacetal soaked in concentrated additive D (3 weeks at 70°C) prior to erosion.

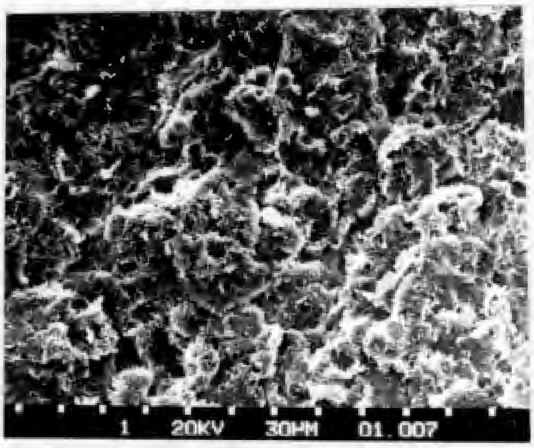

FIG. 4.25 Eroded surface of Polyacetal soaked in concentrated additive E (3 weeks at 70°C) prior to erosion.

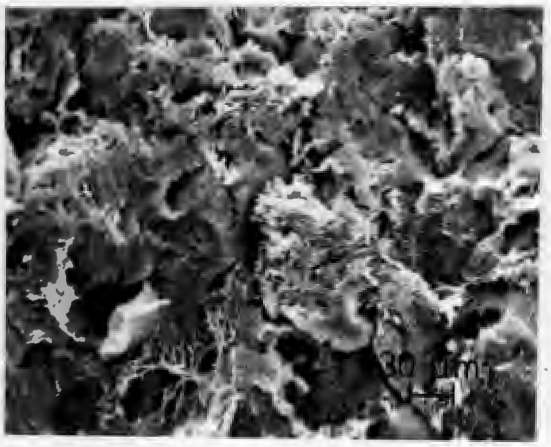

FIG. 4.26

Eroded surface of Polyacetal soaked in water (3 weeks at 70°C) prior to erosion.

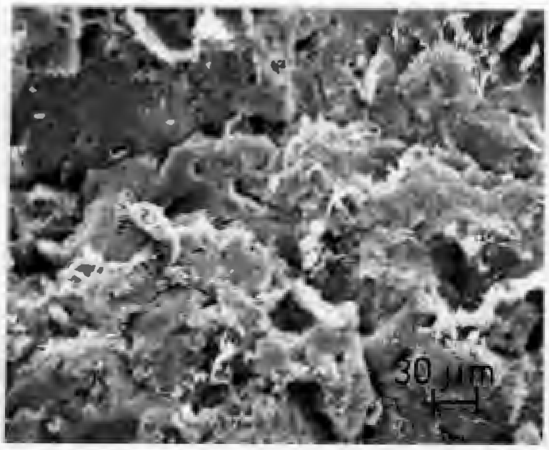

FIG. 4.27

Eroded surface of Polyacetal kept in air (3 weeks at 70°C) prior to erosion.

CHAPTER 5: RESULTS OF COATED AND SURFACE TREATED MATERIALS

5.1 ELECTROLESS NICKEL PLATING

5.1.1 Effect of varying the coating thickness

The results of the erosion tests performed on En24 samples which had been quenched and tempered at 600°C and then coated with electroless nickel to various thicknesses, are shown in Figs. 5.1 and 5.2.

An electroless nickel coating thicker than 15 m improves the erosion performance, relative to an uncoated substrate. A coating of 100 m electroless nickel has similar erosion performances to that of a 25 m thick coating. However, below 15μm the coating is removed by 'spalling' (Fig. 5.14), and the rate of volume loss for a 10μm thick coating is extremely high during the first few seconds of erosion.

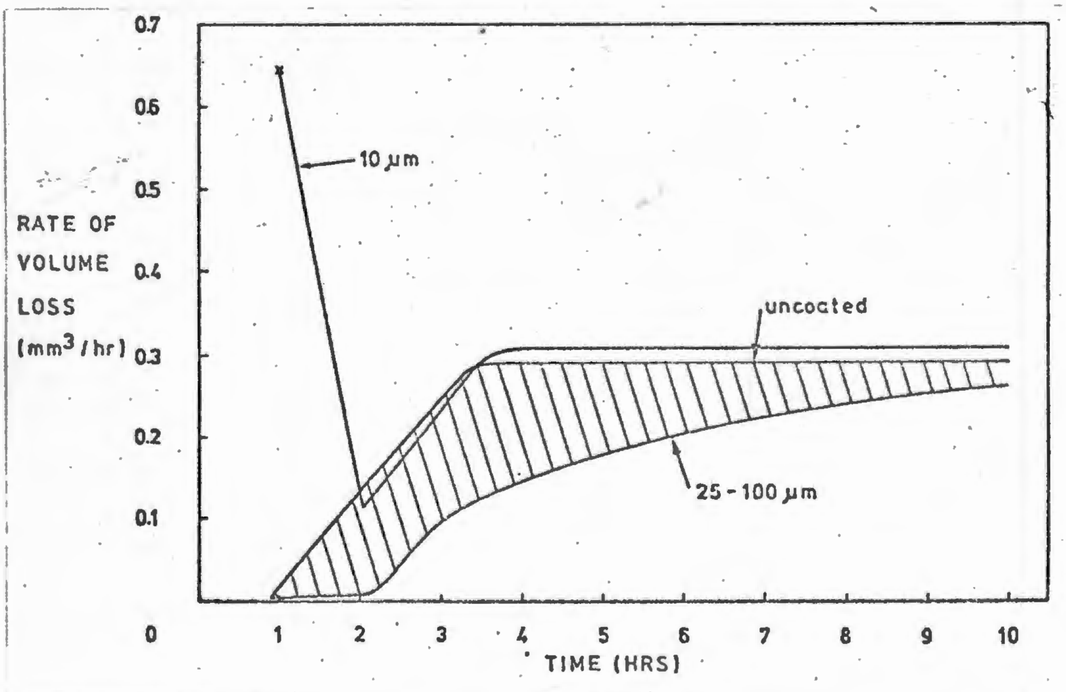

FIG. 5.1 General effects of varying coating thickness on the erosion performance of electroless nickel coated En24 (Q & T 600°C)

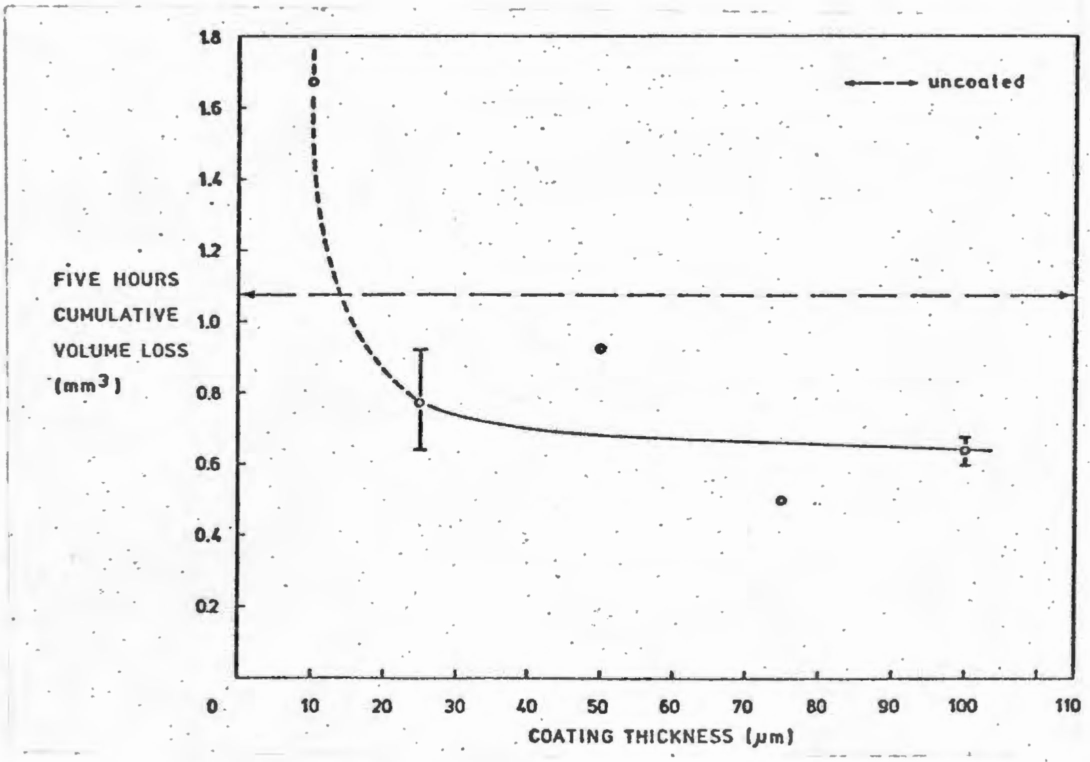

FIG. 5.2 Five hour cumulative volume loss for electroless nickel coatings of varying thickness (10 μm to 100 μm). Erosion performance is measured relative to uncoated En24 (Q & T 600°C)

5.1.2 Effect of post coating heat treatment

5.1.2.1 Erosion tests

Samples of En24 in the Q & T (600°C) condition were coated with electroless nickel to a thickness of 25μm and then heat treated (post heat treated - PHT) at temperatures in the range 200° to 600°C for 3 hours. These samples were then subjected to the standard erosion test discussed in Section 2.3. The results are shown in Fig. 5.4. A PHT of 200°C has no beneficial effect on the erosion resistance and the coating is 'stripped off' during the first hour of cavitation. However, PHT above 200°C improves the erosion resistance relative to the uncoated base metal (En24), for periods up to 10 hours.

A plot of the five hours cumulative volume loss vs post heat treatment temperature is shown in Fig. 5.3. A PHT of 400°C results in optimum erosion resistance with similar erosion performances attributed to the 500° and 600°C PHT samples.

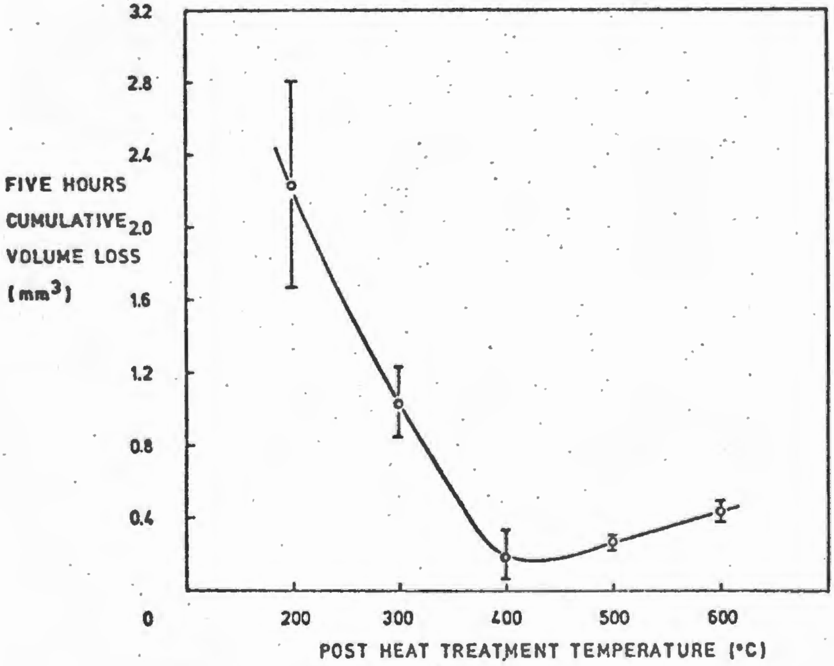

FIG. 5.3 Effect of PHT on the 5 hour CVL of a 25μm thick coating of electroless nickel.
Base metal: En24 (Q & T 600°C)

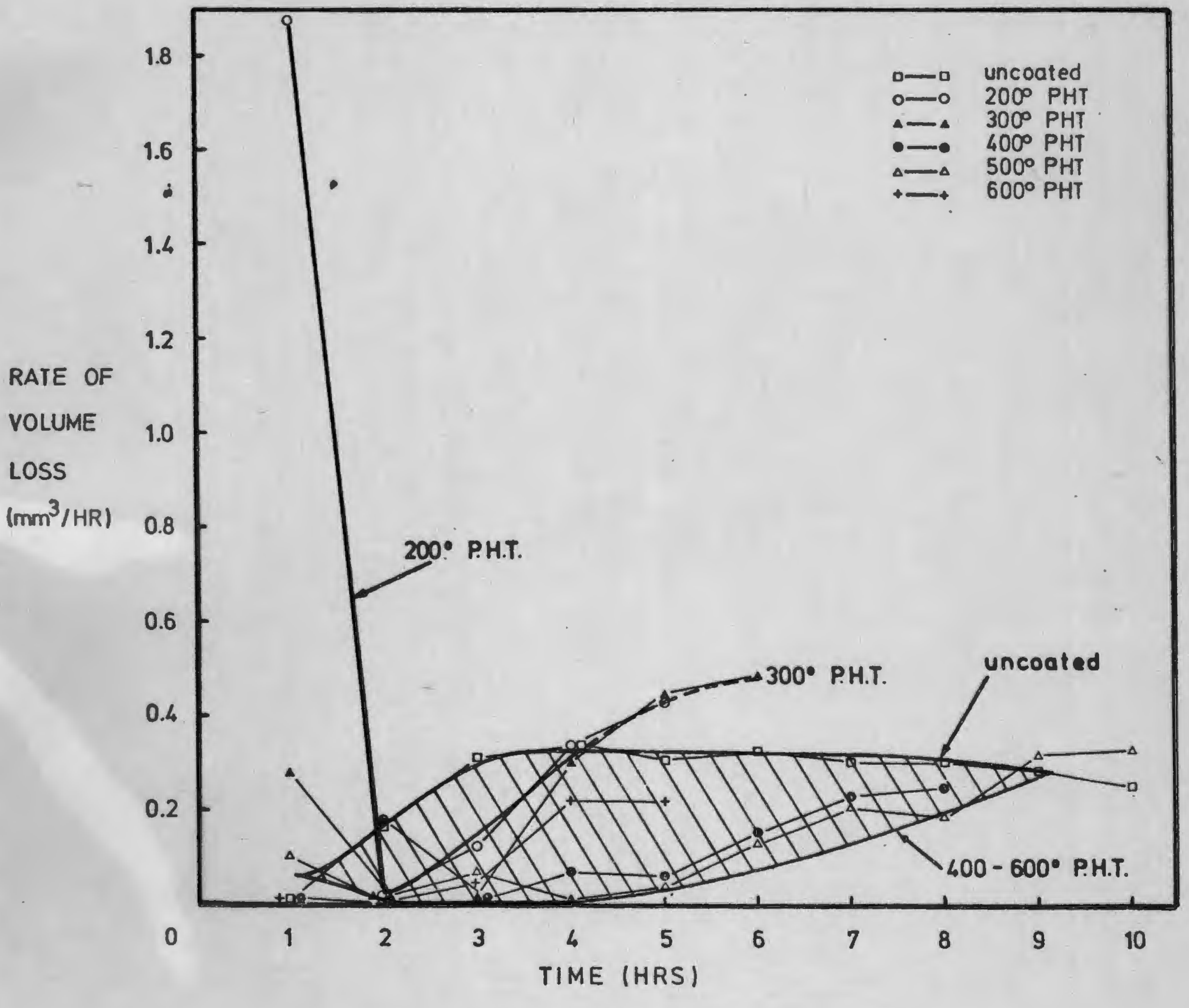

Fig. 5.4 Effect of P.H.T. on the rate of value loss vs. time for a 25μm thick electroless nickel coating. Base metal: (Q & T 600°C).

5.1.2.2 Microhardness measurements

As shown in Fig. 5.5 hardnesses as high as 1000 to 1100 MHN_{20} can be produced by the post heat treatment. Hardening of electroless nickel is due primarily to the formation of nickel phosphide particles within the alloy. Even though a decrease in hardness occurs above 400°C the erosion performances (Fig. 5.3) for specimens treated at 500°C and 600°C are very similar. This suggests an improved adhesion of coating to substrate after elevated temperature treatments.

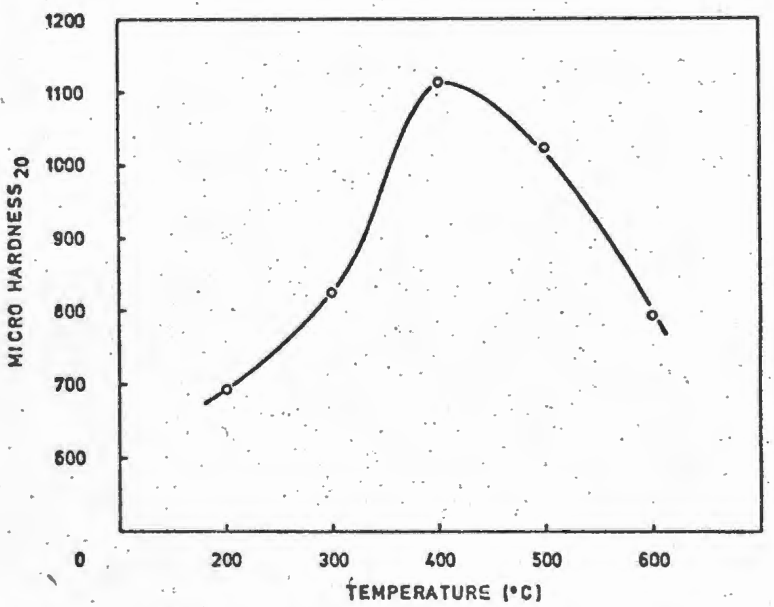

FIG. 5.5 Effect of post application heat treatment on the hardness of electroless nickel.
Base metal: En24 (Q & T 600°C)

5.1.2.3 Coating - substrate interdiffusion

A Ni-Fe interdiffusion layer was observed by optical microscopy for an electroless nickel sample which had received a 600°C PHT for 3 hours. An Energy Dispersive X-ray Analysis technique confirmed that the interdiffusion layer, which was optically observed, was indeed Ni-Fe. The results of this spot analysis are presented in Fig. 5.6. The Ni-Fe interdiffusion layer was not observed optically in a specimen which had received a 500°C PHT for 3 hours (Fig. 5.7). Identical specimen preparation and etching techniques were employed in both cases.

5.1.2.4 X-ray diffraction (XRD) analysis

The XRD spectra for coatings which received heat treatments ranging from 200° - 600°C are shown in Figs. 5.8 to 5.12. The d-spacings obtained are comparable to the theoretical d-spacings for $(FeNi)_3P$ (Table 5.1), which confirms the presence of Ni_3P for PHT's above 200°C. All XRD analysis was performed after erosion and areas of substrate were exposed. This accounts for the Fe peak seen in Fig. 5.8, even though electroless nickel is totally amorphous (and contains no Fe) at 200°C. A linear relationship between intensity (cps) and PHT (Fig. 5.13) suggests that at 600°C crystallisation is not totally complete. This will be fully discussed in Chapter 7.

5.1.2.5 Scanning electron microscopy (SEM)

Two major mechanisms of coating removal are displayed in Fig. 5.14 and 5.15. They are:

1. spalling
2. erosion of the coating by removal of brittle cleavage facets.

EN 24 Q & T 600°C - ELECTROLESS NICKEL (25µm)

600° P.H.T. (3 hrs.). Spot analysis displaying Ni-Fe diffusion layer.

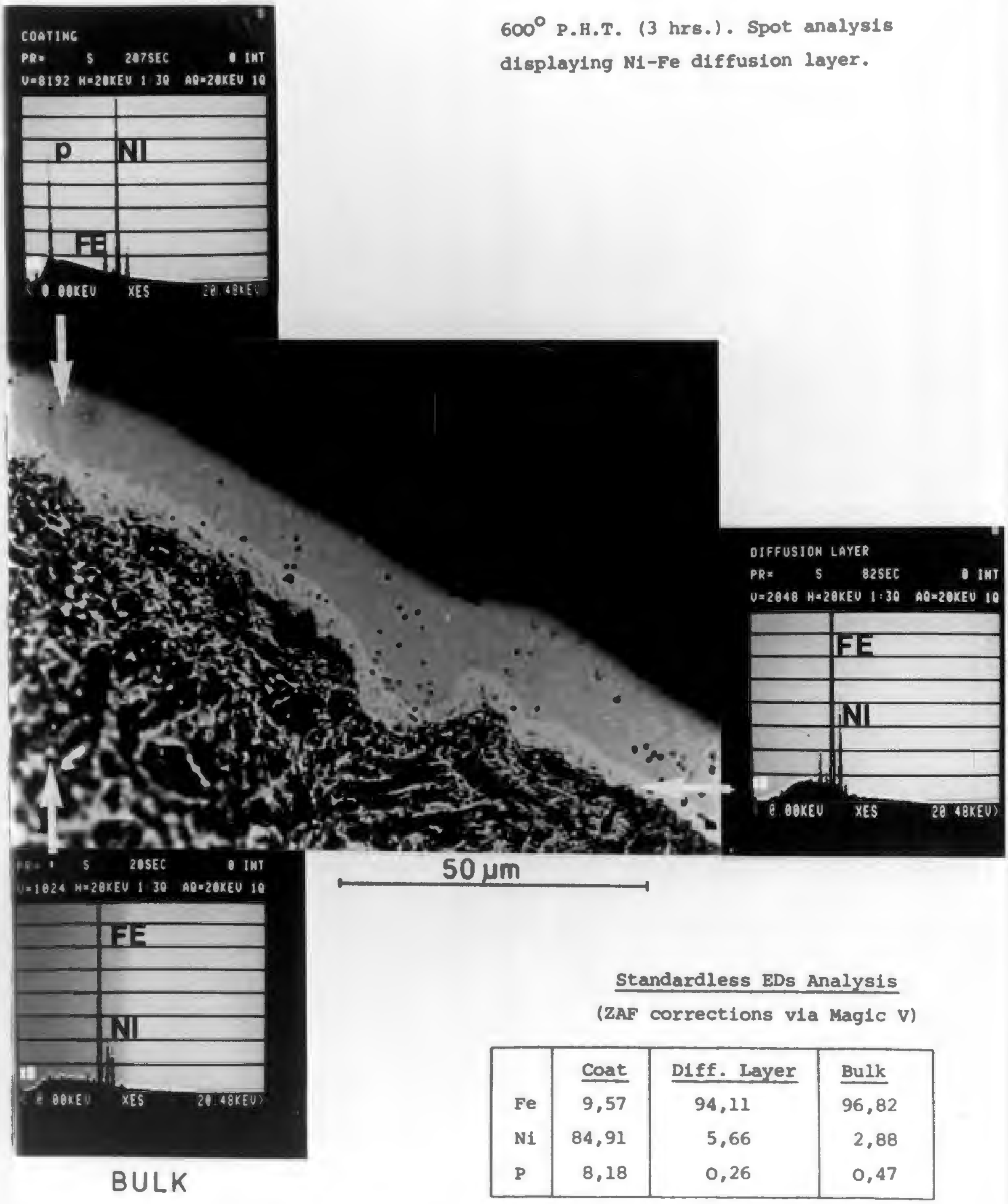

Standardless EDs Analysis
(ZAF corrections via Magic V)

	Coat	Diff. Layer	Bulk
Fe	9,57	94,11	96,82
Ni	84,91	5,66	2,88
P	8,18	0,26	0,47

FIG. 5.6 Spot analysis traces for an electroless nickel coating (25µm) which had received a 600°C PHT for 3 hours.

FIG. 5.7 Optical micrograph showing no sign of Ni-Fe interdiffusion layer for an electroless nickel coating (25µm) which had received a 500°C PHT for 3 hours.
Base metal: En24 (Q & T 600°C)

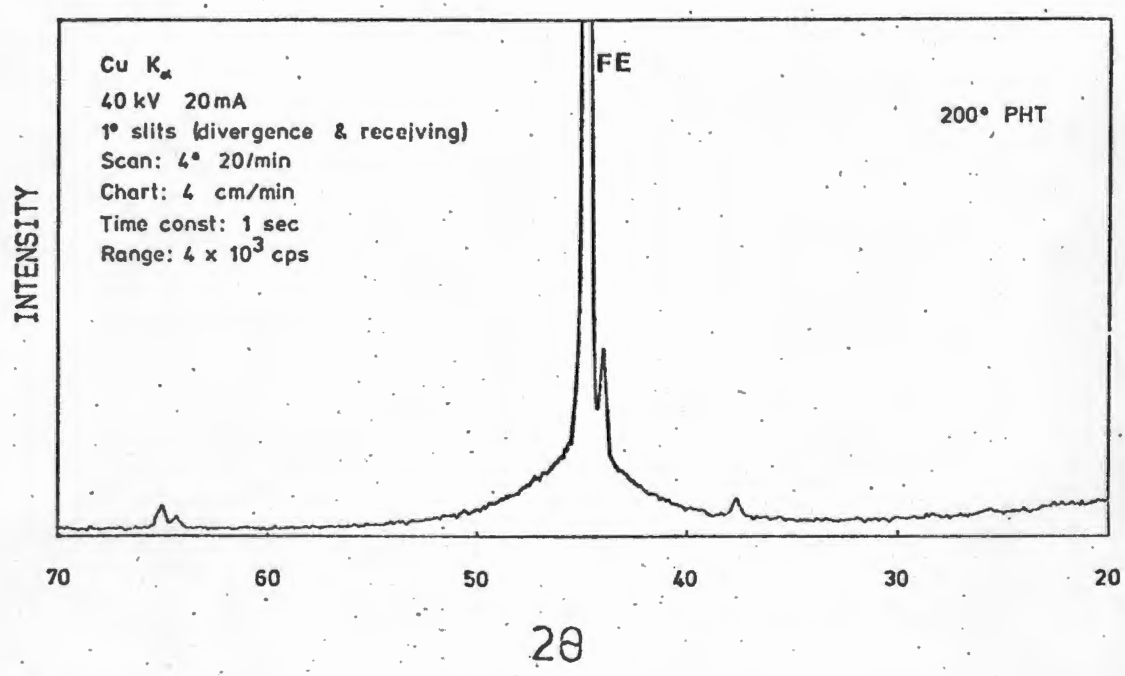

FIG. 5.8 XRD trace of an electroless nickel coating which received a 200°C post application heat treatment. Structure is totally amorphous and presence of the Fe peak is due to an area of exposed substrate.

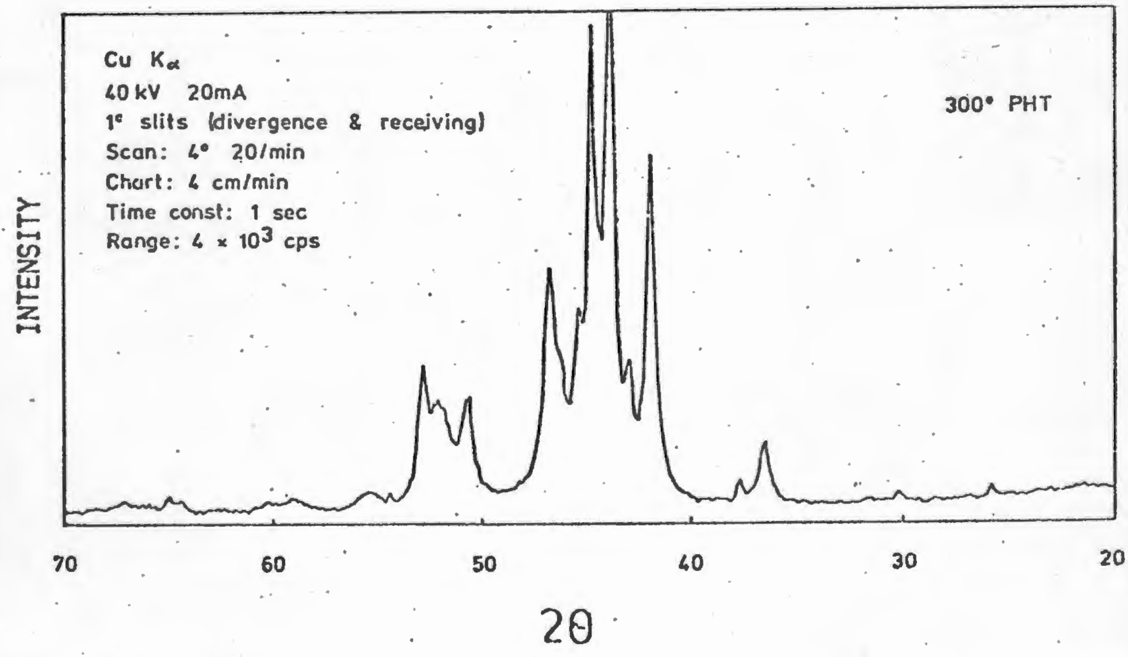

FIG. 5.9 XRD trace of an electroless nickel coating which received a 300°C post application heat treatment.

TABLE 5.1 D-SPACINGS FOR $(Fe\ Ni)_3P$

$2\ \theta$	Peak Intensity	d-spacing obtained	d-spacing quoted
36,6	S	2,50	2,45
42,0	VS	2,19	2,15
43,1	S	2,13	2,10
43,7	VVS	2,11	2,07
46,8	VS	1,97	1,94
50,8	M	1,83	1,80
52,2	MS	1,77	1,75
53,0	S	1,76	1,73

Good match between theoretical d-spacings of $(FeNi)_3P$ and those obtained for Ni_3P.

S : strong

VS : very strong

VVS : very very strong

M : medium

MS : medium strong

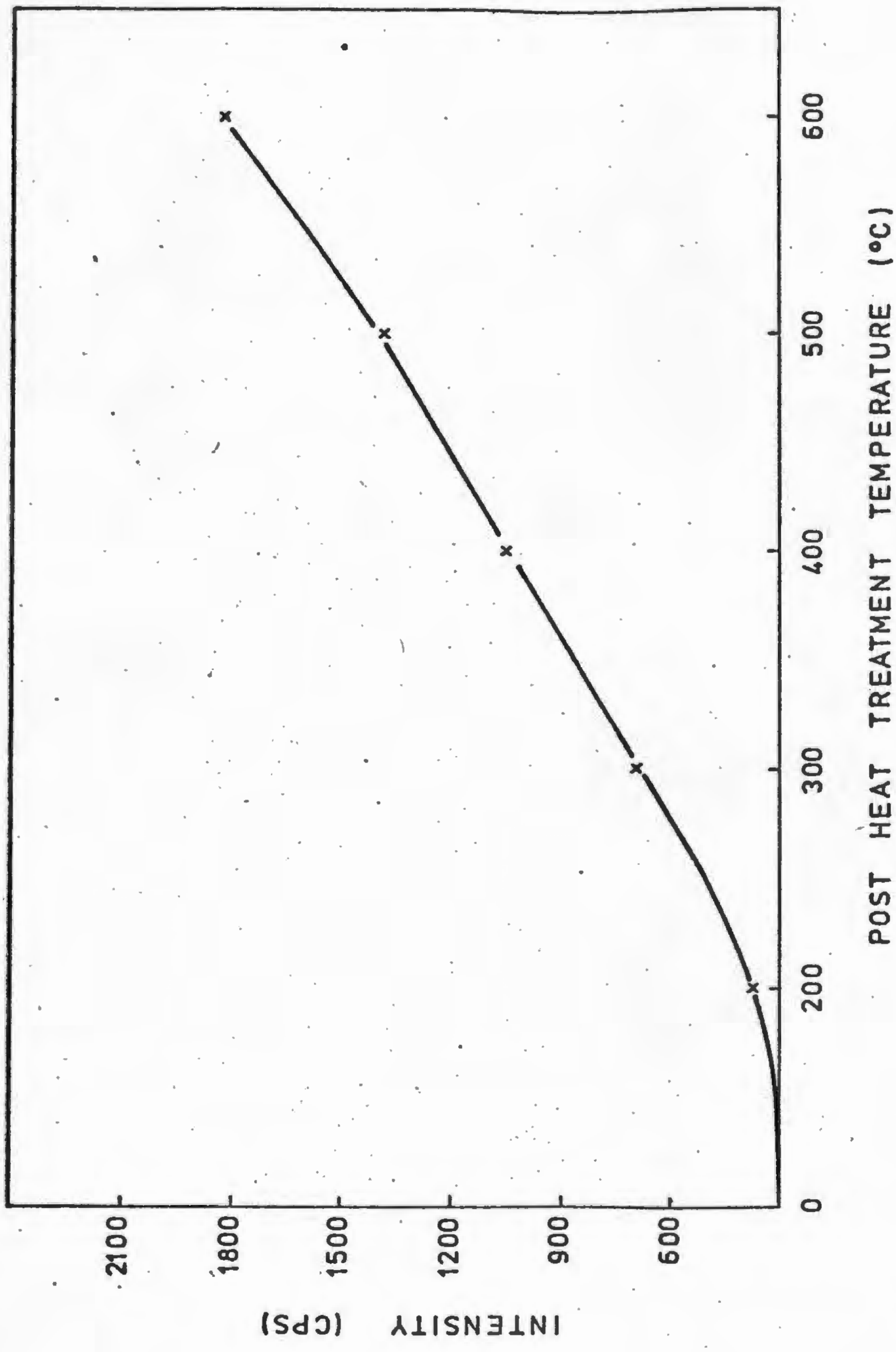

3hrs

FIG. 5.13 XRD peak intensity ($2\theta = 36°$) as a function of post heat treatment temperature, for nickel phospide.

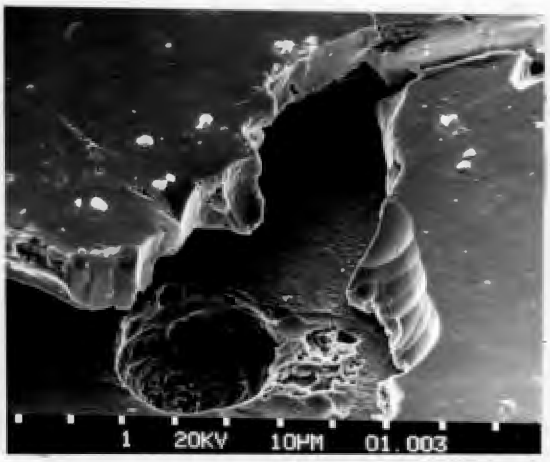

FIG. 5.14 SEM micrograph showing removal of 25μm electroless nickel (200°C PHT for 3 hours) by 'spalling' and brittle cracking.

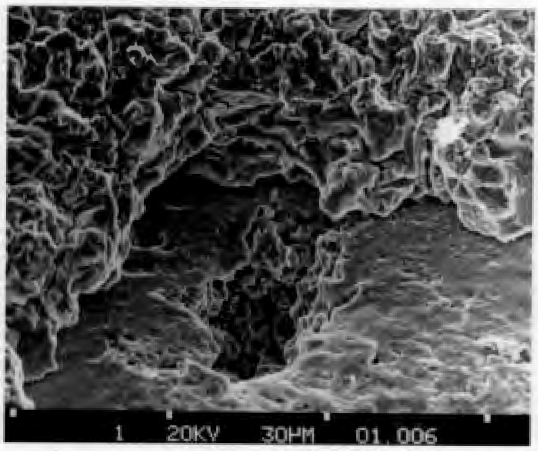

FIG. 5.15 Erosion of 75μm thick electroless nickel coating exposing En24 substrate. Micrograph shows evidence of brittle cleavage facets.

5.2 CHEMICALLY VAPOUR DEPOSITED COATINGS (CVD)

It will be shown in this section that the CVD coatings do not provide any improvement in erosion resistance, relative to the uncoated substrate.

5.2.1 Tungsten and Titanium carbide coatings on En24

The erosion performance of the tungsten and titanium carbide coated En24 samples is shown in Fig. 5A (page 95). The titanium carbide (TiC) coatings showed poor adhesion to the En24 substrate (see Fig. 5.16) and this is reflected in the erosion profile presented in Fig. 5A. The coating is removed by spalling, during the first hour of erosion, accounting for the high initial rate of volume loss. This large scale coating removal causes localised erosion of the substrate, and this is shown in Fig. 5.18. In addition, an edge-on view of the coating-substrate interface is presented in Fig. 5.17.

In contrast, the W_2C coating showed superior adhesion (Fig. 5.19) and evidence of the shot blasting treatment, prior to coating, is clearly visible. A micrograph of the coating-substrate interface is shown in Fig. 5.20. From Fig. 5.20 and Fig. 5.21 it appears that material loss occurs by brittle 'chip' removal and preferential erosion of the substrate can aid large scale coating removal (Fig. 5.21).

5.2.2 W_2C and TiC on grey cast iron

The erosion performance of the TiC coated and W_2C coated grey cast iron is shown in Fig. 5B (page 98). From this graph it is clear that the TiC coatings showed extremely poor erosion resistance, relative to the uncoated substrate.

These coatings showed poor adhesion to the substrate (Fig. 5.22) and large scale material removal occurred. This is clearly displayed in Fig. 5.24. From this micrograph it can also be noted that once the coating is removed, preferential erosion of the hard graphite occurs. A micrograph (Fig. 5.23) of the coating substrate interface demonstrates the poor adhesion.

Once again, the W_2C coatings showed superior adhesion to the substrate (Fig. 5.25) and coating loss does not occur by spalling but by brittle 'chip' removal (Fig. 5.26 and Fig. 5.27).

5.2.3 W_2C and TiC on nodular cast iron

From Fig. 5C (page 101) it is clear that the TiC coatings showed extremely poor erosion resistance. In addition, coating with W_2C does not provide improved resistance, relative to uncoated nodular cast iron.

An interesting feature of the W_2C and TiC coatings is the preferential removal of the spheroidal graphite from the softer matrix, once areas of the coating are removed (see Fig. 5.28 and Fig. 5.31). Scanning electron micrographs of the eroded surfaces (Figs. 5.29 - 5.32) clearly demonstrate the preferred graphite removal. Once these graphite spheres are extracted (Fig. 5.33) large scale coating removal is encouraged.

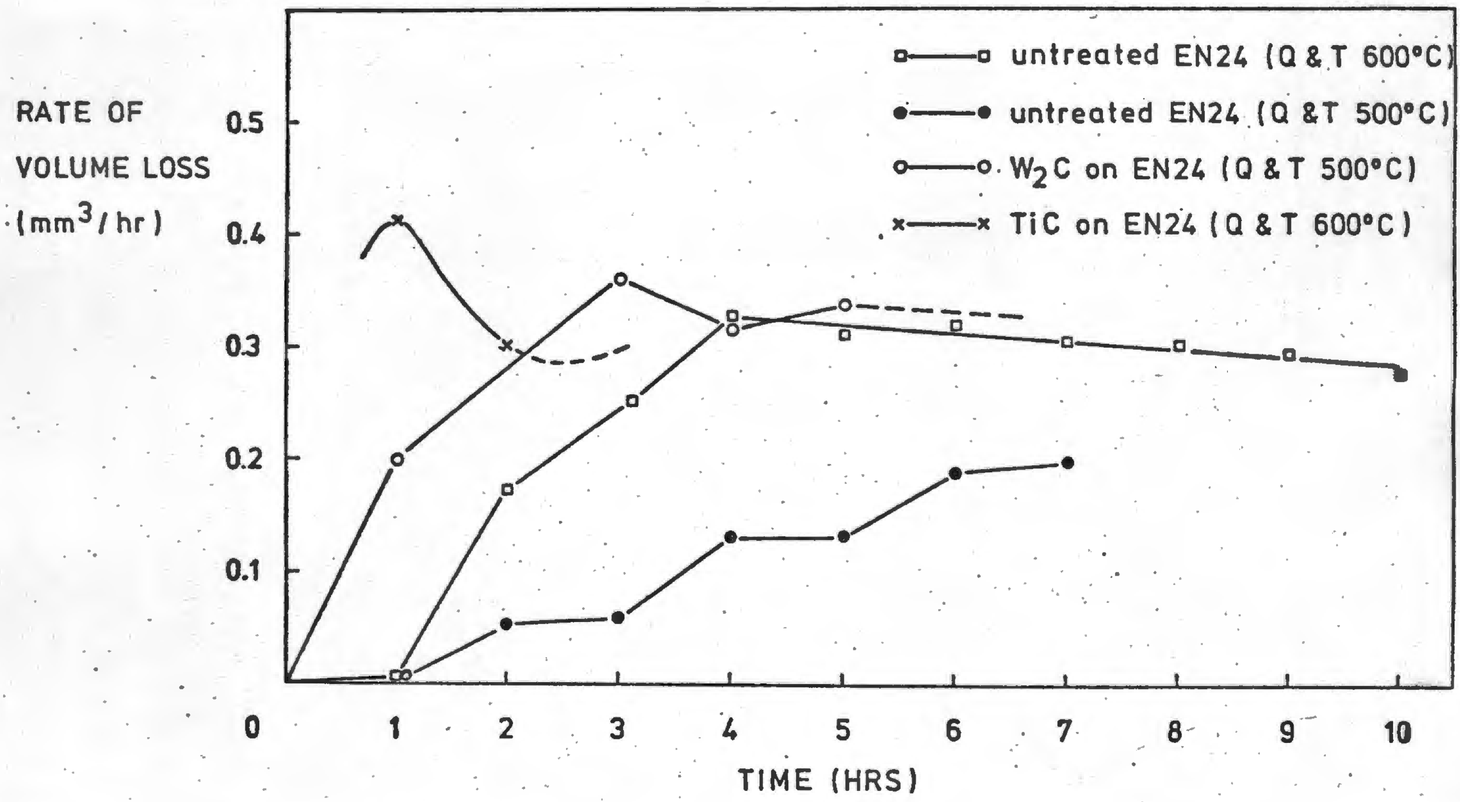

FIG. 5A Rate of volume loss as a function of time for W_2C and TiC coated En24.

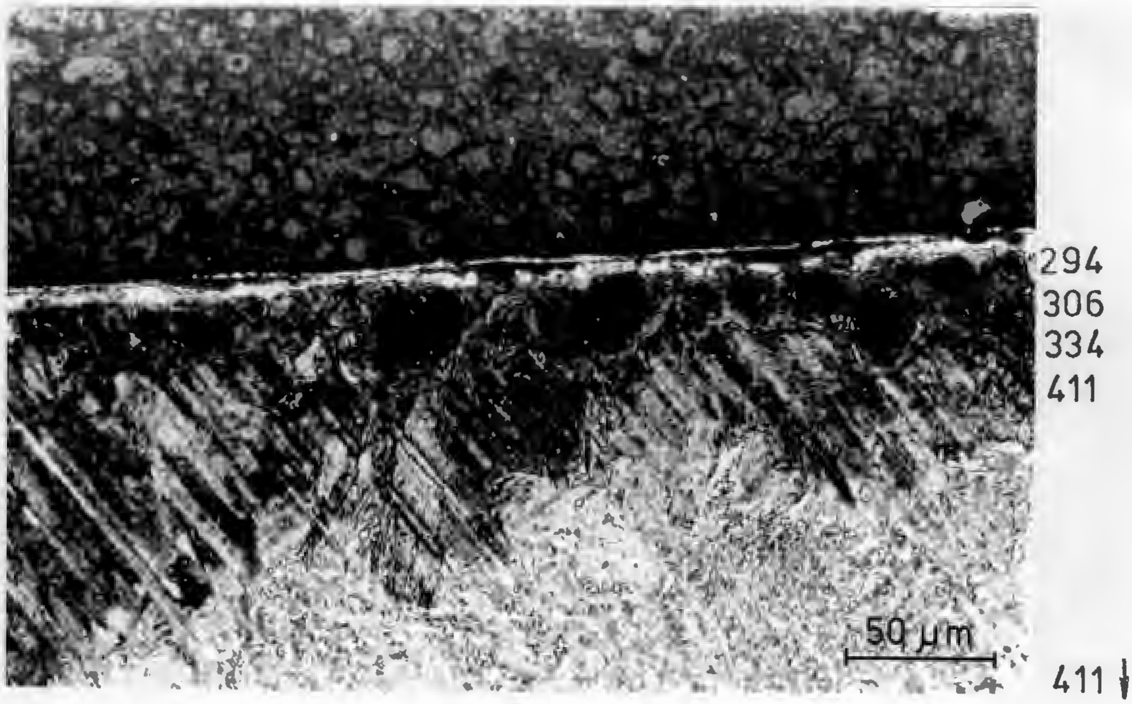

FIG. 5.16 Titanium carbide (TiC) coating on En24 (Q & T 600°C). Note double nature of applied coating. Micrograph is taken some distance away from the site of erosion.

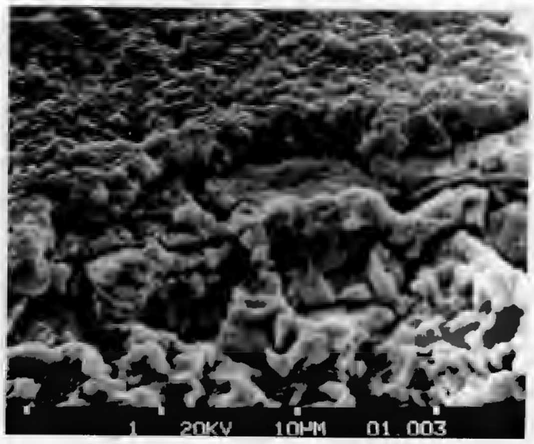

FIG. 5.17
Edge-on view of coat and substrate

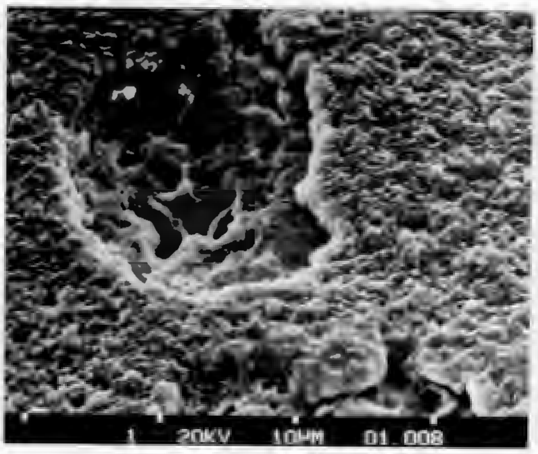

FIG. 5.18
Localised erosion initiated at site of coating removal.

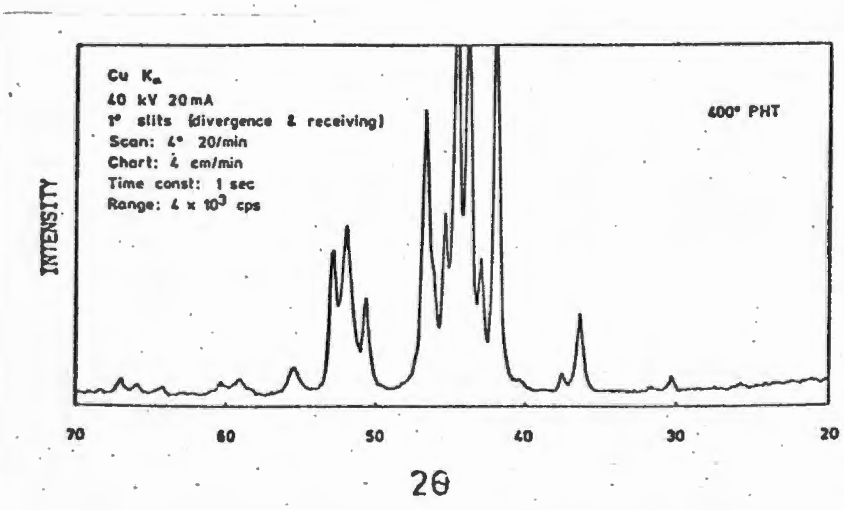

FIG. 5.10 XRD trace of an electroless nickel coating which received a 400°C post application heat treatment.

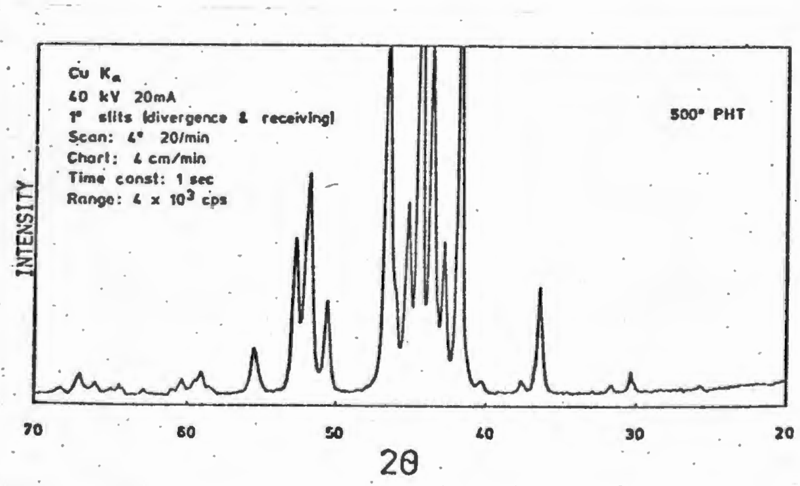

FIG. 5.11 XRD trace of an electroless nickel coating which received a 500°C post application heat treatment.

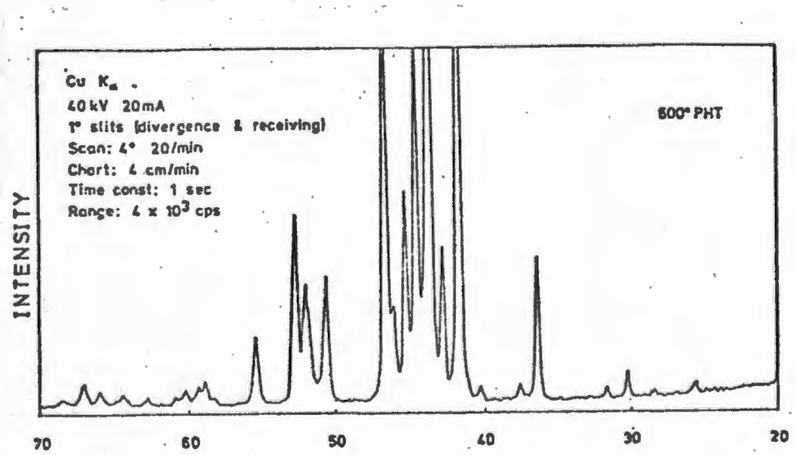

FIG. 5.12 XRD trace of an elctroless nickel coating which received a 600°C post application heat treatment.

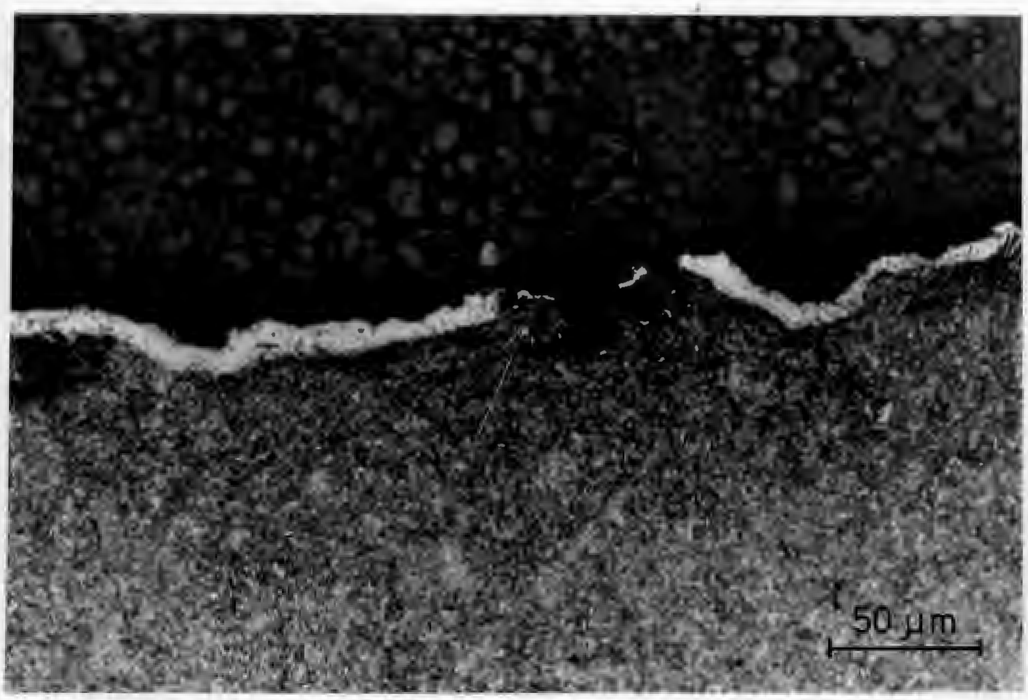

1819
374
341
334

334

FIG. 5.19 Photomicrograph of tungsten carbide (W_2C) on En24 (Q & T 500°C). Note the unevenness of the surface finish with respect to the TiC application.

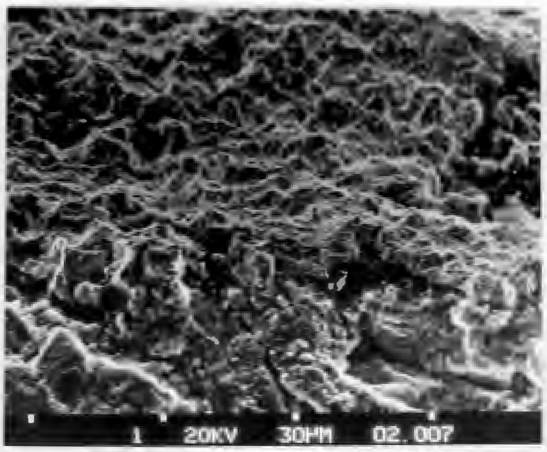

FIG. 5.20
Edge-on view of coating and substrate. Apparent brittle nature and 'chip' removal of coat evident.

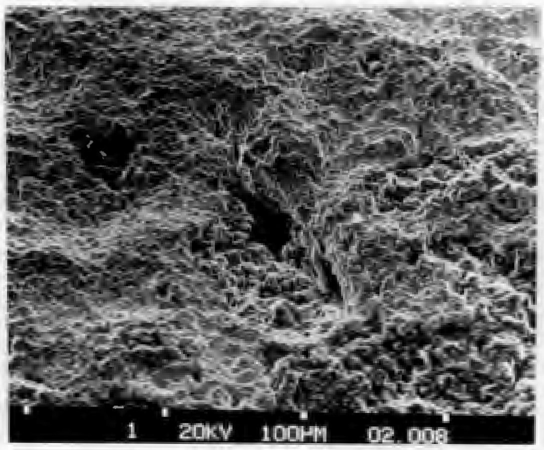

FIG. 5.21
Erosion of substrate causing undercut of the surface which results in large scale material removal.

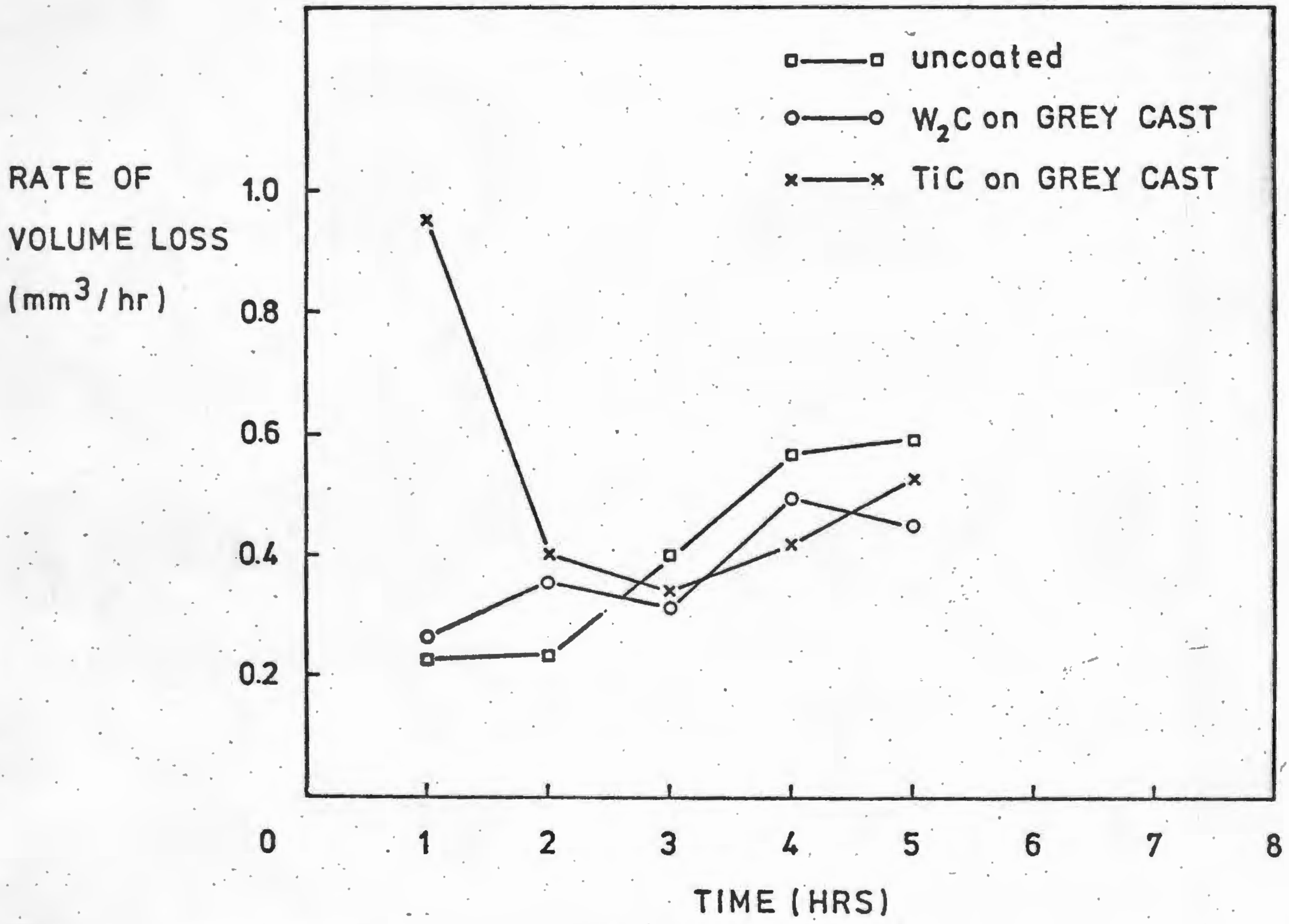

FIG. 5B Rate of volume loss as a function of time for W_2C and TiC coated grey cast iron.

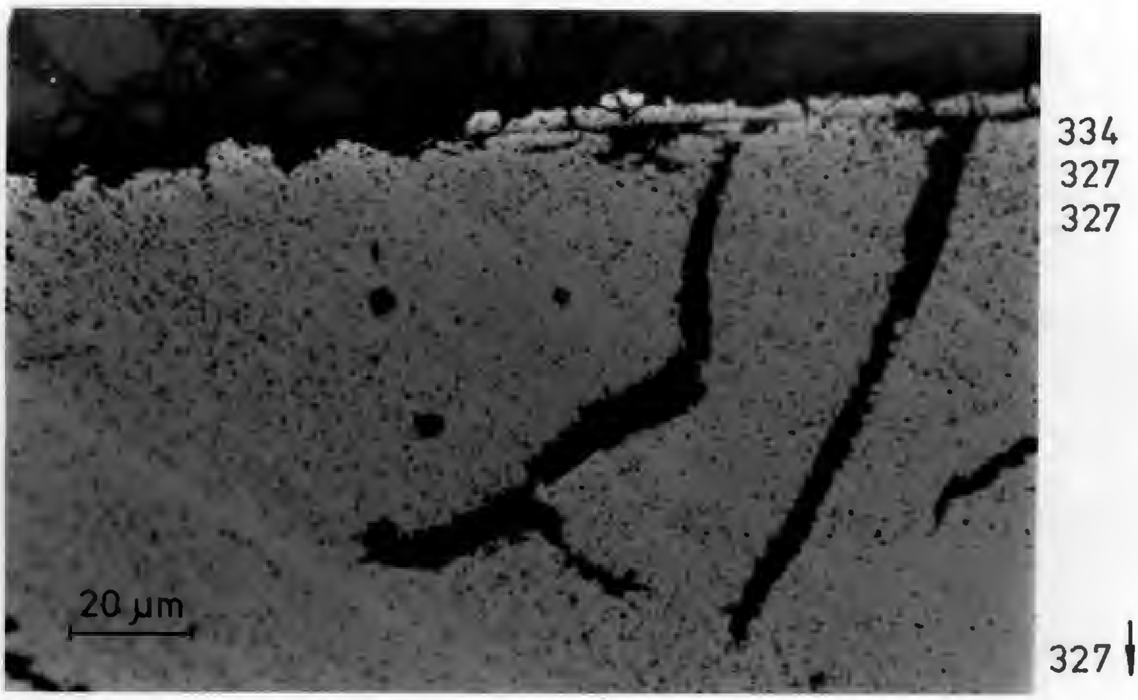

FIG. 5.22 TiC on grey cast iron. Coating adhesion appears to be poor relative to the TiC on En24.

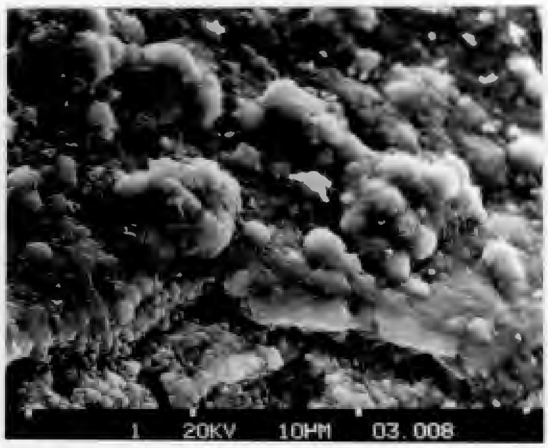

FIG. 5.23
Edge-on view of coating and substrate. Coating appears to be stripped off by removal of nodules.

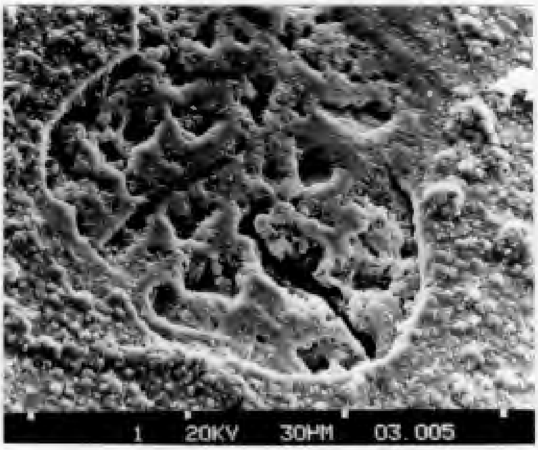

FIG. 5.24
Large scale coating removal exposing grey cast iron substrate.

FIG. 5.25 W_2C on grey cast iron. Once again note the irregulrity of surface finish when applying the W_2C coat.

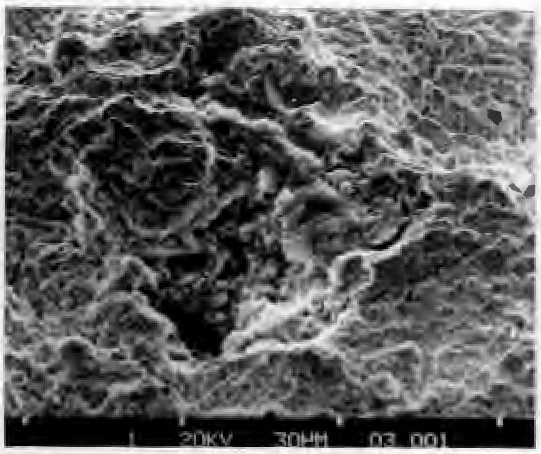

FIG. 5.26
Brittle nature of coating removal is evident from the above micrograph.

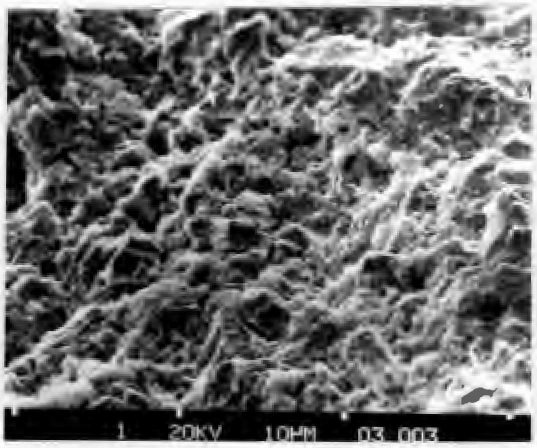

FIG. 5.27
Micrograph of coated surface. Note material loss occurs by brittle 'chip' removal.

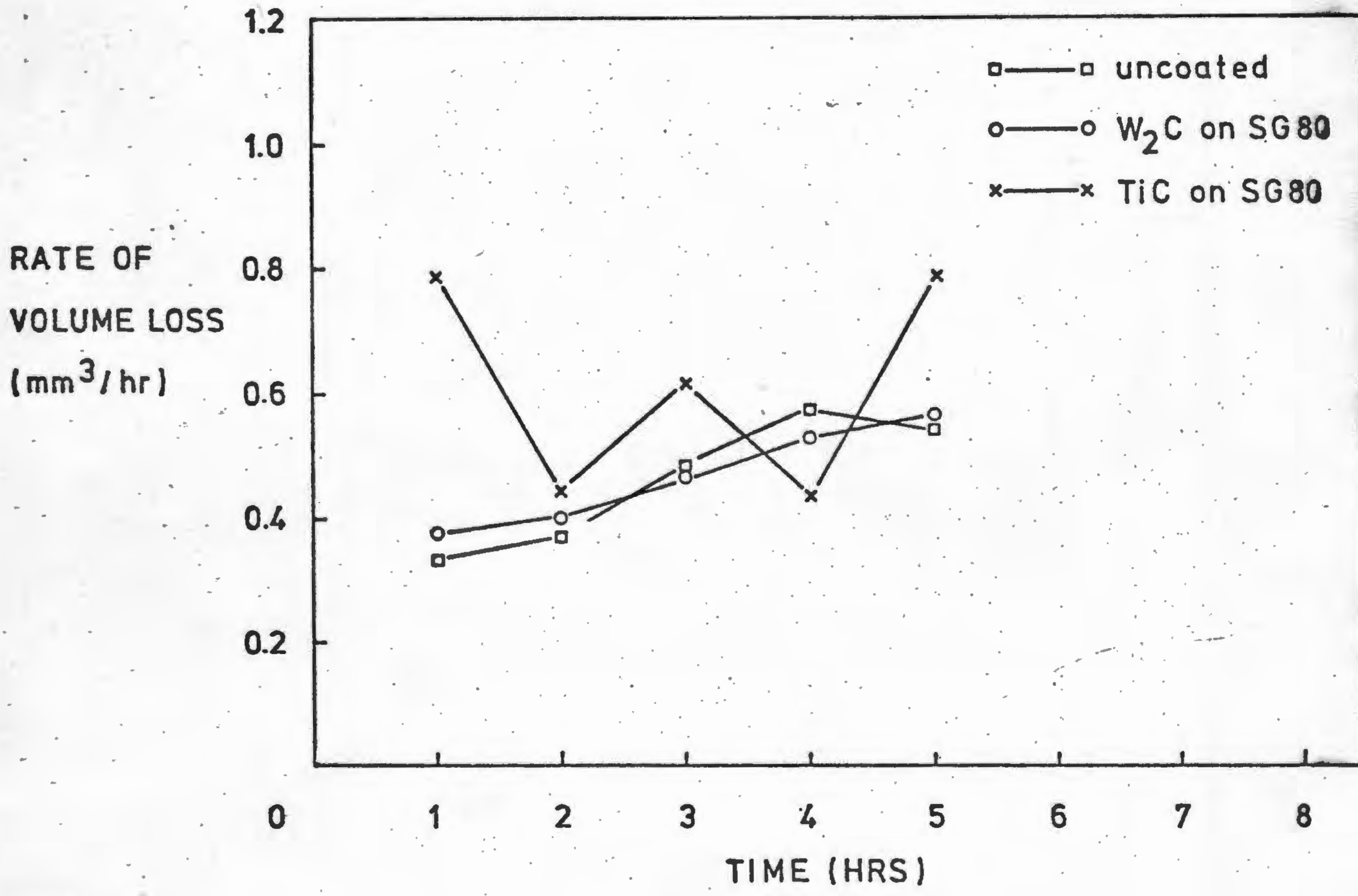

FIG. 5C Rate of volume loss as a function of time for W_2C and TiC coated SG80.

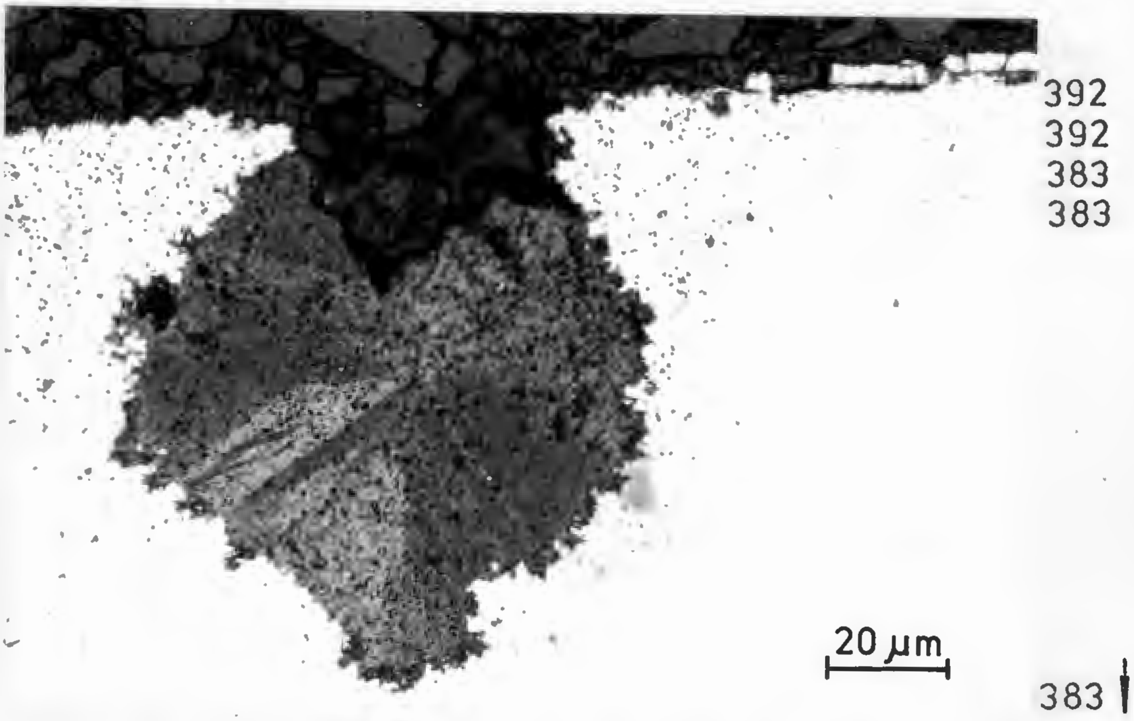

FIG. 5.28 The poor nature of the TiC coated SG80 is displayed. Once the coating is removed the hard spheroidal graphite is easily eroded.

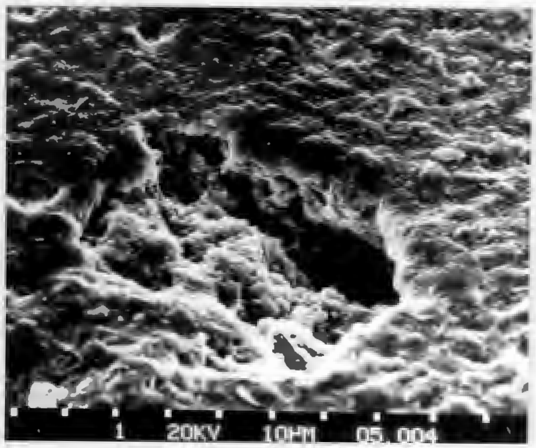

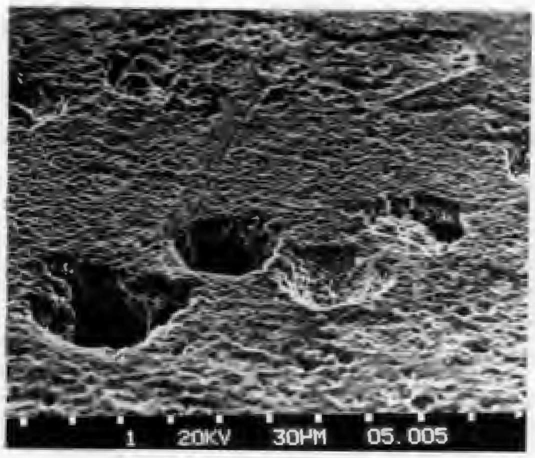

FIG. 5.29
Crater formed due to ease of graphite removal. This causes 'undercut' of the surface and encourages coating removal.

FIG. 5.30
Craters can join up and in doing so large strips of TiC are removed.

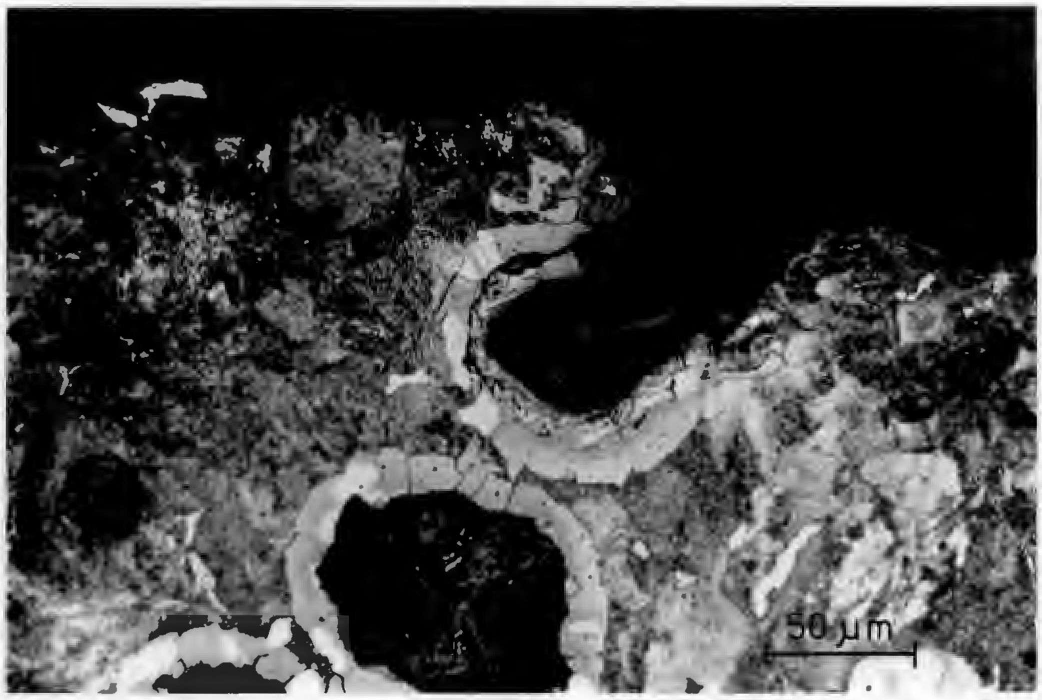

FIG. 5.31 Removal of spheroidal graphite just below surface of W_2C coated SG80.

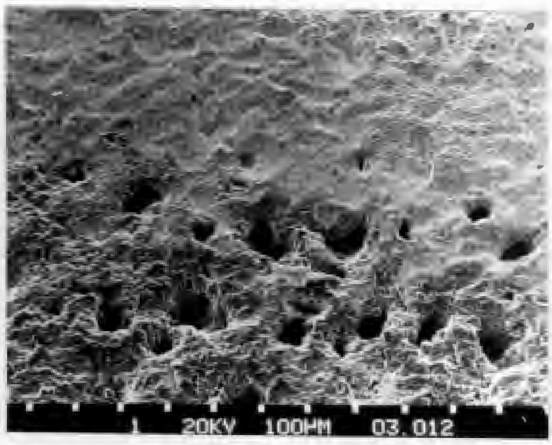

FIG. 5.32

Formation of crater due to removal of graphite sphere.

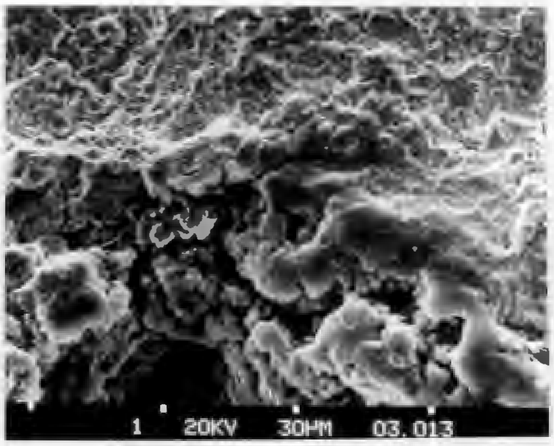

FIG. 5.33

High magnification shot of coating-substrate-crater interface.

5.3 SPRAYED COATINGS

5.3.1 Plasma sprayed Triballoy

Mild steel samples which were coated with Triballoy T-100, T-400 and T-800 were cavitated employing the standard conditions discussed in section 2.3. The volume losses together with coating thicknesses, measured by optical observation of sectioned discs, are shown in Table 5.2, below.

TABLE 5.2 MASS LOSS OVER 2 HOURS FOR TRIBALLOY COATINGS OF DIFFERING LAVES PHASE CONTENT AND UNIFORM THICKNESS

Coating	Mass loss (2 hrs) (mg)	Coat [I] thickness (μm)	Laves phase content Vol %
T-100	82,3	75	65
T-400	60,0	75	50
T-800	69,5	75	55

[I] measured by optical observation of sectioned discs.

It is clear from Table 5.2 that the Triballoy coatings provide extremely poor erosion resistance. An optical micrograph of a sectioned disc specimen, showing the coating-substrate interface, is presented in Fig. 5.34. This micrograph was taken some distance from the site of maximum erosion. Evidence of vertical cracking in the coating, together wtih a high degree of porosity, is clearly visible.

Once the coating is eroded to about 50 μm (see Fig. 5.35), large scale removal occurs. The poor adhesion and brittle nature of this failure is evident from the scanning electron micrographs of the eroded surfaces, presented in Figs. 5.36 and 5.38. In addition, the mismatch between the hard Laves phase and softer matrix is shown by the scanning micrograph presented in Fig. 5.37. Microhardness measurements reveal the Triballoy coatings to be extremely hard (MHN_{20} = 1569) relative to mild steel (MHN_{20} = 220) (see Fig. 5.34).

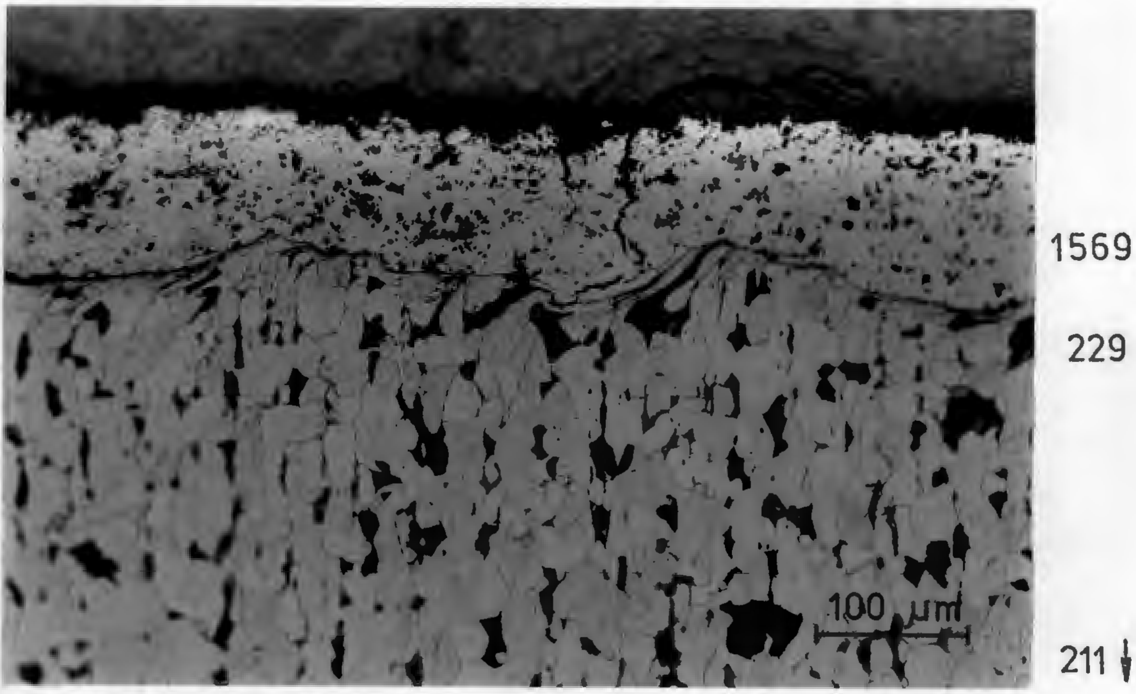

FIG. 5.34 Triballoy T-100 on mild steel. Note the vertical cracking of the coating and high degree of porosity some distance away from erosion site

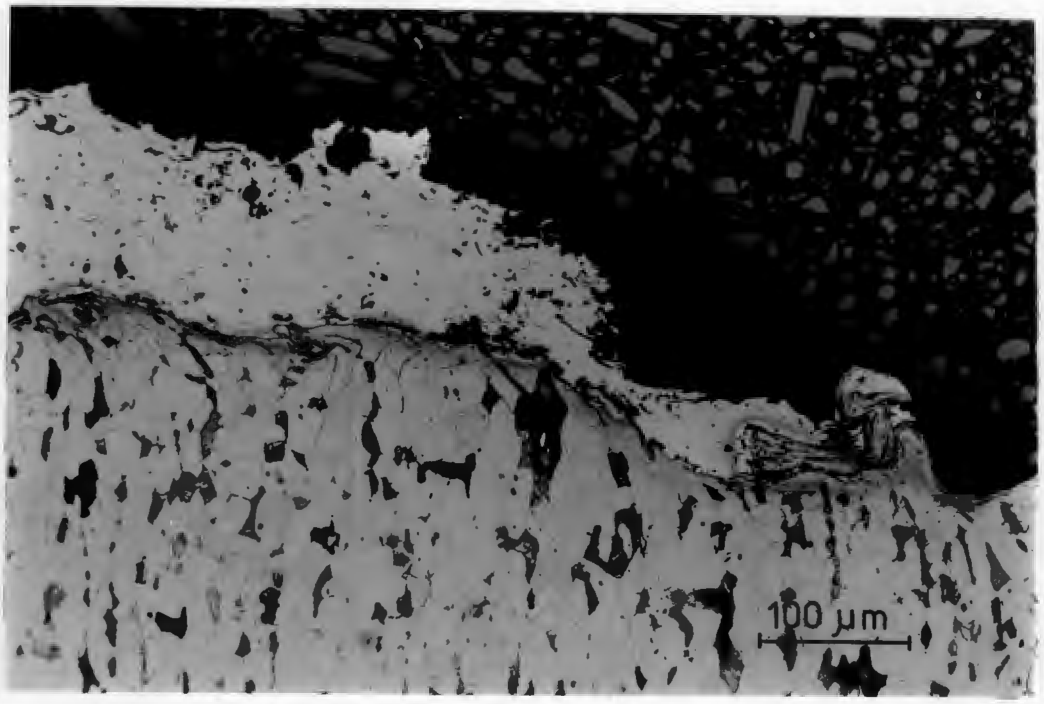

FIG. 5.35 Large scale coating removal of Triballoy T-800

MICROGRAPHS OF TRIBALLOY COATINGS ON MILD STEEL

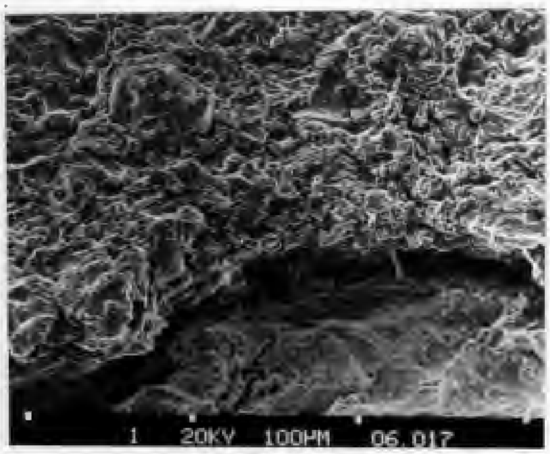

FIG. 5.36 T-100
Brittle mode of coating removal evident

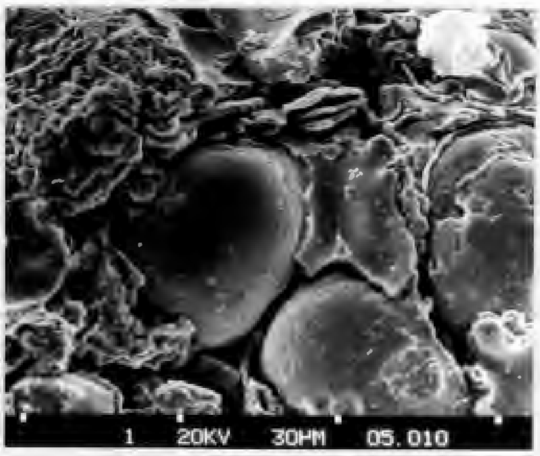

FIG. 5.37 T-400
Micrograph of hard Laves phase in cobalt matrix. Evident is the mismatch between the two phases.

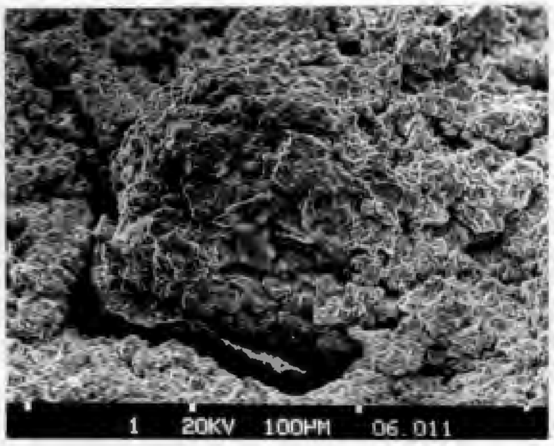

FIG. 5.38 T-800
Edge on view of coating and substrate showing apparent lack of good adhesion.

5.3.2 D-Gun carbide coated En3

Four D-gun carbide coated En3 samples, two of which were polymerically sealed, were cavitated. The plots are presented in Fig. 5.39. Coating markedly improves the erosion performance of En3. Five hour CVL's together with the optically measured coating thicknesses are shown in Table 5.3, below. It is clear from Fig. 5.39 that the coatings which had been polymerically sealed showed a higher rate of volume loss when compared to the unsealed coatings. Evidence of this polymeric sealent is shown in Fig. 5.40.

TABLE 5.3 FIVE HOUR CVL AS A FUNCTION OF COATING THICKNESS FOR SEALED AND UNSEALED D-GUN CARBIDE COATED EN3

Material	5 hr CVL (mm^3)	Coat thickness (μm)	Percentage Scatter $\pm \bar{\delta}$ %
Sealed	2,91	150	9,18
Unsealed	2,39	150	14,2

Material removal ocurred by cleavage cracking (Fig. 5.41) and these coatings showed good adhesion to the substrate, even in regions of severe erosion (Fig. 5.42).

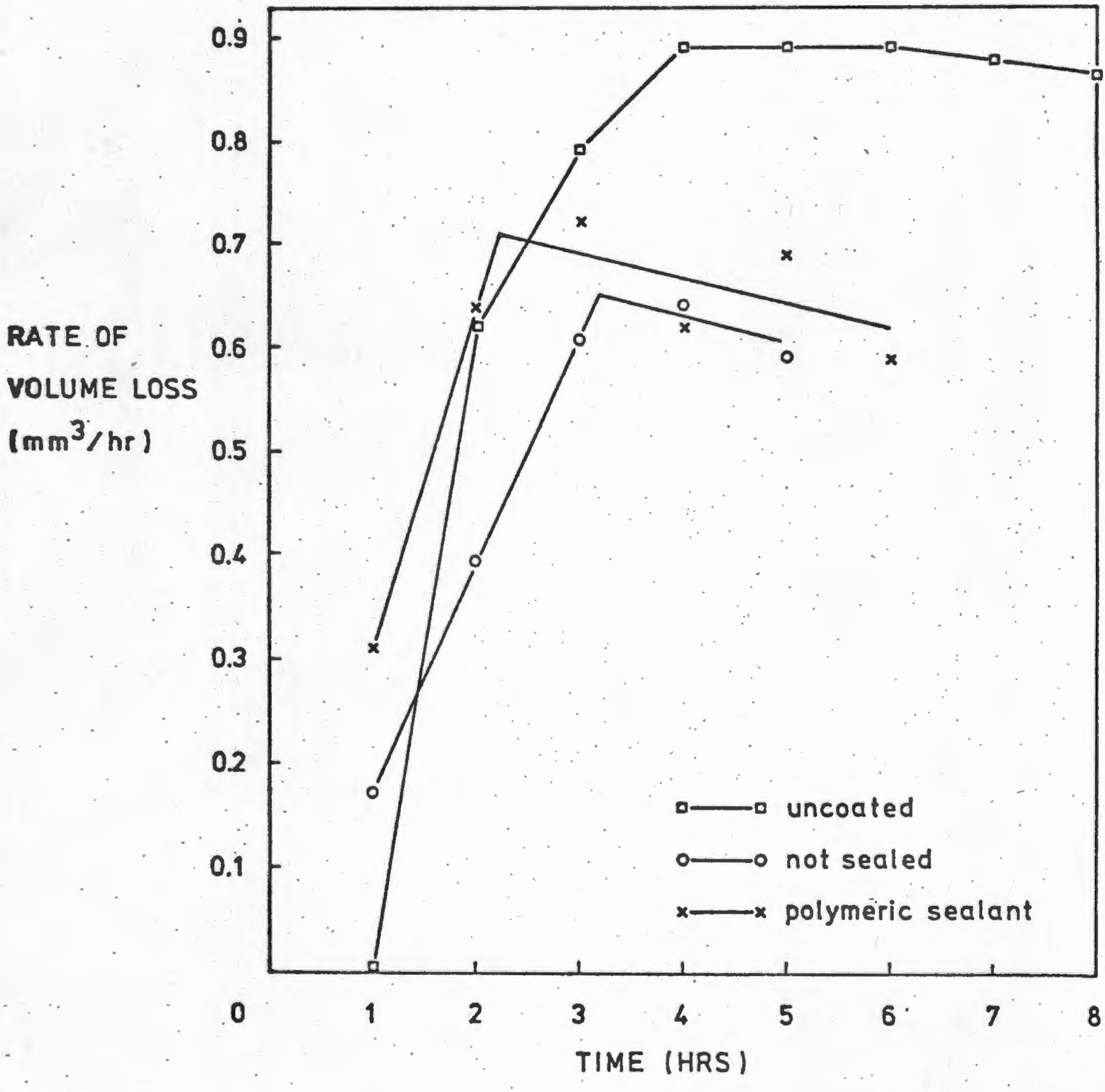

FIG. 5.39 Rate of volume loss as a function of time for D-Gun carbide coated En3.

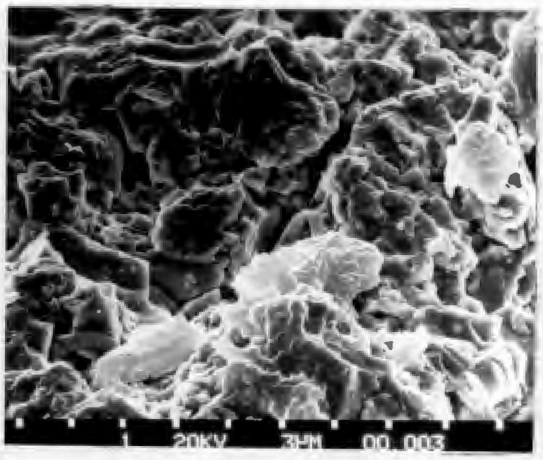

FIG. 5.40
Micrograph of eroded surface of D-Gun carbide coated En3 showing evidence of polymeric sealent.

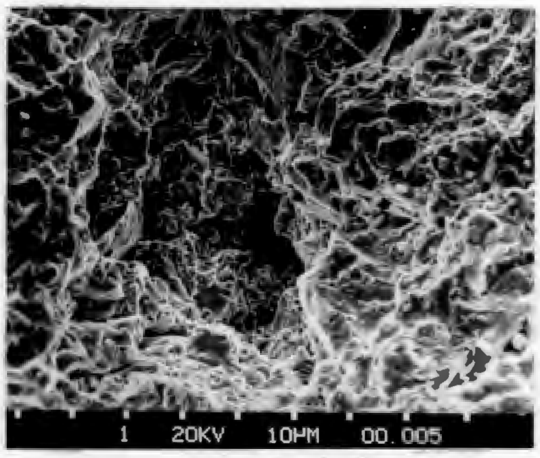

FIG. 5.41
Erosion of D-Gun carbide coated En3 displaying cleavage cracking.

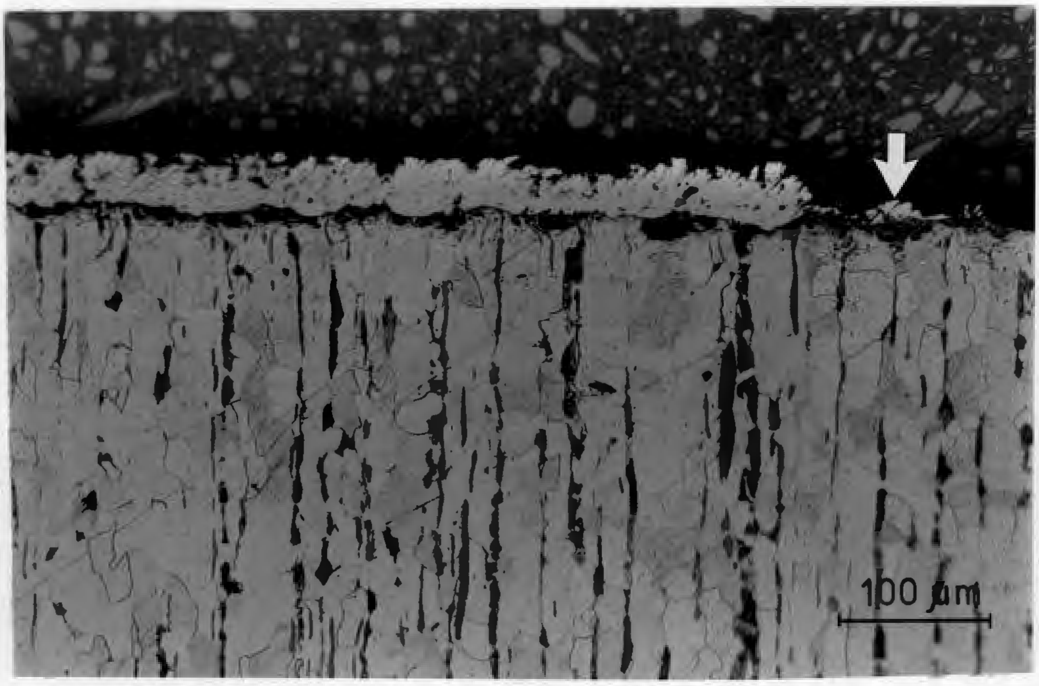

FIG. 5.42 Sectioned view of eroded D-Gun carbide coated En3, at the coating-substrate interface. Note the evidence of good adhesion (↓) in region of severe erosion.

5.4 SURFACE TREATED MATERIALS

5.4.1 Gas and ion nitrided steel (En41B)

The erosion curves for both gas and ion nitrided En41B (Q & T 600°C) are shown in Fig. 5.43. There is approximatley a four fold decrease in the steady state erosion rate when compared with the untreated specimen. However, a large volume loss is recorded in the first hour because of the removal of the brittle iron nitride layer (generally a mixture of Fe_4N and Fe_2N). Removal of this layer exposes a 200-250μm deep diffusion layer (determined by optical observation of sectioned samples) which provides erosion resistance once the brittle 'white' layer is removed.

Furthermore, it is clear that gas nitriding provides superior erosion protection when compared with the ion nitrided samples. The microhardness profiles of the sectioned samples confirm the depth of diffusion to be between 200 and 250μm (Fig. 5.44).

An optical micrograph of En41B which had received an ion nitriding treatment for 36 hours is shown in Fig. 5.45. The brittle iron nitride layer is clearly visible.

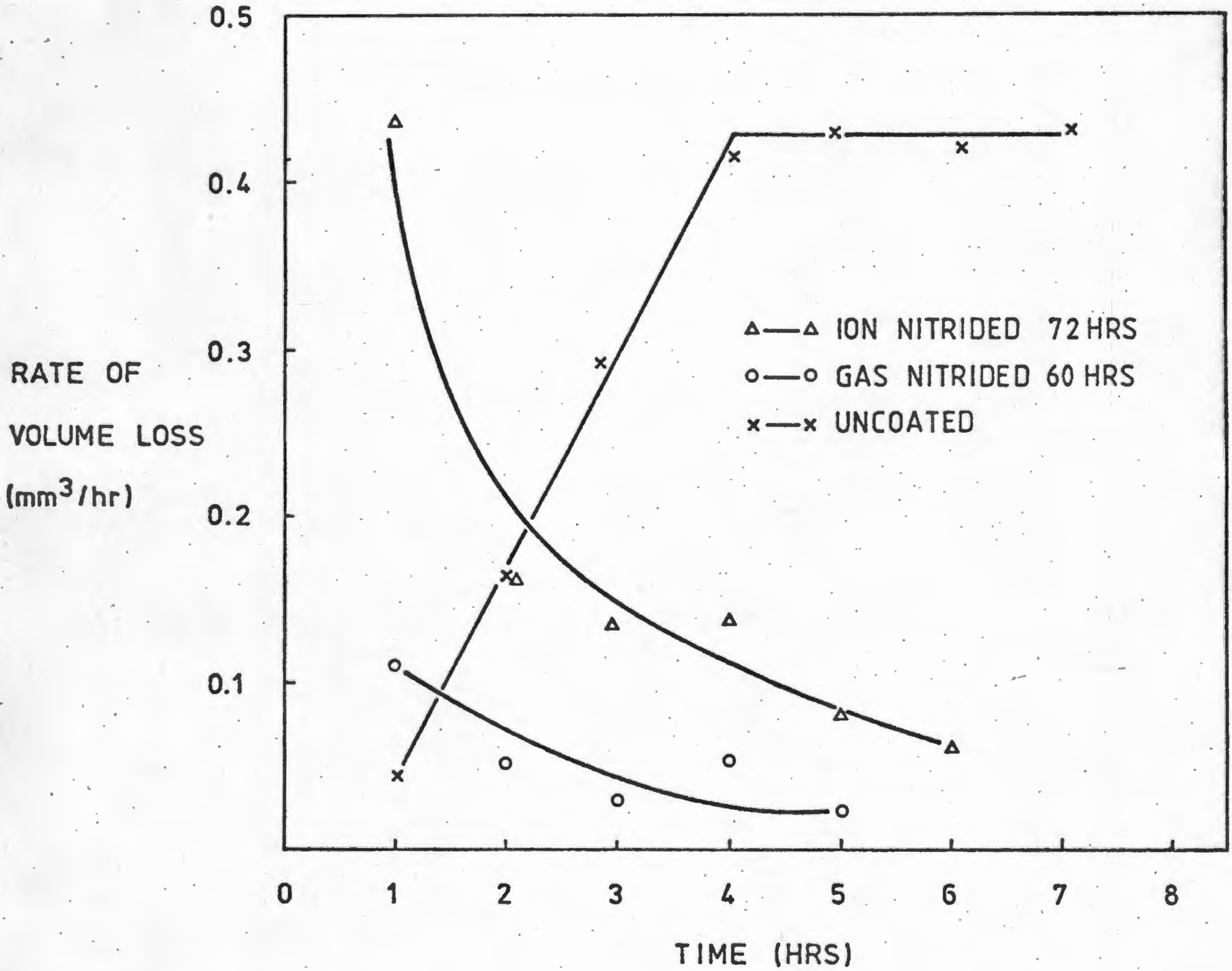

FIG. 5.43 Rate of volume loss as a function of time for Gas and Ion nitrided En41B (Q & T 600°C)

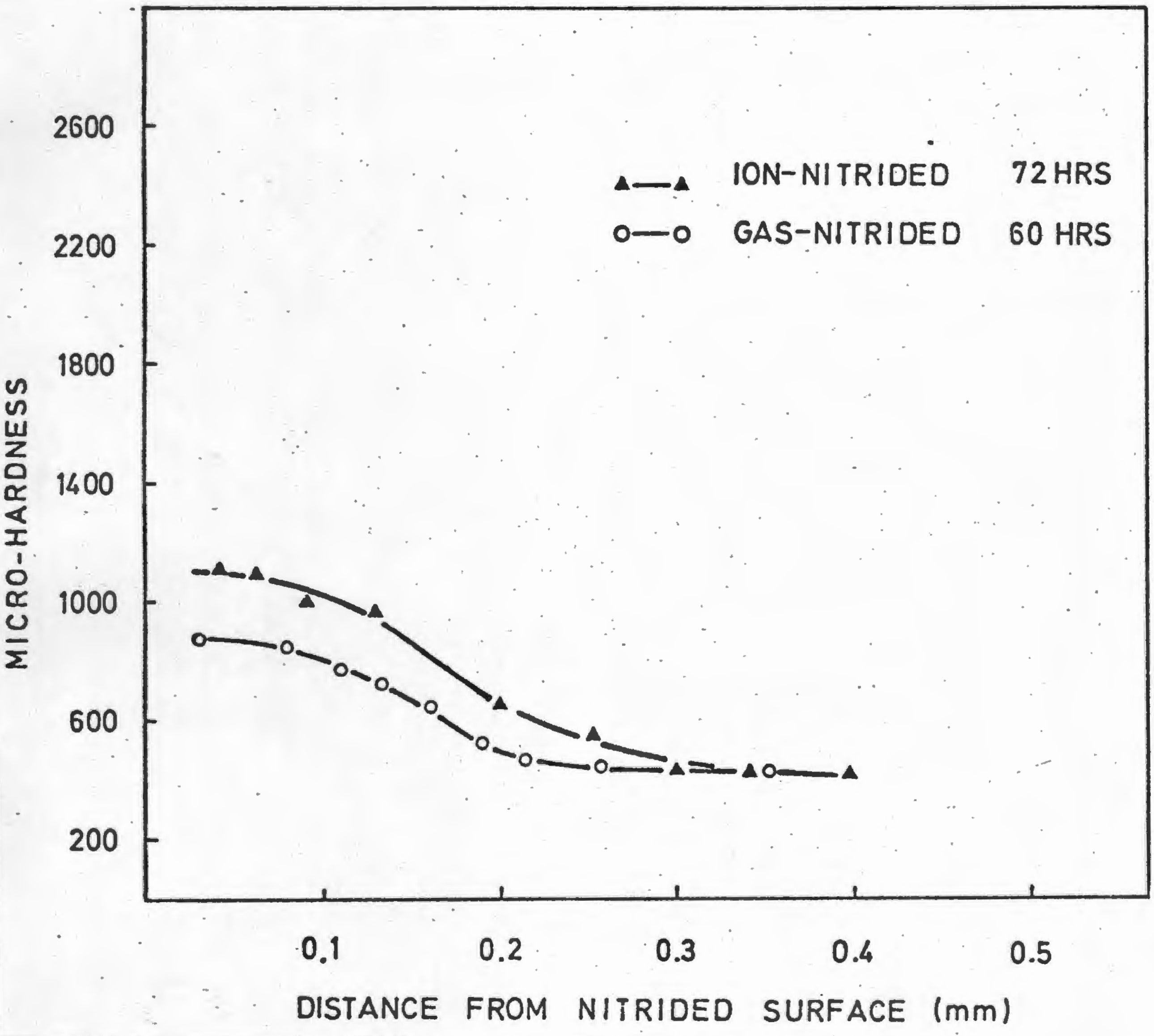

FIG. 5.44 Microhardness profile of Gas and Ion nitrided En41B (Q & T 600°C)

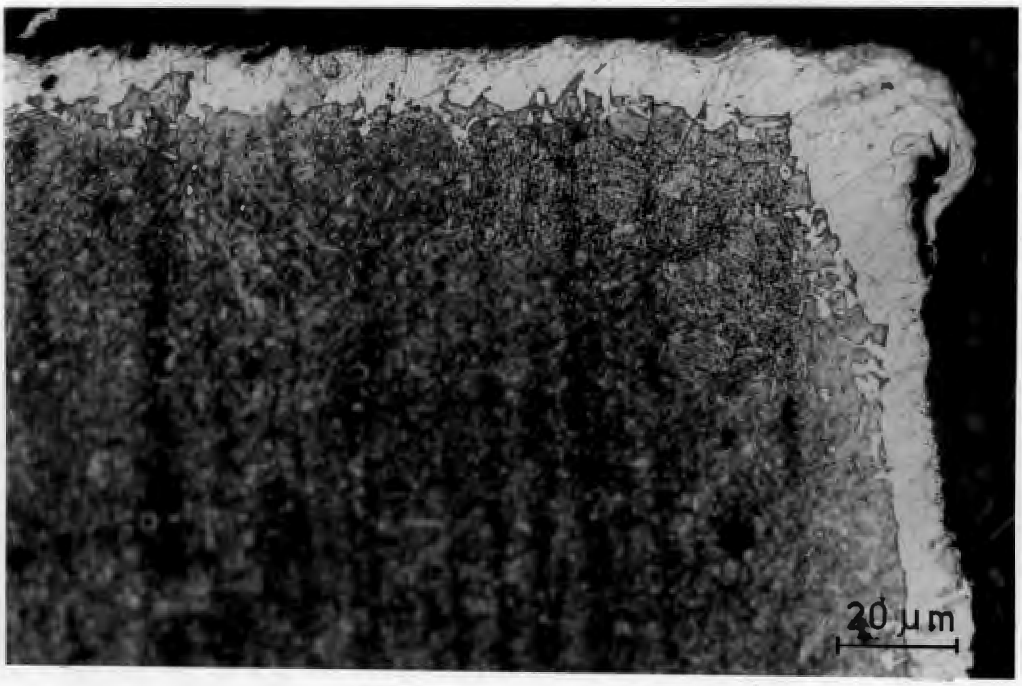

FIG. 5.45 En41B (Q & T 600°C) - ion nitrided for 72 hours. Note the brittle 'white' layer consisting of an iron nitride mixture of Fe_4N and Fe_2N.

5.4.2 Boronised steel (En1A and En24)

The erosion curves for boronised En1A and En24 are shown in Figs. 5.46 and 5.47. Boronising En24 does not provide any improved erosion resistance and the steady state of erosion is increased three-fold. Conversely, boronising En1A slightly reduces the steady state rate of volume loss. However, in both cases the initial rate of volume loss is high when compared with the substrate. Varying the boronising time appears to have little influence on the erosion performance. The depth of this boronising layer as a function of time is shown in Fig. 5.48. Both maximum depth and complete coverage depth were measured.

Optical micrographs together with microhardness readings of the boronised layer and substrate (En24 and En1A) are shown in Fig. 5.49 and 5.50. An XRD analysis was performed on samples (En24) which were boronised for time periods ranging between 1 and 5½ hours. The boronised layer consists in all cases of Fe_2B and a selective XRD trace is shown in Fig. 5.51. The d-spacings for this trace are presented in Table 5.4.

Complete coverage - *the distance from sample edge to the point where any substrate fingers begin to appear.*

Maximum depth - *the distance from the sample edge to the end of the fingers of iron boride protruding into the substrate, (ref. 58).*

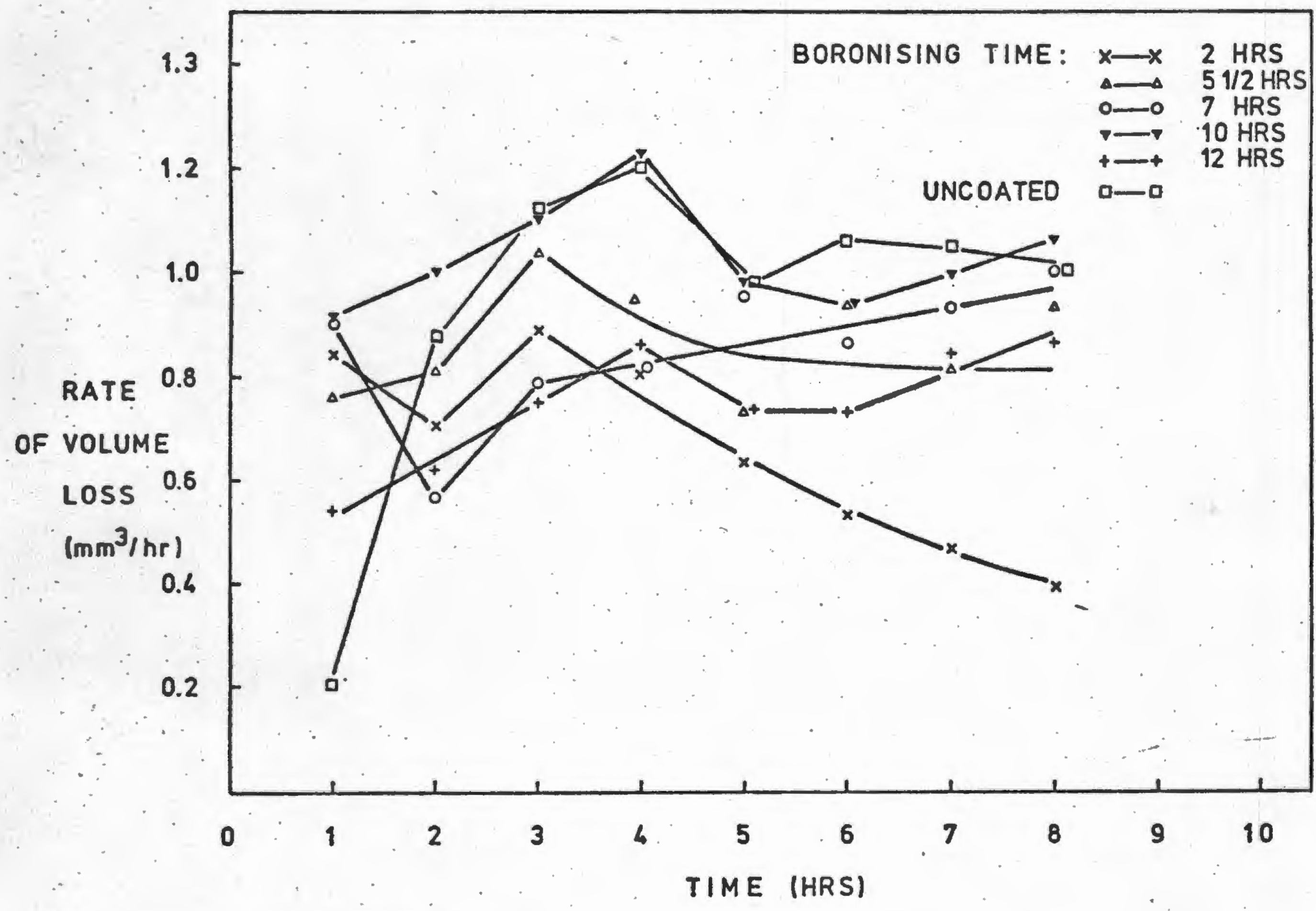

FIG. 5.46 Effect of varying the boronising time on the rate of volume loss.
Base metal: En1A.

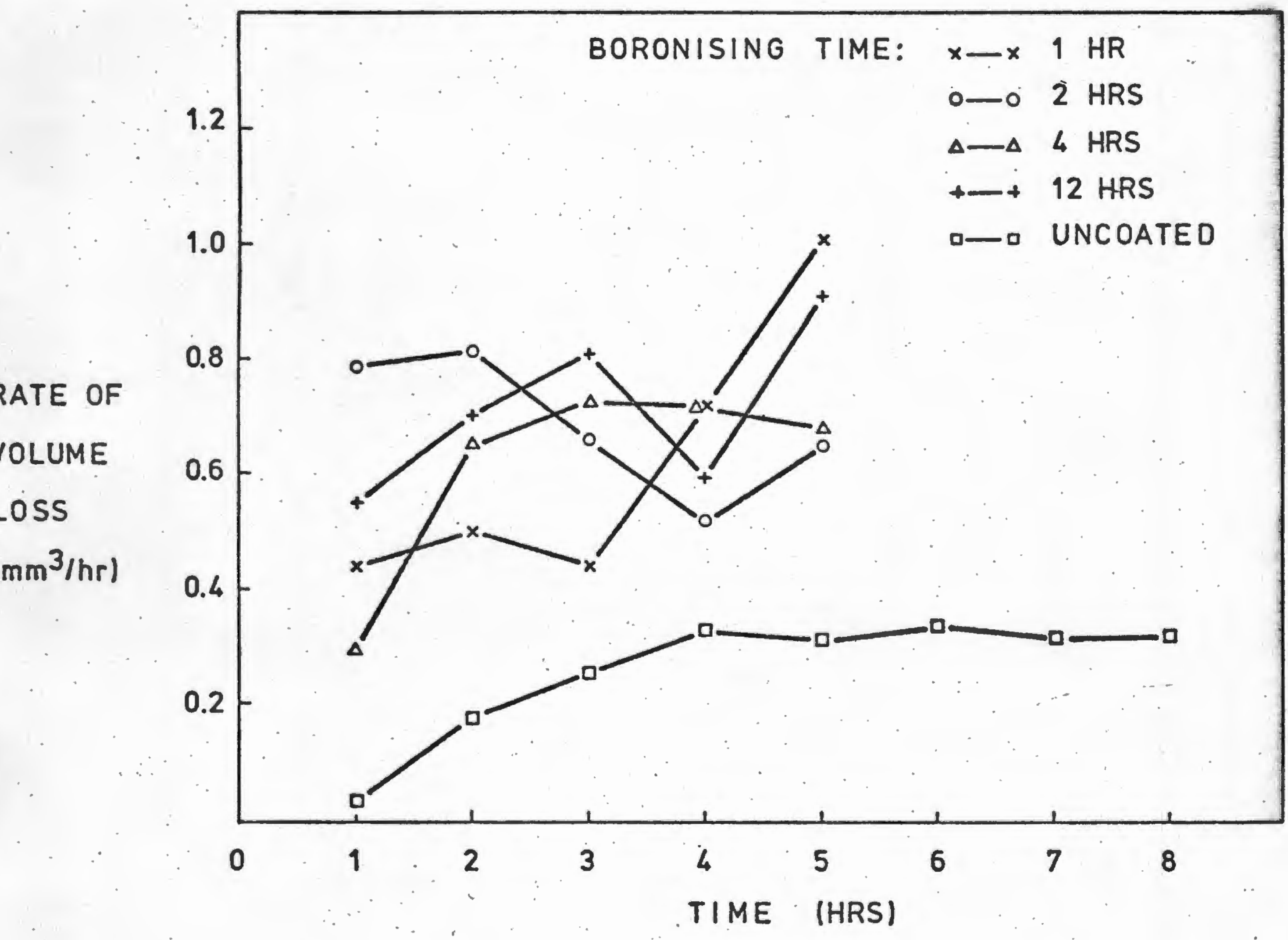

FIG. 5.47 Effect of varying the boronising time on the rate of volume loss.
Base metal: En24.

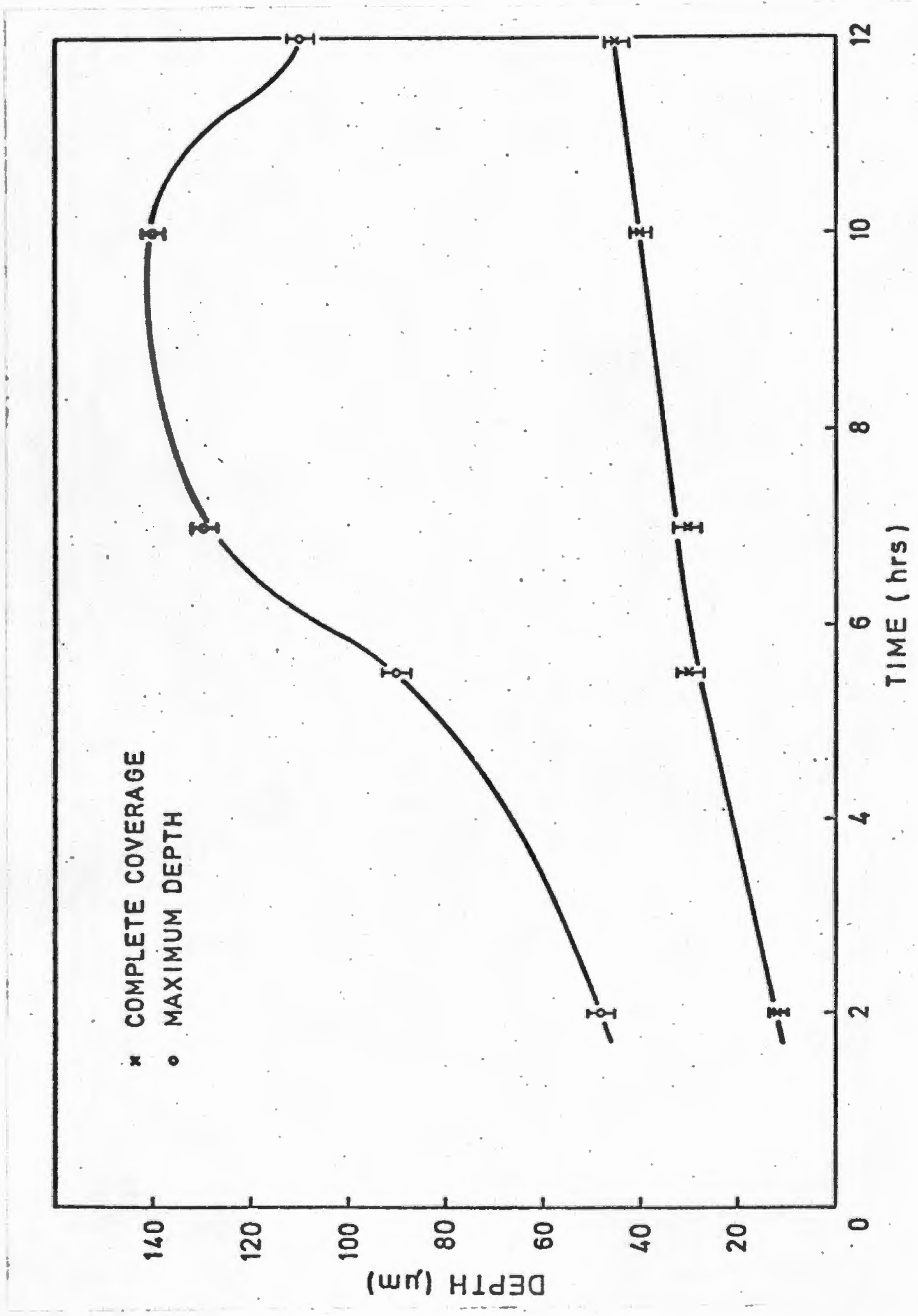

FIG. 5.48 Variation in case depth as a function of boronising time (application temperature 930°C). Base metal: EnlA.

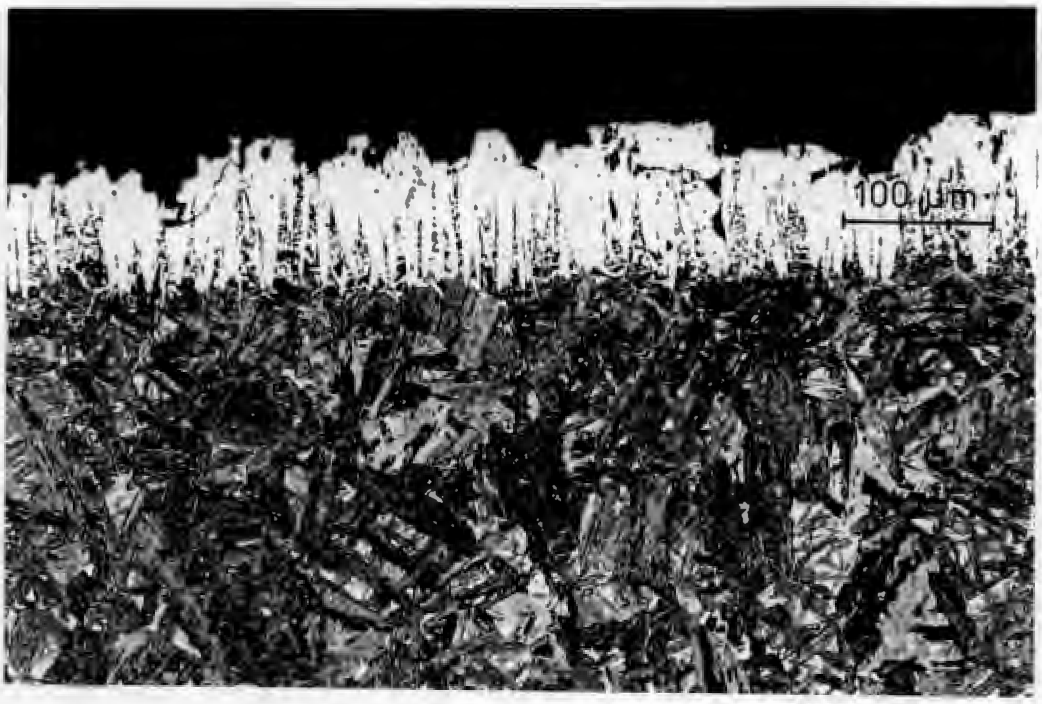

FIG. 5.49 En 24 boronised for 5½ hours at 930°C.
Note brittle cracks in hard boronised layer.

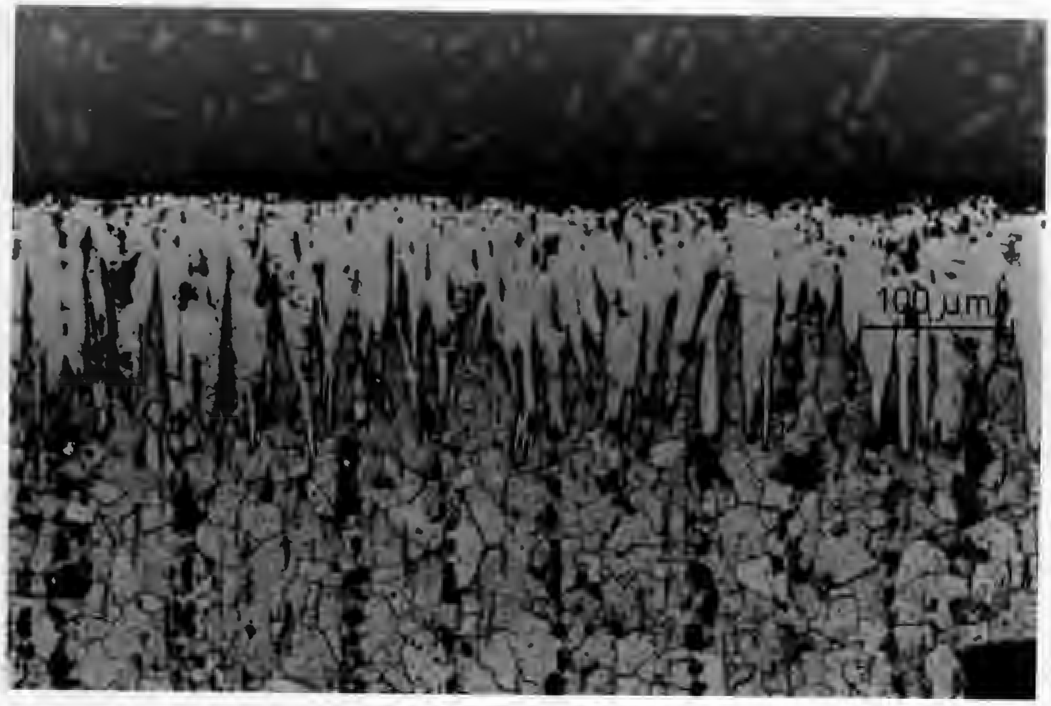

FIG. 5.50 En 1A boronised for 5½ hours at 930°C.
Note difference in saw tooth geometry when contrasted to boronised En 24.

TABLE 5.4 D-SPACINGS FOR Fe_2B

2θ	Peak Intensity	d-spacings obtained
78,0	-	1,20
56,5	W	1,63
45,0	VS	2,01
42,6	VS	2,12
35,1	W	2,56
24,6	W	3,61

VS : very strong

W : weak

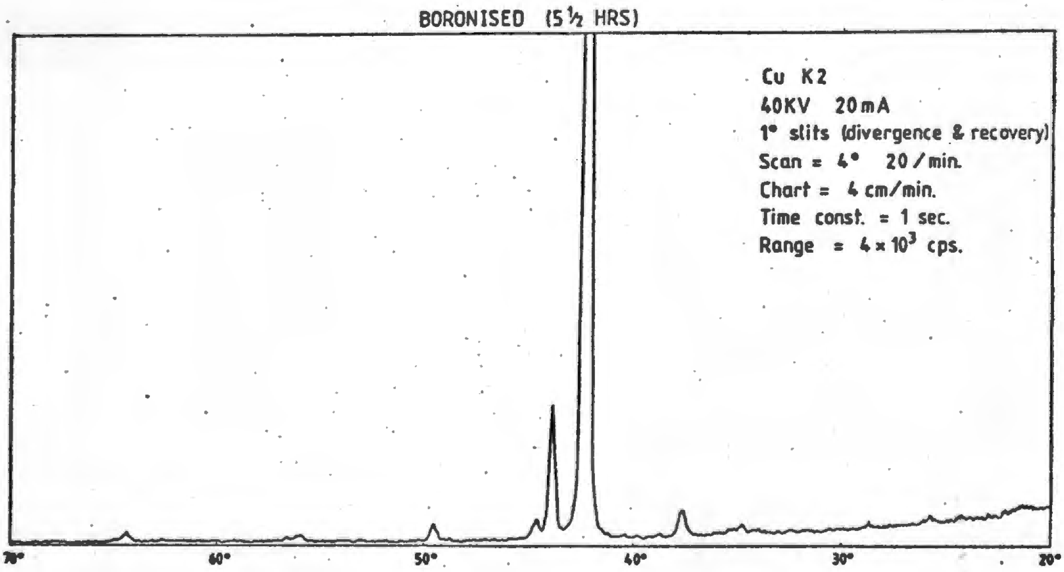

FIG. 5.51 XRD trace of En24 boronised for 5½ hours at 930°C shows boronised layer to consist of Fe_2B.

5.4.3 Carburising

Results of the erosion tests conducted by Yamey (54), are presented for comparative purposes in Fig. 5.52. These results are included because of the excellent erosion performances of the carburised En36 steels. These surface treated steels show an eight-fold decrease in the steady state erosion rate.

Both optical and scanning micrographs are displayed in Figs. 5.53 to 5.55, together with a microhardness profile of the sectioned disc (Fig. 5.53). From the hardness profile it is evident that hardness gradually decreases with depth (ie. a diffuse hardness gradient exists).

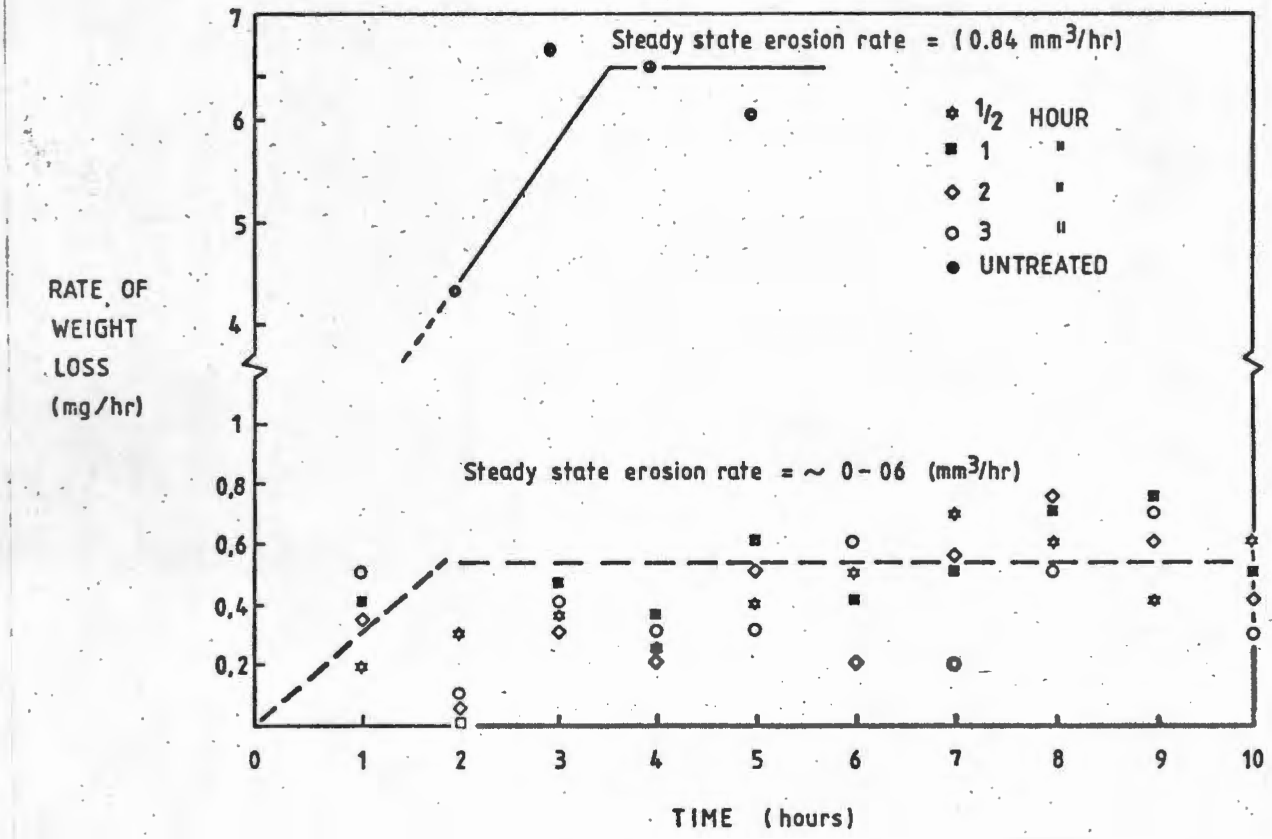

FIG. 5.52 Effect of varying the carburising time on the rate of weight loss over ten hours.

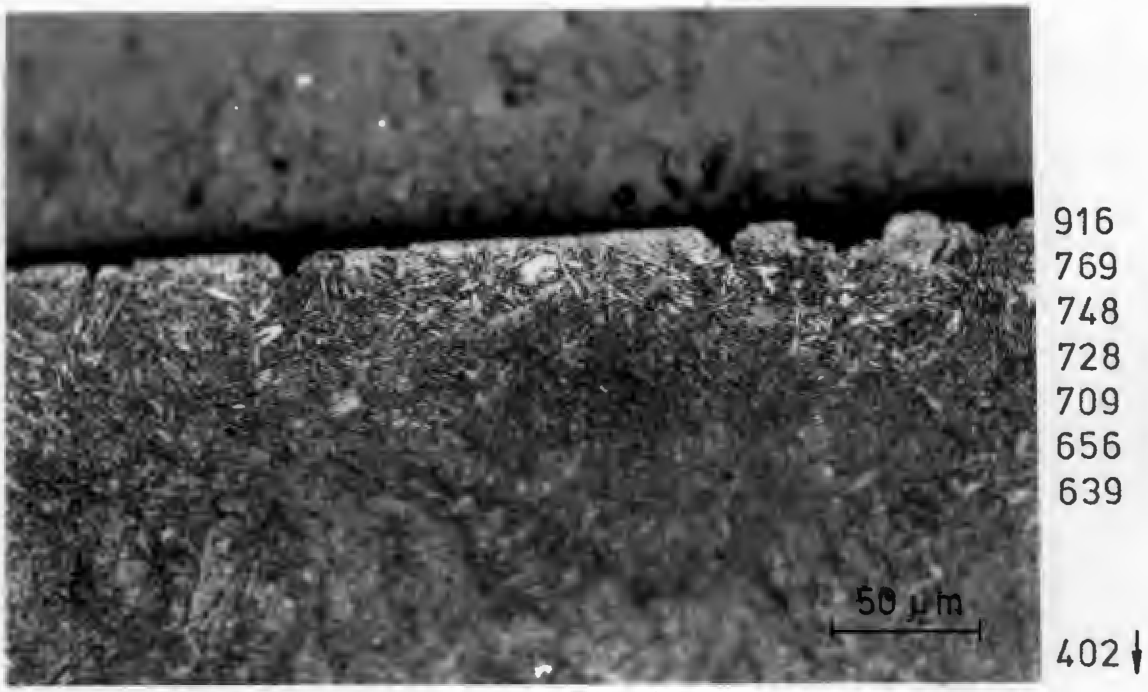

FIG. 5.53 Optical micrograph of carburised En36 (½ hour) together with microhardness readings at varying intervals below the surface.

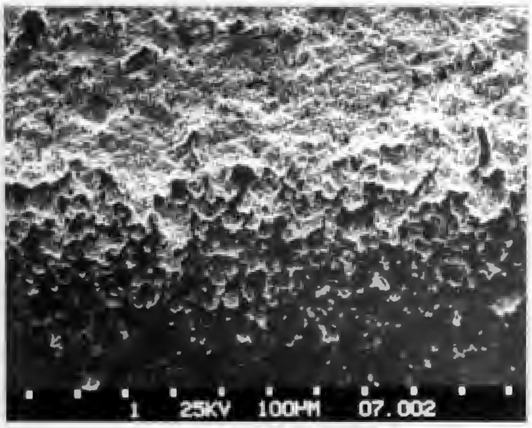

FIG. 5.54
Carburised layer-substrate interface.

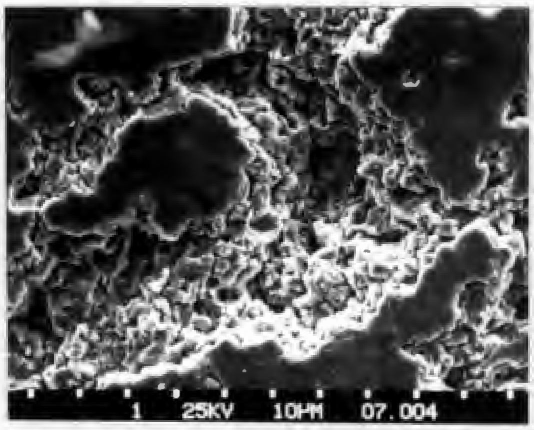

FIG. 5.55
Preferential erosion of substrate once surface treated layers are removed.

CHAPTER 6 : DISCUSION - BULK POLYMERS

6.1 THE CORRELATION OF EROSION PERFORMANCE WITH MECHANICAL PROPERTIES

The erosion resistance of polymeric materials (Table 4.1) shows broad correlations with the mechanical properties. Precise correlations are not observed because of the complex erosion process associated wth high frequency collapse of cavities in a fluid. Conventional mechanical properties are determined by employing simple stress conditions, whereas erosion occurs at high strain rates producing complex stress patterns (43).

6.2 RESILIENCE NUMBER

The rebound resilience of a material is related to its dynamic and viscoelastic properties. It represents a measure of a material's response to rapid impact and strains which approach conditions imposed by the collapse of cavities.

From Table 4.1 it is notable that a group of polymers, Group IV, eroded in a catastrophic manner. This occurred either by melting, in the case of the urethanes (A → C) and polyvinyldiene flouride, or by brittle failure in the case of polycarbonate.

The elastomeric polymers of this group, namely polyurethane A → C, are characterised by their extremely low resilience (<55) together with low melting points (± 90°C). In contrast, PTFE which has a much higher melting point did not fail catastrophically in spite of its low resilience (Rn = 36). The behaviour of Group IV elastomers is best understood in terms of their relatively high mechanical hysteresis. This leads to the generation of heat, which coupled with their low thermal conductivity does not allow the heat to be dissipated sufficiently quickly to prevent a marked rise in temperature. Thus failure occurs by melting rather than by mechanical damage.

The more erosion resistant materials, such as polyamide 66 + PE (Group I) and polyacetal, have melting points ca. 165-225°C. Thus whenever high frequency cavitation is encountered, there is a possibility of thermal softening and, in order to establish a satisfactory stress level for a particular design, it may be necessary to test at the relevant frequencies encountered in service. On the other hand, polycarbonate (Group IV) failed catastrophically as a result of the extremely high resilience (Rn = 91) which is an indication of its brittle character since it could not absorb the strains generated due to cavitation.

It should be noted that polyethylene terephalate (Group III) although having a higher resilience number (Rn = 103) did not fail catastrophically, probably as a consequence of its greater chemical stability. Group III polymers, with the exception of polypropylene, are all 'glassy' at room temperature and this accounts for their high resilience numbers (Table 4.1). These polymers have a low mechanical damping ability and their failure mechanism approximates the normal erosion mechanism of hard metals (ie. brittle chip removal).

The polymeric materials (Group I and Group II) with resilience numbers between 45 and 75 have the optimum behaviour (see Fig. 6.1). These polymers are generally 'leathery' (characterised by low Tg) and their relaxation times are probably shorter than the cavitation frequency and thus these plastics can release energy elastically between cyclic stress pulses generated by cavitation. Resilience numbers are not high, hence indicating a non-brittle failure of the matrix (Figs. 4.6, 4.8 and 4.11). Damage accumulation is slow and materials show excellent erosion resistance.

There is a gradual transition between the properties of Group I and Group II with the properties of Group II being closer to the limits of the optimum (Fig. 6.1). But since no one property determines the erosion behaviour of polymers it is difficult to separate the two groups on the basis of a single property. The upper level of resilience is more critical, and polyacetal and poly(amide-imide), though having almost identical resilience, have greatly differing volume losses (Table 4.1).

6.3 HARDNESS

Although the term 'hardness' is sometimes used to donate scratch resistance or rebound resilience the definition is restricted in the present context to resistance to indentation, ie. the response of a material to a statically applied compressive deforming load. When the Shore hardness exceeds approximately 82 (Fig. 6.2) the materials behave in a brittle manner and the approach to characterisation can be the same as used for resilience (discussed in section 6.2). There appears to be no simple relationship between resilience and Shore hardness (Fig. 6.3) because the first is a dynamic method of determining hardness, and the latter is static. It will be noted, however, that the materials with optimum behaviour have a resilience between 45 and 75 and a Shore hardness between 65 and 82. Although three distinct groupings are observable in Fig. 6.3 no clear-cut trends present themselves and this joint approach gives no extra information in terms of understanding the interrelating factors which determine erosion resistance.

6.4 PERCENTAGE ELONGATION TO FRACTURE (PERCENT ε_f)

Fig. 6.4 suggests that there is no direct relationship between percent ε_f and the 5 hour CVL. However, for a material to have good erosion resistance the ε_f should, in general, exceed 100 percent. Values less than this sometimes result in a brittle failure mode; nonetheless the low ε_f of heterogeneous polymers obviously does not inhibit their good performance.

6.5 GENERAL DISCUSSION : ANALYSIS OF EROSION MECHANISMS

6.5.1 Homogenous polymers

The mechanical properties of the polyethylenes are very dependent on the molecular weight and degree of branching of the polymer chains. It is essentially a long chain aliphatic hydrocarbon of the type $-CH_2-CH_2-CH_2-$ and would thus be thermoplastic. The density as in HDPE's is taken as a measure of the degree of short chain bonding. In addition, the higher the molecular weight (ie. in UHMWPE), the greater the number of points of attraction and entanglement between the molecules. Differences in branching (and hence degree of crystallinity) largely affect properties characterised by solid displacement, molecular weight differences will affect properties that involve large deformations such as UTS and percent ε_f (Table 6.1).

TABLE 6.1 HOMOGENOUS POLYMER PROPERTIES

Polymer	5 hr CVL (mm^3)	Tg (C)	Percent εf	UTS (MPa)	Shore Hardness (D)	Rn
Polyamide 66	0*	20	90,00	80,00	77	89
DS UHMWPE	0,53	-	467,30	30,41	66	46
UHMWPE	0,85	-120 to 70	485,50	19,33	66	55
HDPE	1,06	-120	1030	25,78	68	45
Polyacetal	2,79	-2 to 0	30,65	65,65	81	76
Polypropylene	11,20	-27	234,00	26,52	76	60
Polysulfone	21,53	175 to 190	20,70	70,22	83	83
Polyethylene terephalate	35,57	63 to 80	17,30	78,83	86	103
Polycarbonate	VVB	-	38,89	70,10	83	91
Polyvinyldiene flouride	M	-62	59,82	44,29	78	76

*The high ranking of the polyamides samples can be misleading and cannot be viewed purely in terms of their 5hr CVL (see discussion on polyamides, section 6.5.1)

VVB : very, very brittle M : melt

Both HDPE and HMWPE have excellent erosion resistance because of their high elongations to fracture (Table 6.1). The effect of high $_f$ is reflected in the ductile fibril tearing of the eroded surface of these materials (Fig. 4.8 and Fig. 4.11).

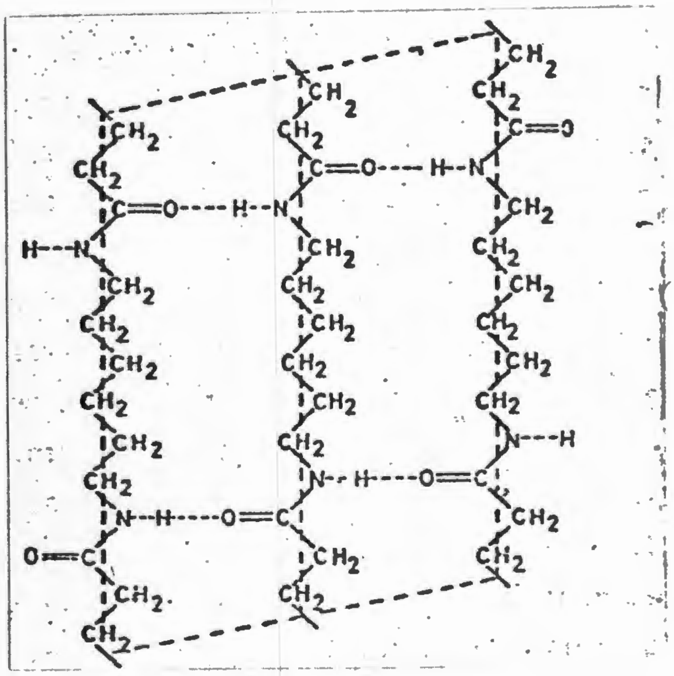

FIG. 6.1 Structure of Nylon 66 (Ref. 5)

Polyamides such as Nylon 66 (Fig. 6.1) contain polar groups spaced out at regular intervals so that the polymers crystallise as a result of intermolecular attraction. Hydrogen bonds with an NH-O distance of 2.8A are produced and are the reason for the high strength and melting point of Nylon 66. These polymers have aliphatic chain segments which give a measure of flexibility in the amorphous region. Nylons are hygroscopic and water absorption will cause a reduction in tensile strength and an increase in toughness. Absorbed water is bound to the polyamide by diffusing into the amorphous regions, when the H_2O content increases from 0,2 to 2,5 percent. Once this water content exceeds 2,5 percent aggregates of water form loosely bound bridges between the C=O and N-H groups. Thus the absorption of more than 2 or 3% of H_2O causes a reduction in interchain attraction with a corresponding decrease in the mechanical properties (5). The critical water content of Nylon 66 was calculated by Heathcock (5) to be approximately 2,2%. The reason for the high Rn is that the Tg of Nylons is generally below room temperature so that the materials have a measure of flexibility in spite of their high crystallinity. Nylon 66, in addition to small amounts of fibrous tearing, loses material during cavitation attack in a brittle manner (Fig. 4.5). This is possibly due to the high resilience in conjunction with a relatively high percent ε_f (Table 6.1).

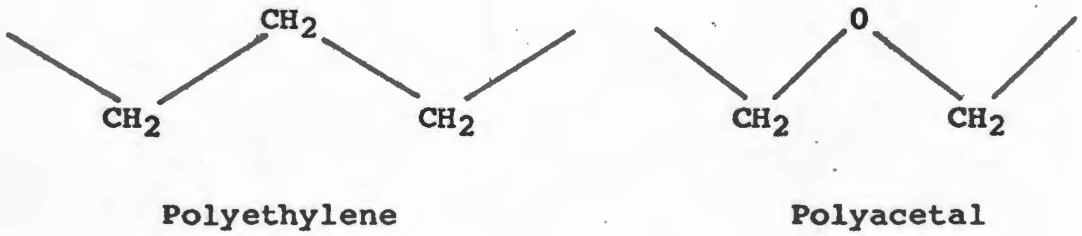

FIG. 6.2 Structure of polyacetal and polyethylene

Both polyethylene and polyacetal (Fig. 6.2) are linear with a flexible chain backbone. The acetal polymer molecules have a shorter backbone (- C - O -) bond and they pack more closely together than polyethylene resulting in higher UTS, Shore hardness and Rn. The erosion resistance of polyacetal is lower than that of polyethylene. A possible explanation is that the polyacetal responds in a more brittle manner because of the closer molecular packing. This is reflected by a higher Rn and percent ε_f (Table 6.1), which results in a 'mixed' (Group II) mode of erosion (Fig. 4.6).

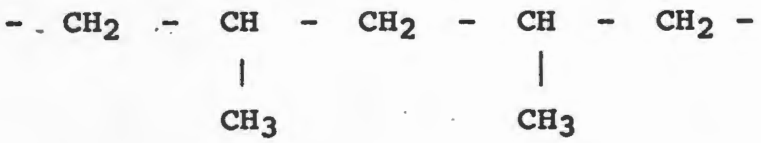

$$\begin{array}{ccccccccc} -CH_2 & - & CH & - & CH_2 & - & CH & - & CH_2 - \\ & & | & & & & | & & \\ & & CH_3 & & & & CH_3 & & \end{array}$$

FIG. 6.3 Structure of polypropylene

Polypropylene is a linear hydrocarbon polymer which has methyl groups attached to alternate carbon atoms on the chain backbone (Fig. 6.3). The most significant influence of the methyl group is that it can lead to products of different tacticity*. Commercial polymers are usually about 90 - 95% isotactic. If resilience

---

** If a new monomer unit, eg. CH_3, is added onto the side of the previous one, the polymer is called isotactic; if it is on the opposite the polymer is called syndiotactic (tactic - stereo regular).*

number, percent ε_f and Shore hardness determine the erosion resistance then polypropylene would have a ranking in the order of polyethylene. However, the lower elongation to fracture compared with polyethylene combined with the increased resilience and hardness suggests a decrease in erosion resistance.

Even when all of these factors are taken into account the high level of the cumulative volume loss cannot be simply explained.

In the case of polysulfone, polycarbonate and polyethylene terephalate the presence of benzene rings in the main chain leads to a somewhat 'stiffer' chain resulting in a higher Tg. This high Tg together with Rn, Shore hardness and UTS (Table 6.1) accounts for the brittle behaviour of these polymers. The effect of a low ε_f is seen in the eroded surface (Fig. 4.7).

6.5.2 Glass fibre reinforced polymers

The presence of fibres in a thermoplastic material confer an increase in tensile modulus, strength and hardness. However, properties are highly dependent on fibre anisotropy. The erosion resistance of the reinforced plastics such as Polyamide 66 + GF (30,1%) and Polyacetal + GF (20,1%) is lower than that of the homogenous polymer (Fig. 4.2). The polyacetal + GF contains 20,1% by weight of GF.

5 hr CML (mg)	Polyacetal	Polyacetal + GF
	3,70	5,0

From the above figures it can be seen that the composite has an increased weight loss of 35%. Thus erosion of more than the mass contribution of the glass fibre occurs (ie. 20% by weight of GF). The glass fibre is not contributing to the erosion resistance and the fibres are removed (Fig. 4.9) due to the elastic mismatch between matrix and fibre. Once the fibres have been removed the exposed matrix is about 15% weaker than that of the homogenous polymer.

6.5.3 Heterogenous polymers

No simple explanation can be given for the optimum behaviour of polyamide 66 + PE and polyacetal + PE. Heterogenous polymers consist of at least two chemically different substances (polyethylene spheres in a polyacetal matrix), and the properties of the composite materials are determined by the separate components.

Unlike the fibre reinforced polymers, the components are elastically compatible and the mixture of the two polymers resutls in an intermediate Shore hardness and resilience from that of the individual homogenous polymer (Table 4.1). It is the optimum resilience and hardness properties attained by these heteropolymers (Figs. 6.1, 6.2) that account for their excellent erosion resistance. A micrograph of the eroded surface of polyamide 66 + PE (Group

I) is shown in Fig. 4.5. The possibility of enhanced damping of cavitation stresses by the dual phase matrix cannot be discounted, especially when the low ε_f is considered.

6.5.4 Specifications for optimum materials

a) The polymer likely to give the best erosion performance on the basis of our work will be heterogenous (eg. PE spheres in a polyacetal matrix).

b) It will have a resilience number between 45 and 75 with optimum of $\sim$60.

c) It will ahve a Shore hardness between 66 and 84 with an optimum of $\sim$75.

d) The elongation to fracture in general must exceed 100 percent. Higher ε_f's are preferable.

e) No glass fibre reinforcements or macroscopic fillers should be used as these tend to lower the erosion resistance.

f) The Tg should be below room temperature so that the polymer is in the leathery state under normal working conditions.

g) Polyamides should be avoided in an aqueous environment.

If the above criteria are satisfied and it is borne in mind that all of the factors are inter-relating, the resultant polymer will have a good erosion resistance to vibratory cavitation at ambient temperatures.

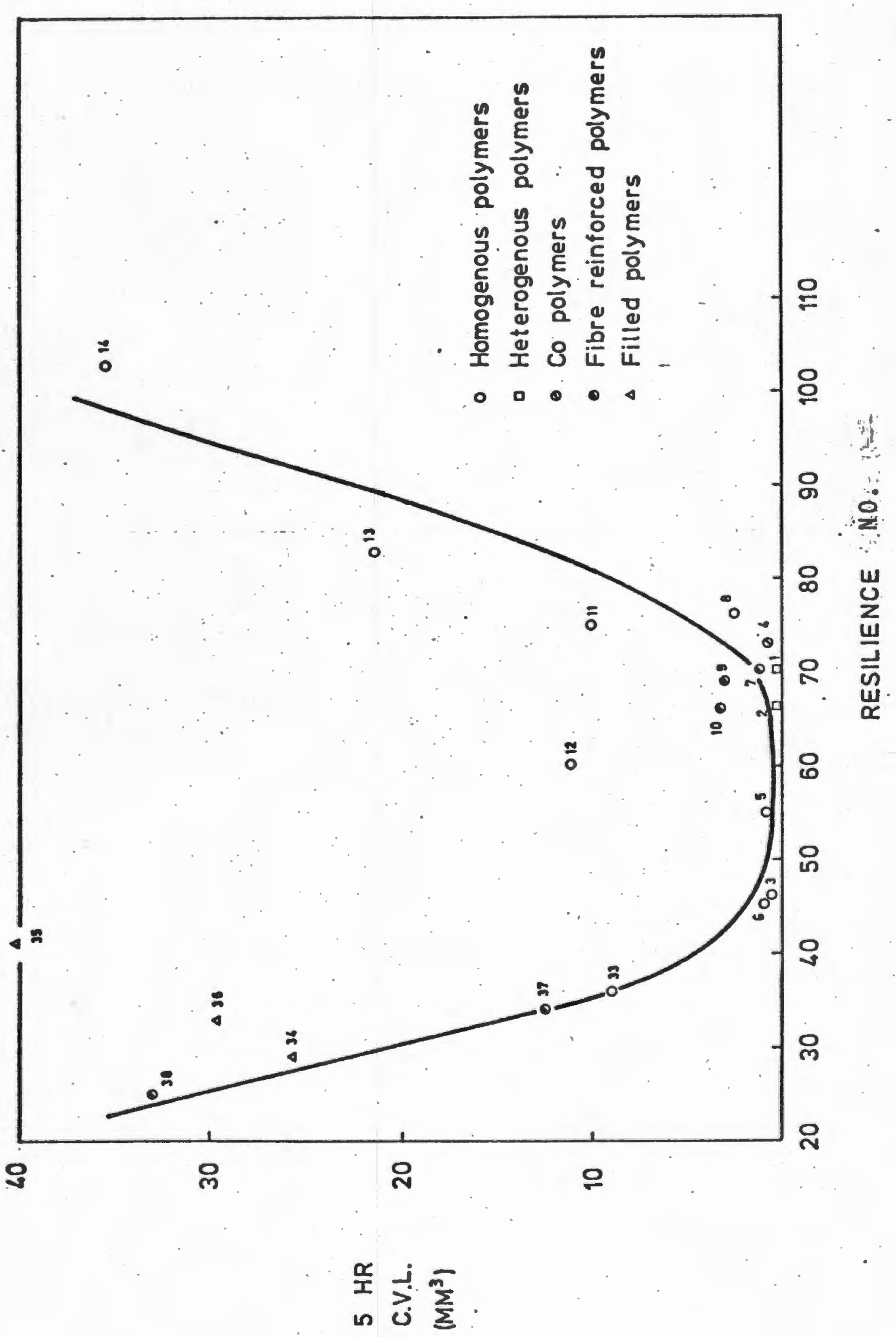

FIG. 6.1

Effect of varying resilience on the five hour cumulative volume loss

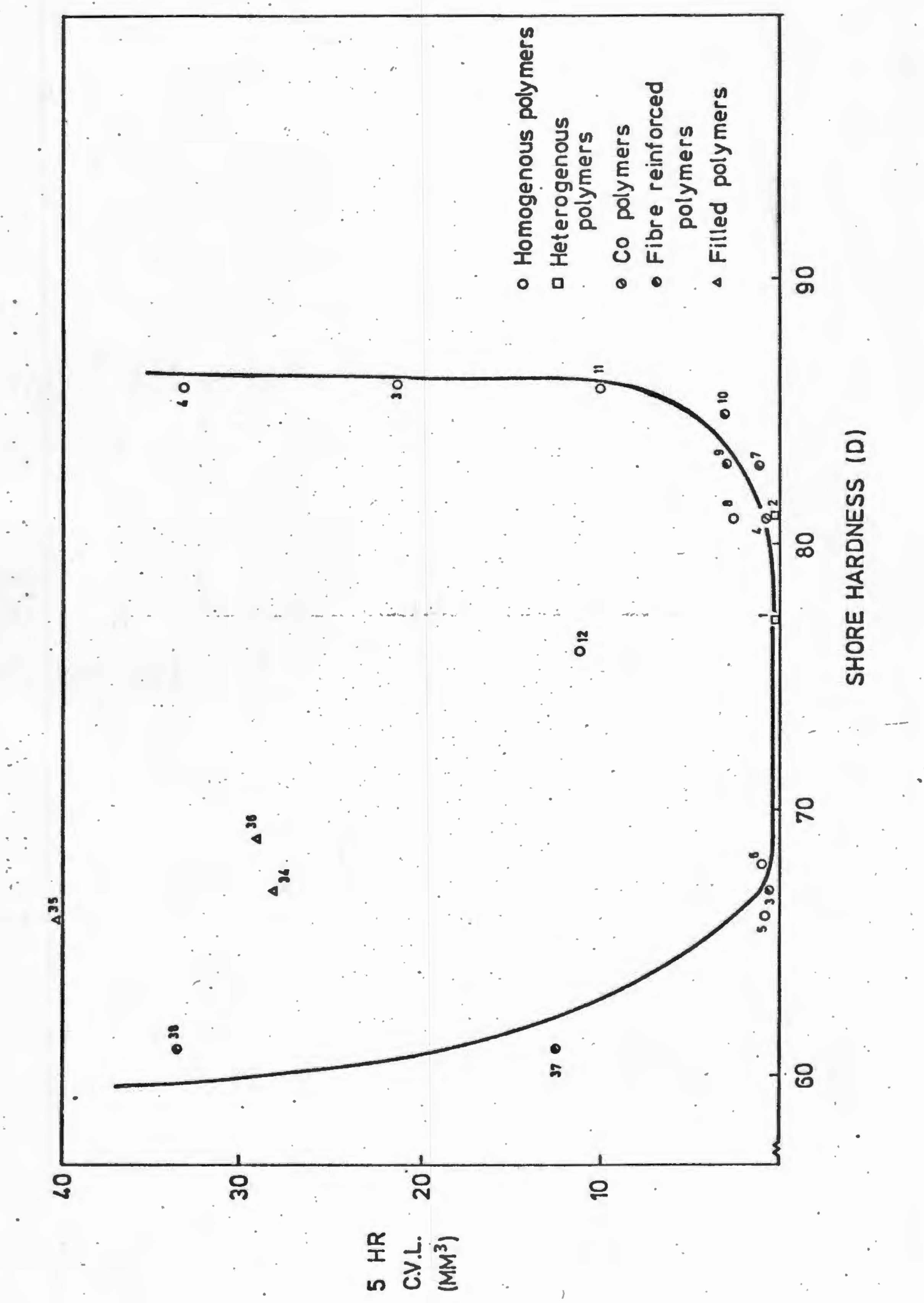

FIG. 6.2

Effect of varying Shore hardness on the five hour cumulative volume loss

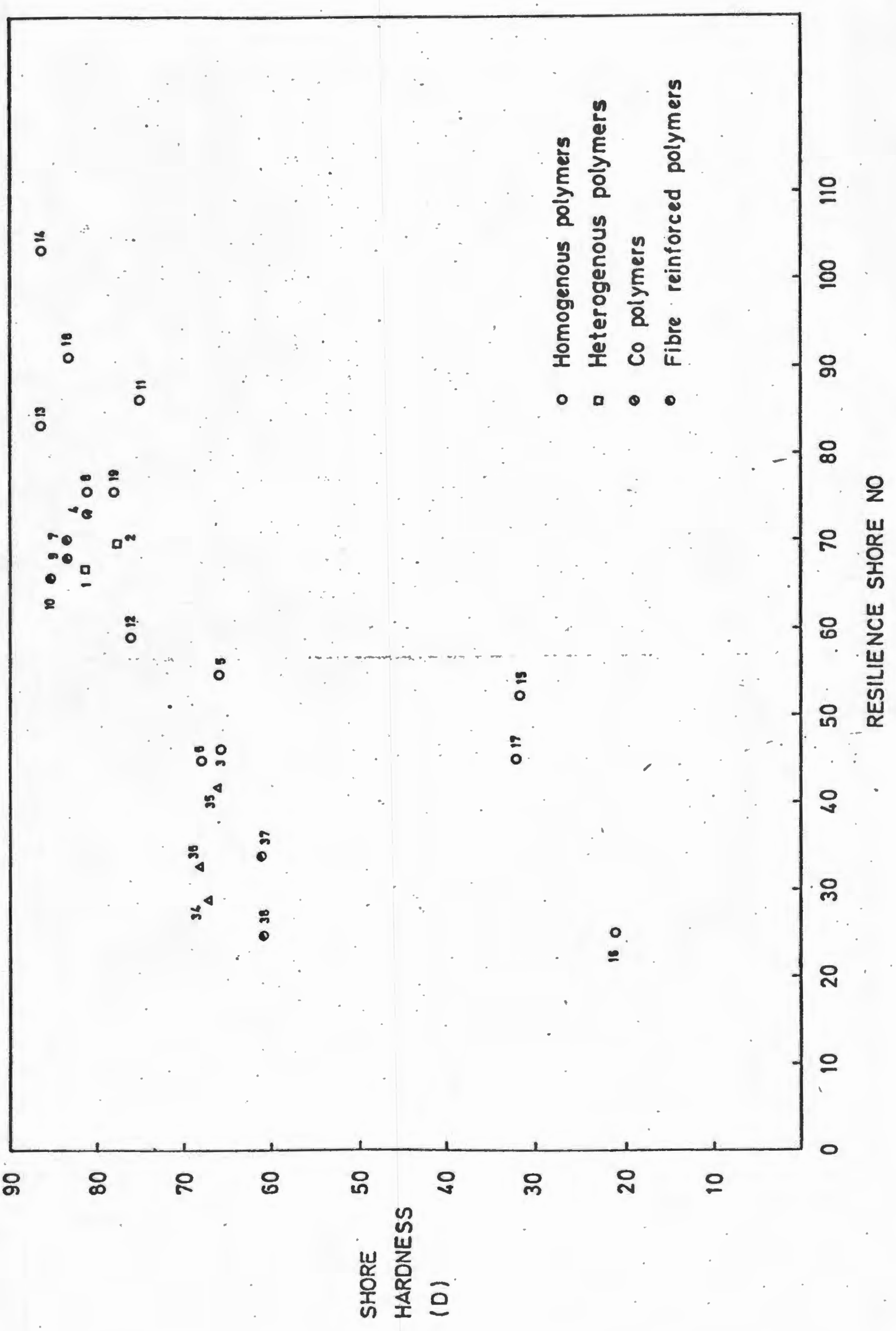

FIG. 6.3

Relationship between resilience and Shore hardness

6.6 INFLUENCE OF PRE-EROSIVE TREATMENTS ON EROSION OF POLYMERIC MATERIALS

From Table 4.3 it will be noted that the polyacetal samples which were soaked in various concentrated additives for three weeks at 70°C all had better erosion resistance than those kept in either air or water under the same conditions. Additionally, there appears to be no correlation between the 5 hr CVL and the percentage by weight of concentrated fluid absorbed (Fig. 4.15). In contrast, the polyacetal samples, which were soaked in the dilute media (5/95), exhibited no well defined trends relative to the erosion performances of the samples stored in either air or water prior to erosion. The ability of the oil layer to wet the polymer surface may account for an improved erosion resistance which can be explained as follows:

Firstly, the presence of the fluid film would eliminate the potential nucleii which form on irregular surfaces of the polymer (5). In addition, the fluid film increases the distance between the cavities collapse centre and the surface of the polymeric material. This is significant as the potentially damaging pressure front developed as a result of cavity collapse is rapidly attenuated and can only cause damage if the collapse occurs no further that ½ its initial radius from a boundary surface (7).

Brunton (79), in his investigation of liquid drop impact erosion of a wetted surface, suggested that a fluid layer would prevent direct impact of microjets (drops) and dissipate the transmitted pressure pulse. This pressure pulse is attenuated if the layer is much thicker than the diameter of the droplet (attentuation of the pulse varies as a square of layer thickness). Thus in the case of the polymers soaked with the diluted concentrate (5/95), the layer thickness could be much thinner than the diameter of the cavity. This could account for the fact that there is no marked improvement in the erosive performance relative to that of air or water. Notable, is that there is no correlation between the erosion performances of the polyacetal polymers pre-soaked in the concentrate and dilute fluids.

Micrographs of the eroded surfaces of the 'treated' polyacetal samples are shown in Figs. 4.21 to 4.27. The micrographs of the polyacetal samples which were treated in both air and water prior to erosion (70°C for 3 weeks) are shown in Figs. 4.26 and 4.27. These fracture surfaces display the characteristic 'intermediate' mode of erosion. However, a more ductile mode of erosion, characterised by a larger proportion of free fibril ends, could possibly account for the lower cumulative volume loss for these samples immersed in the concentrated additives (Figs. 4.21 - 4.25). The role the fluids play in altering the ductility of the polyacetal samples is not clear and it is possible that a plasticising effect is responsible.

Consulting Table 4.3 it is clear that the UHMWPE discs which were pre-soaked in both concentrate and dilute forms of fluids B, C, D failed 'catastrophically' when eroded by cavitation (standard conditions discussed in section 2.3 were employed). An optical micrograph depicting the mode of failure is shown in Fig. 4.20. This failure mode can be discussed in terms of the phenomenon known as solvent stress cracking. Stress-cracks in plastics are defined in ASTM D-883-62T as internal or external cracks caused by tensile stresses less than the short time mechanical strength of the material. Additionally, inception of these cracks may be hastened by the presence of a suitable environment. The state of knowledge in this area has been extensively reviewed by Howard (77) and VOL. 17 of the Enclyclopaedia of Polymer Science (78). The solvents (typically those of B, C, D) which induce solvent failures, weaken the surface layers by solvation or swelting. This results in a lowering of the cohesive bond energies of the surface layers by replacing polymer to polymer bonds with polymer to solvent bonds. A high loading situation, as encountered in cavitation, can result in a ductile form of failure due to the possible plasticising of the polymer by the solvent. Thus, if the applied stress exceeds the strength of the weakened cohesive bonds, plastic flow occurs as shown in Fig. 4.20. 'Catastrophic' failure did not occur in the case of the discs pre-soaked in fluids A and E. The reason for this is not clear; however, it is generally accepted that the chemical nature of the absorbed solvent appears to be the factor determining failure rather than the amount of solvent absorbed.

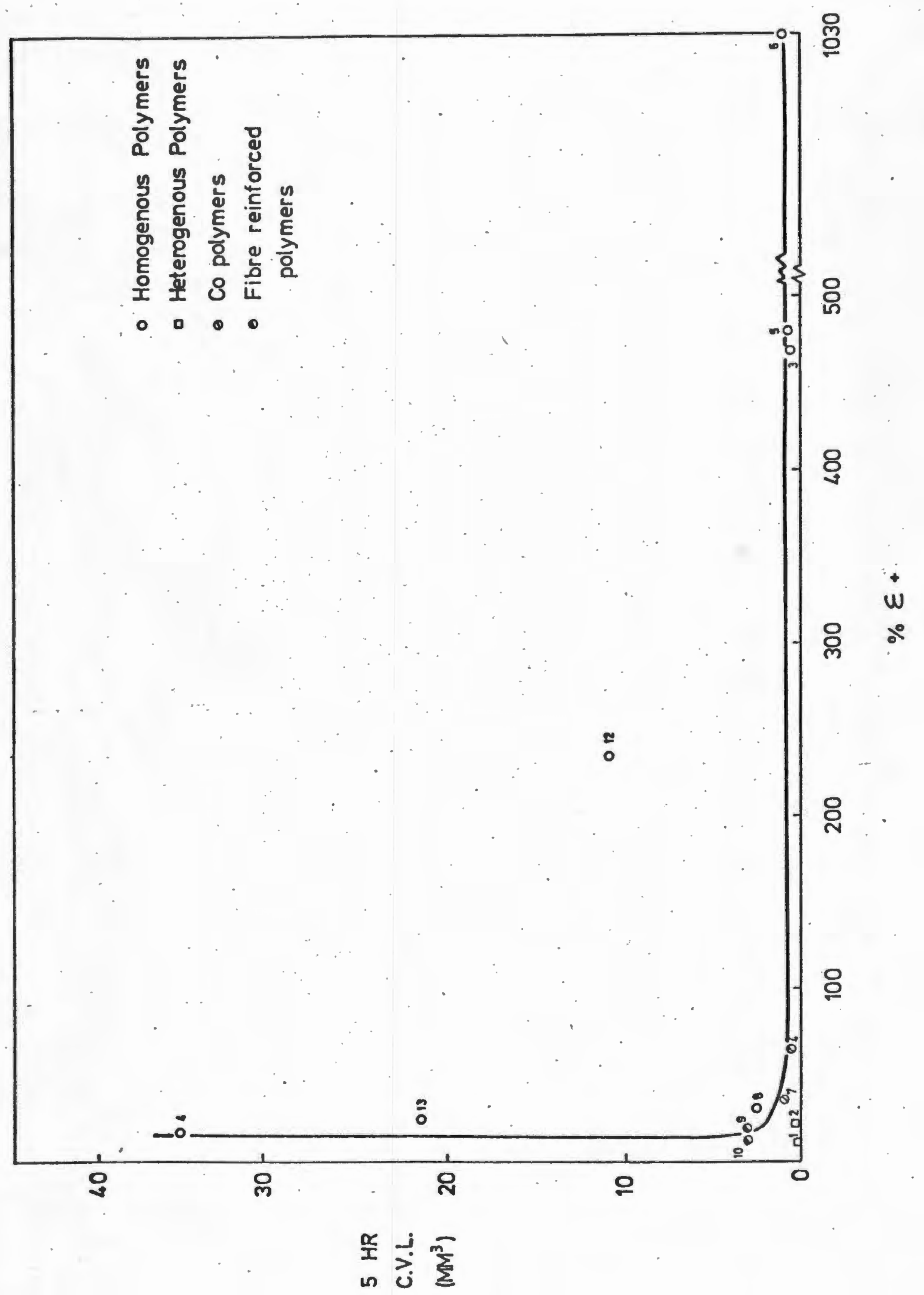

FIG. 6.4

Five hour cumulative volume loss as a function of percent ε_f.

6.7 CONCLUSIONS - POLYMERIC MATERIALS

The results of the erosion tests performed on the nineteen different polymers, together with the effects of a pre-erosive treatment in concentrated and dilute forms of HWBF's, has lead to the following conclusions:

1. The samples fell into four classes of resistance to cavitation erosion. Seven of the nineteen samples have very high erosion resistance (Group I), three have intermediate resistance (Group II), and four have low erosion resistance (Group III). Group IV polymers failed catastrophically (by melting or brittle failure).

2. The heterogenous polymers, namely polyamide 66 + PE and polyacetal + PE, had the highest erosion resistance.

3. Fibre reinforced polymers and macroscopically filled polymers were less erosion resistant than the homogenous base component.

4. There were no clearly defined trends which related cavitation erosion to any single mechanical or chemical property. Thus erosion resistance depends on an inter-relation between the various properties and in particular, glass transition temperature, elongation to fracture and resilience.

5. Scanning electron micrographs of eroded surfaces showed correlations with the various groupings, viz.:

   a) Group I polymers failed by a 'ductile' tearing mechanism.

   b) Group II showed an 'intermediate' mode of erosion.

   c) Group III was characterised by a 'brittle' failure mode.

6. The polyacetal samples which were pre-soaked in the concentrated additives A - E all showed improved erosion resistance. The effects of the absorbed fluids may prevent nucleation of surface cavities or dampen the effects of cavity collapse.

7. The polyacetal discs pre-soaked in the 5/95 dilutions showed no defined correlations relative to the erosion performances of the samples stored in air and water or the concentrated additives.

8. A more ductile failure mode, characterised by a larger proportion of free fibril ends, suggests that the polyacetal samples were plasticised by the concentrated additives.

9. Failure as a result of solvent stress cracking ocurred in the case of the UHMWPE samples pre-soaked in both the concentrate and dilute forms of fluid B, C, D, prior to erosion.

10. The UHMWPE discs which were pre-soaked in fluids A and E did not fail catastrophically when eroded. Thus it is beleived that the chemical nature of the absorbed solvent appears to be the factor determining failure rather than the amount of solvent absorbed.

CHAPTER 7 : DISCUSSION - COATED AND SURFACE TREATED MATERIALS

7.1 EFFECT OF VARYING THICKNESS OF ELECTROLESS NICKEL COATINGS

The erosion performance of an En24 sample (Q & T 600°C) coated with less than ∿15μm of electroless nickel is inferior to that of the uncoated substrate (Fig. 5.1, Fig. 5.2). The reason for the high volume loss is that the coating is removed by spalling (see Fig. 5.14). In contrast coatings thicker than and equal to 25μm eroded by removal of brittle cleavage facets. Increasing the coating thickness above 25μm does not improve the erosion resistance (Fig. 5.2).

An explanation for this behaviour can be provided employing the theoretical arguments developed by Rieger and Boche (6).

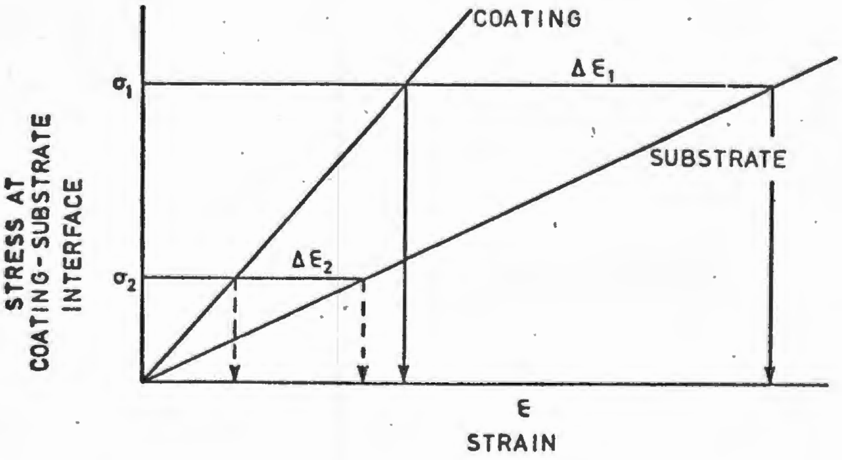

FIG. 7.1 Hypothetical stress-strain diagram for a particular coating-substrate system.

A hypothetical elastic stress-strain diagram for both coating and substrate is shown in Fig. 7.1. Assume that a coating of thickness 25μm receives the impact from a microjet or shock wave due to cavitation. The coating is placed in compression and expands laterally to allow for this (Fig. 7.2).

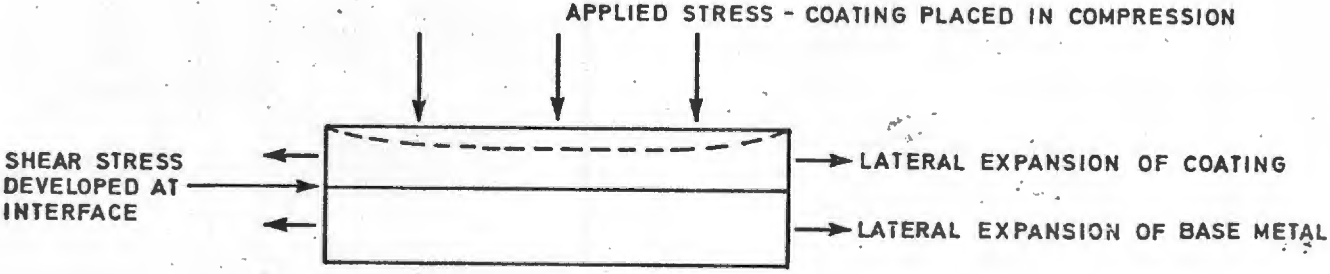

__FIG. 7.2__ Schematic representation of the stress developed at a coating-substrate interface due to an applied stress on the coating surface.

Once the cavitation stress pulse reaches the base metal it is also placed in compression. The mismatch in transverse expansion between the coating and substrate sets up a shear stress at the interface (Fig. 7.2). Consulting Fig. 7.1, assume (for a coating $< 25\mu$m) that the stress at the interface is σ_1, then the strain differential between coating and substrate is $\Delta\varepsilon_1$.

Considering now a coating of 25µm and thicker; because the stress pulse is attenuated as a function of depth, the shear stress experienced at the interface, σ_2, and hence the differential strain, $\Delta\varepsilon_2$, is lower and thus delamination will not occur. The interface will spall at a critical value of the strain differential with which will be associated a critical shear stress in the plane of the interface. The shear stress is a function of the thickness of both the surface layer and the supporting layer and is given by the equation below (ref. 6).

$$\sigma_s = \frac{\frac{1}{2}\, d(\nu_1 E_2 - \nu_2 E_1)\, G_1 G_2 \sigma_{p2}}{E_1 E_2 \left[l_{x1} G_2 \left(1 - \frac{\sigma_{p2}}{E_1}\right) + l_{x1} G_1 \left(1 - \frac{\sigma_{p2}}{E_2}\right)\right]}$$

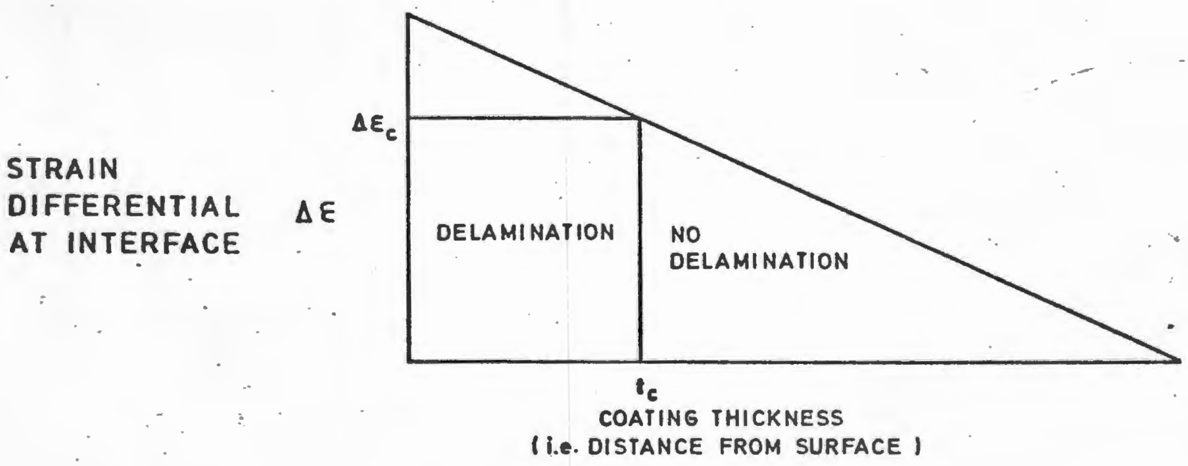

FIG. 7.3 Magnitude of the strain differential at the interface as a function of distance from the surface.

Consulting Fig. 7.3 there must be a critical coating thickness, t_C, below which delamination occurs, because the strain differential becomes too high at the interface. Thus if the shear stress at the interface exceeds the adhesive strength of the coating, removal occurs by spalling. Conversely, if the shear stress is less than the adhesive strength of the coating (coatings 25μm and thicker) then it erodes by brittle chip removal.

Clearly from Fig. 7.1 the greater the elastic mismatch between coating and substrate, the greater the possibility of delamination.

7.2 EFFECT OF POST COATING HEAT TREATMENT ON THE EROSION RESISTANCE OF ELECTROLESS NICKEL

The erosion curves, together with an erosion envelope (overlay transparency) is shown in Figs. 5.4. This figure demonstrates that a post application heat treatment (PHT) of 200°C, for 3 hours, (performed on a 25μm thick electroless nickel coating deposited on En24 [Q & T 600°C]), does not improve the erosion resistance relative to the uncoated substrate. In contrast, PHT's of 400°C (3 hours) and above, improve the erosion resistance (see Fig. 5.3). The coated samples which were used to investigate the effects of coating thickness on erosion resistance were all heat treated at 300°C for periods ranging from 10 to 12 hours. Fig. 5.4 shows that a 25μm electroless nickel coating failed by spalling after having received a 200°C PHT for 3 hours. However, Fig. 5.1 shows that spalling did not occur in the case of the 25 μm thick coating receiving a 300°C PHT for 10 to 12 hours. This demonstrates the possibility of improved adhesion of the coating to substrate due to higher heat treatment temperature performed over an increased time period. Trends similar to those attained by Heathcock et al (48) were observed. However, minor discrepancies existed because a 10μm coating thickness was used in the investigation unlike the 25 μm thick coating used in this research. Heathcock noted that a post heat treatment above 400°C improved the erosion resistance, with an optimum resistance at a 600°C PHT.

The effects of heat treating electroless nickel above 200°C have been investigated by Parker (72) and reported by Kofsky (71). The bell shaped curve shown in Fig. 5.5 depicting microhardness as a function of temperature can be explained as follows:

As-deposited electroless nickel is a microcrystalline or amorphous structure (72). XRD analysis performed on eroded samples (this accounts for the presence of the iron peak) demonstrates the amorphous character of the 200°C PHT sample which has a microhardness of $700MHN_{20}$. The reported (71) increase in hardness for temperatures above 260°C is primarily due to the formation of coherent and then distinct forms of Ni_3P. The d-spacings for $(FeNi)_3P$ are shown in Table 5.1. It is clear from Fig. 5.9 that at 300°C PHT nickel phosphide begins to precipitate.

According to Parker (72), a rapid increase in hardness occurs between the temperatures of 300° and 375°C because a crystalline mixture of nickel and nickel phosphide (Ni_3P) is formed. A peak hardness of 1100 MHN_{20} (Fig. 5.5) is attained at 400°C PHT and this is in agreement with that reported by Kofsky (71) for a sample containing 10-11% phosphorous.

Parker (72) noted that above 400°C a rapid drop-off in hardness occurs which he attributed to recrystallisation and grain growth. However, another softening mechanism has been noted and is described below.

As PHT temperature increases a notable sharpening of the Ni_3P peaks (Figs. 5.9 to 5.12) occurs, suggesting increased crystallinity. Fig. 5.13 shows a linear relationship between intensity (cps) and post heat treatment temperature. So it appears that Ni_3P is still precipitating out above 400°C, even though a reduction in hardness is occurring. Thus the variation of hardness with temperature can also be likened to the age-hardening of aluminium alloys.

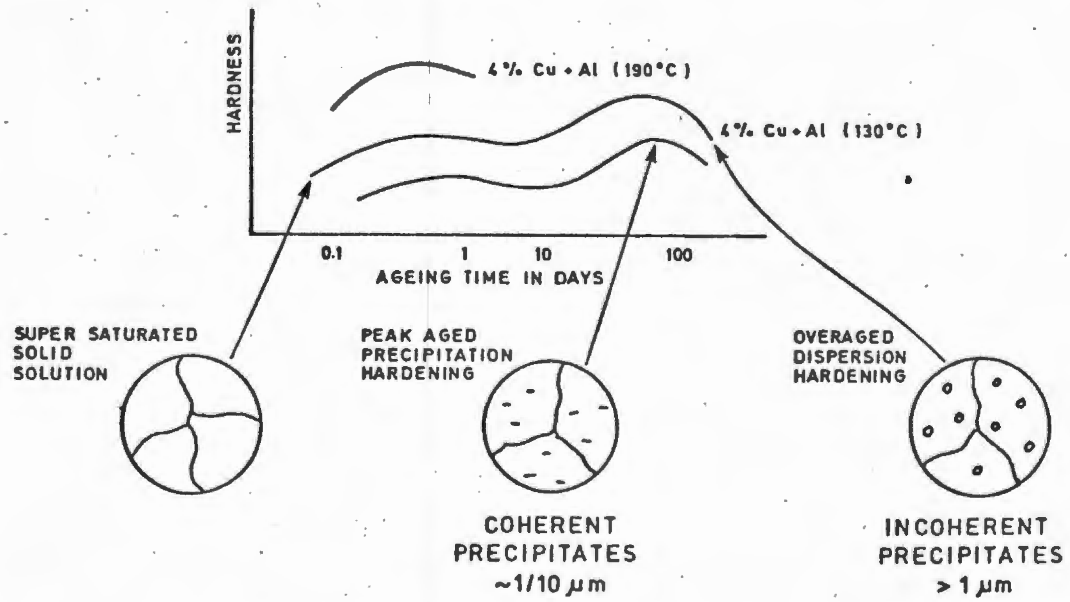

FIG. 7.4 Variation of hardness with ageing time for a Cu-Al system.

Overageing of aluminium leads to the formation of incoherent precipitates (∿ 1 μm) with a corresponding reduction in hardness. It is probable that the electroless nickel is undergoing a similar precipitation hardening plus overageing process. This together with the possibility of recrystallisation and grain growth could account for the reduction in hardness above 400°C. Parker (72) investigated the effects of PHT electroless nickel above 600°C. He observed a 5μm nickel-iron interdiffusion layer for a sample which received a PHT for 4 hours at 621°C. The results of the present work, shown in Fig. 5.6, substantiate the findings of Parker. A semi-quantitative spot analysis technique (using a Kevex) confirmed the optically observable diffusion layer to be nickel-iron. An interdiffusion layer was not observed for a PHT of 500°C for 3 hours (Fig. 5.7).

From the scanning electron micrographs shown in Figs. 5.14 and 5.15 it is clear that two major mechanisms of material removal are operational. Firstly removal by spalling, and secondly erosion of the coating itself. The erosion curve for a 200°C PHT sample is shown in Fig. 5.4. It displays a high rate of volume loss during the first hour because removal of material occurred by spalling (see micrograph 5.14). However, in the case of the 300°C PHT sample, the erosion curve suggests a 'mixed' mode of material removal. Namely, erosion of the coating for the first two hours, followed by material removal due to spalling. Thus the improved erosion resistance could possibly be due to improved adhesion at 300°C PHT.

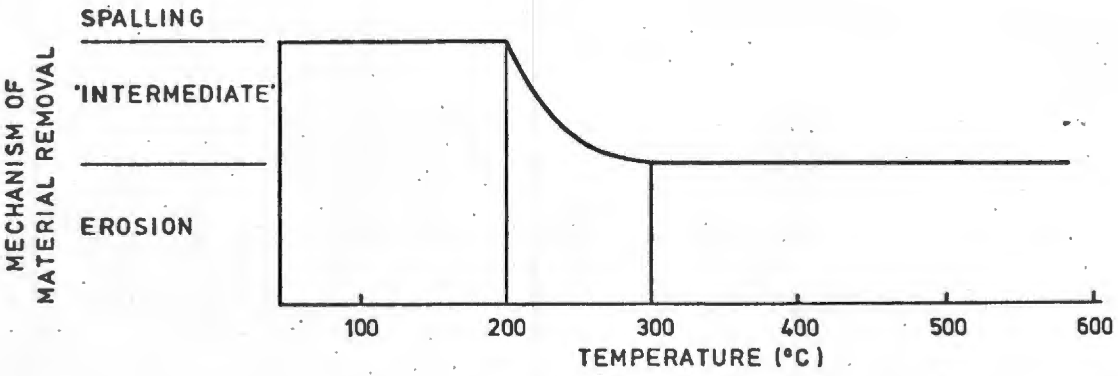

FIG. 7.5 Affect of post heat treatment on the mode of material removal.

From the schematic diagram shown in Fig. 7.5 above, it is probable that the mechanism of erosion is a function of the adhesive strength at the interface which is in turn related to the post application heat treatment. Therefore, even though hardness falls off dramatically above 400°C, a corresponding decrease in erosion resistance does not occur. The fact that the hardness provided by 600°C and 200°C treatment are equal, suggests that the improved adhesion due to interdiffusion at 600°C is playing a role. Thus the size of the interdiffusion layer is related to the PHT temperature (shown optically in Fig. 5.6 and 5.7) which in turn influences the erosion characteristics of material removal. This in turn overrides any adverse affects which may arise from the dramatic reduction in hardness above 400°C.

7.3 CHEMICAL VAPOUR DEPOSITED COATINGS

Consulting Figs. 5A to 5C it is clear that CVD coatings do not improve the erosion resistance of either En24, grey cast iron, or nodular cast iron. A number of possible reasons can be proposed, viz.:

1. The development of residual stresses in the CVD deposits. These may be due to -

   A) the growth of the CVD layer is nucleation controlled and well ordered, free standing shapes devoid of porosity are formed. However, stresses may arise in these deposits due to the competition between neighbouring growth centres (ref. 64).

   B) differences in the thermal expansion coefficients between coating and substrate can develop shear stresses at the interface upon cooling. Hintermann (64) reported the expansion coefficients to be a factor of 1,2 to 2 lower than steels. However, this shear stress only becomes significant in coatings thicker than 10 μm and limits the applied thickness of wear resistant coatings such as TiC.

2. The brittle nature of TiC may render it unable to accommodate applied mechanical overloading as it can only deform elastically with a fracture strain of 2% (64).

3. The poor industrial application of TiC is shown in Fig. 5.16. Obviously this has deleterious effects on the erosion resistance.

As a consequence of the high temperatures associated with the application of TiC (900°C) there is the possibility of interdiffusion and strong interfacial bonding may result (63,64,65). However, this is not reflected in the erosion profiles presented in Fig. 5A, 5B and 5C. The TiC coatings were removed by spalling. In contrast, the W_2C coatings showed superior erosion resistance, when contrasted to the TiC coated samples. Better adhesion in possibly achieved as a consequency of the shot blasting of the base metal prior to the application of W_2C, at a temperature of 500°C. This may aid the mechanical 'keying' and be more effective than interdiffusion which would occur at 900°C in the case of TiC (see Fig. 5.25).

Once the coating had been removed, the mechanism of erosion of the cast irons was by large scale preferential removal of the hard graphite. This occurred as a result of the elastic mismatch between hard graphite and softer iron matrix (5). This is depicted in the micrographs 5.24, 5.28 and 5.31. It is thought that the removal of the graphite produces an 'undercut' (see Fig. 5.29) which results in the wholesale spalling of TiC. In contrast, the W_2C's superior adhesive, discussed above, is reflected in the erosion profiles shown in Fig. 5B and Fig. 5C where the erosion curve approximates that of the uncoated substrate.

7.4 SPRAYED COATINGS

In general spraying techniques such as plasma spraying or D-gun spraying are characterised by depositing heated coating material at high velocities onto a relatively cold substrate (53).

7.4.1 Plasma sprayed Triballoy

Consulting Table 5.2 it is clear that Triballoy coatings provide extremely poor erosion resistance. A number of possible reasons exist:

Firstly, the mismatch in the elastic modulus between the Triballoy phases (hard Laves phase in a soft matrix) could result in an erosion mechanism similar to nodular cast iron, where erosion occurs by the removal of the hard graphite phase from the ferrite matrix. A micrograph displaying cracking which is a consequence of the mismatch between the phases in Triballoy is shown in Fig. 5.37. It is interesting to note that the higher the volume percentage of Laves phase the higher the weight loss (see Table 5.2).

From Fig. 5.35 it appears that once the coating thickness reaches ∿ 50μm (initially 75μm), large scale coating removal occurs. At a 50 μm thickness the shear stress generated at the interface must reach a critical value and exceed the adhesive strength of the coating (see Fig. 5.38).

A second important phenomenon is the difference in thermal expansion coefficients between Triballoy and Mild Steel (Triballoy = 11.2 x 10^{-6}/K; Mild Steel = 12.8 x 10^{-6}/K). Thus large residual stresses can develop upon cooling resulting in cracking and even spalling of the coating prior to erosion (see Fig. 5.34).

7.4.2 D-gun carbide coatings

From Fig. 5.39 it is clear that D-gun carbide coating improves the erosion resistance of En3. In fact D-gun coatings have the highest reported bond strength of any of the sprayed coatings (53). This D-gun technique produces an extremely dense coating applied at high velocity by a series of overlapping deposits. Heat treating at elevated temperatures would result in improved adhesion between coating and substrate (75) [eg. 1080°C for 4 hours in vacuum].

A typical micrograph of the eroded surface is shown in Fig. 5.41 and evidence can be seen for cleavage cracking. From the erosion profiles shown in Fig. 5.39 it appears that both coating and sealent are being eroded in the case of the polymerically sealed sample, and this accounts for the consistently higher erosion rate of these specimens. Evidence for the presence of this polymeric sealent is clearly visible in Fig. 5.40.

The improved erosion performance is probably as a result of the extremely dense nature of the coating together with a strong interfacial bond. (See Fig. 5.42)

7.5 SURFACE TREATMENTS

7.5.1 Nitrided steels

It is clear from Fig. 5.43 that the steady state erosion rate is lowered by a factor of approximately 4, relative to the untreated base metal. However, the initial rate of volume loss is extremely high (during the first hour). This is due to the removal of the brittle 'white layer' shown in Fig. 5.45. This white layer consists of a mixture of iron nitrides Fe_4N (gamma nitride) and Fe_2N (epsilon nitride) (62). It is undesirable, as it can be responsible for the initiation of fatigue cracks in the underlying nitride layer. The white layer froms because the nitrogen potential is too high in the treatment process. However, a thickness of up to 0,02mm is acceptable for most commercial applications (76). Removal of this white layer prior to erosion (by soaking the sample in a hot cyanide solution, followed by layer removal with alumina grit or vapour blasting) would probably result in excellent erosion characteristics, in view of the low steady state rate of erosion of the underlying nitrided steel.

A number of possible explanations exist for the extremely 'good' steady state of erosion:
Firstly, nitriding En41B places the surface and sub-surface layers in compression (62). This residual compressive stress can be as high as 750 N/mm^2 and has obvious advantages in terms of

improving the fatigue strength of the material. Secondly, the dimensional changes which take place as a result of nitriding are extremely low because no metallurgical phase transformations are involved during the process which is performed at 500°C.

The superior erosion resistance of the gas nitrided sample (see Fig. 5.43) can be explained by consulting the microhardness profiles presented in Fig. 5.44. Clearly the case depth in both samples is approximately 250 μm. However, the gas nitrided sample is consistently lower in hardness. This could result in a slightly more ductile mode of erosion, resulting in the lowered rate of volume loss. It also appears (Fig. 5.43) that the extent of 'white layer' formation is lower in gas nitriding than in ion nitriding for the conditions particular to specimen preparation.

7.5.2 Boronised steels

The boronised steels showed an extremely high rate of volume loss during the first hour of exposure to cavitation. Possible reasons are as follows:

1. The abrupt transition in hardness (Fig. 5.49) between the surface layer and base metal (56). This transition would result in the creation of interfacial stresses, due to cavitation, and failure mechanisms could approximate that of coated systems.

2. Additionally the creation of residual stresses, upon cooling (55), could account for the poor erosion resistance of the boronised steels.

St John and Sammels (58) performed an XRD analysis of AISI 1008 steel boronised for periods ranging between 1 and 5 hours. They noted that crystallinity was only achieved after heating times in excess of one hour. The Fe_2B phase initially predominated and after approximately 5 hours the brittle FeB phase formed in the saturated Fe_2B layer. This FeB layer is avoided in industry by employing low boron potentials (55) and only the Fe_2B phase is formed. This was confirmed by XRD analysis performed on En24, boronised for periods ranging between 1 and 5½ hours. No evidence of the FeB phase was observed (Fig. 5.51) and the d-spacings for Fe_2B are presented in Table 5.4. In addition, a similar parabolic relationship, to that observed by Eyre (55), was noted for the relationhip between coating depth and varying diffusion time (see Fig. 5.48).

7.6 GENERAL DISCUSSION

When considering the choice of a coated or surface treated material, for use in a particular erosive environment, a number of important considerations have to be made and numerous important trends have emerged from the research undertaken. In trying to optimise a coated or surface treated material for an erosive environment, the following considerations are of importance:

7.6.1 Coated systems

Firstly, an understanding of how the variation in coating thickness effects the erosion resistance must be obtained. The coating thickness determines the magnitude of the shear stress developed at the interface, which in turn, dictates the mode of material removal. This is demonstrated when considering electroless nickel where a 10 μm coating is removed by spalling; whereas a 25μm coating is removed by brittle failure. However, the optimisation of this thickness is particular to the coating technique employed and the magnitude of the stress created by a cavitating system.

Secondly, it is generally accepted that a 'strong' interfacial bond is crucial for good erosion resistance. This bonding can be achieved by either mechanical keying (low temperature applications - spraying) or interdiffusion (high temperature applications - electroless nickel). The latter, in general, provides a superior adhesion.

7.6.2 Surface treated materials

The surface treated materials (nitrided and carburised steels) generally showed superior erosion resistance when contrasted with the coated systems. Both nitriding and carburising (results presented in section 5.4.3) provide excellent erosion resistance. Nitriding reduces the steady state erosion rate by a factor of four but only after the hard brittle 'white layer' has been removed. Possible reasons for the superior erosion performances are:

Firstly, these surface treatments create large residual compressive stresses in the surface and near surface layers and these compressive stresses result in improved resistance to plastic flow and fatigue. Secondly, the microhardness profiles are characterised by a gradual transition in hardness from the surface through to the substrate.

However, the boronised steels are exceptions and have a well defined interface, reflected by their steep hardness profile, and display poor erosion resistance. A possible reason for this poor performance is that shear stresses can now be developed at this defined interface and the mechanism of erosion approximates that of the coated systems, discussed earlier in this chapter (7.1).

7.7 CONCLUSIONS - COATINGS AND SURFACE TREATED MATERIALS

The work perfomed on the coatings and surface treated materials has lead to the following conclusions.

1. Carburised and nitrided steels showed the highest erosion resistance of all the coated and surface treated materials tested to date.

2. Electroless nickel which received post application heat treatments of 400°C and above showed the best erosion resistance of all the coated systems tested.

3. A coating of 25 μm improves the erosion resistance. However, increasing the coating thickness above 25μm (electroless nickel) does not improve the erosion performance. A 10μm coating performs worse than an uncoated base metal of En24.

4. CVD coatings, such as W_2C and TiC, showed poor erosion resistance.

5. Plasma sprayed Triballoy coatings display extremely poor erosion resistance. However, D-Gun carbide coated En3 has improved erosion resistance relative to the uncoated substrate.

6. Boronising does not improve the erosion resistance relative to En24 or En3.

Thus the following considerations have to be borne in mind when considering a coating or surface treated material for an erosive environment.

A. <u>Coated Systems</u>

   i) Coating thickness

   ii) Interdiffusion (high temperature applications)

   iii) Mechanical keying (low temperature applications)

   iv) Elastic mismatch between coating and substrate.

B. <u>Surface Treated Materials</u>

   i) Magnitude of the compressive residual stress.

   ii) Microhardness profile.

APPENDIX 1.1

CALCULATION OF THE SHEAR STRESSES OCCURRING, DURING RAIN EROSION, IN THE TWO-LAYER JOINT

(Taken from Rieger and Boche, ref. 6)

The following simplifying assumptions are made in the calculation of the shear stress σ_s:

1. The stresses produced in the joint upon drop impact should result only in elastic deformation.

2. Hydrodynamic jet effects upon drop impact are not taken into consideration.

3. Only simple reflections, and no multiple reflections, of shock waves at phase boundaries are considered. (The damping and the dispersion of shock waves are not known with sufficient accuracy.) The stress in the x-direction should be σ_{p2} in the two-layer joint [compare equation (4) in Chapt. 1]. This pre-supposes that, among other things, the duration of the shock upon drop impact is sufficiently great.

4. It is assumed that the diameter of the water drop d is equal to the diameter of the specimen.

The deformations in the x-direction are:

in layer I

$$\varepsilon_{x1} = \frac{\Delta \ell_{x1}}{\ell_{x1}} = \frac{\sigma_{p2}}{E_1} \qquad \text{(A-1)}$$

in layer II

$$\varepsilon_{x2} = \frac{\Delta \ell_{x2}}{\ell_{x2}} = \frac{\sigma_{p2}}{E_2} \qquad \text{(A-2)}$$

Here E_1 and E_2 are the moduli of elasticity of layers I and II.

The transverse expansions in the y-direction are given by the following relationship:

$$\frac{\varepsilon_y}{\varepsilon_x} = \nu \tag{A-3}$$

Here ν is the coefficient of transverse contraction.

Taking $\varepsilon_y \doteq \frac{\Delta d}{d}$ and equation (A-1), (A-2) and (A-3), the tranverse deformations in layers I and II are found to be:

$$\Delta d_1 = \frac{\nu_1 d\sigma_{p2}}{E_1} \tag{A-4}$$

and

$$\Delta d_2 = \frac{\nu_2 d\sigma_{p2}}{E_2} \tag{A-5}$$

The condition for adhesion in the plane of the joint of the two layers necessitates fulfilment of the following relationship:

$$1/2\ (\Delta d_1 - \Delta d_2) = y_1 + y_2 \tag{A-6}$$

Here

$$y_1 \doteq x_1 \frac{\sigma_s}{G_1} = (\ell_{x1} - \Delta\ell_{x1}) \frac{\sigma_s}{G_1} \tag{A-7}$$

and

$$y_2 = x_2 \frac{\sigma_s}{G_2} = (\ell_{x2} - \Delta\ell_{x2}) \frac{\sigma_s}{G_2} \tag{A-8}$$

where G_1 and G_2 are the moduli of shear of layers I and II and σ_s is the shear stress at the common surface of layers I and II.

Bearing in mind (A-1) and (A-2), equations (A-7) and (A-8) can be transformed into:

$$y_1 = \frac{\ell_{x1}}{G_1}\left(1 - \frac{\sigma_{p2}}{E_1}\right)\sigma_s \qquad \text{(A-7a)}$$

$$y_2 = \frac{\ell_{x2}}{G_2}\left(1 - \frac{\sigma_{p2}}{E_2}\right)\sigma_s \qquad \text{(A-8a)}$$

If equations (A-4), (A-5), (A-7a) and (A-8a) are introduced in equation (A-6), then it is found that:

$$\left.\begin{aligned} 1/2\left(\frac{d\nu_1}{E_1} - \frac{d\nu_2}{E_2}\right)\sigma_{p2} &= \sigma_s\left|\frac{\ell_{x1}}{G_1}\left(1-\frac{\sigma_{p2}}{E_1}\right)+\frac{\ell_{x2}}{G_2}\left(1-\frac{\sigma_{p2}}{E_1}\right)\right| \\ \sigma_s &= 1/2\,\frac{\sigma_{p2}d(\nu_1E_2 - \nu_2E_1)G_1G_2}{E_1E_2\left|\ell_{x1}G_2\left(1-\frac{\sigma_{p2}}{E_1}\right)+\ell_{x2}G_1\left(1-\frac{\sigma_{p2}}{E_2}\right)\right|} \end{aligned}\right\} \qquad \text{(A-9)}$$

APPENDIX 2.1 MANUFACTURERS SPECIFICATIONS

1 = ultimate tensile strength
2 = percentage elongation to fracture
3 = melting point
4 = tensile modulus of elasticity
5 = Values not available

Polymer	UTS'[1] (MPa)	$\% \varepsilon_F$[2]	MP_t[3]	Shore Hardness (D)	E[4] (MPa)
Polyamide 66 + PE	44...54	30	Ca. 255	-	1666
Polyacetal + PE	44	10	Ca. 165	82	2156
DS UHMWPE	-	-	-	-	-
Polyacetal Ccpol	61	61	157	-	28
UHMWPE	22	450	137	66	686
HDPE	17 - 28	10-800	-	-	517-1723
Nylon 66 + GF	80	130	255	-	4
Polyacetal	66	20...35	Ca. 165	80 - 83	2744
Polyacetal + PE + GF	-	-	Ca. 165	-	-
Polyacetal + GF	98...127	3...5	Ca. 165	86	7350
Torlon	135	12	650 ± 20	-	-
Polypropylene	31	Ca.650	Ca. 160	69	1176
Polysulfon	Ca. 74	40..100	-	-	-
Polyethylene terephalate	71	750	Ca. 256	-	-
Vulcanol	29 - 34	700-800	-	31	34
Polycarbonate	62 - 72	50-100	514 ± 9	-	1654
Polycast 880	34	600	± 90	80(A)	4.4
Polycast 885	53	575	± 90	85(A)	4.0
Kynar (Pvdt)	38 - 51	50-100	171	70 - 80	-

APPENDIX 4.1

MATERIALS - ORDER OF PERFORMANCE

MATERIAL	C . V. L. (MM)					INC TIME (HRS)	AVERAGE E (MM /HR)	V.H.	R.NO.	+-SCAT (%)
	40 HRS	20 HRS	10 HRS	7 HRS	5 HRS					
NYLON 6,6	-	3.60	-	0.05	0	6.0	0.290	-	89.	
WC/NI:8LC	0.52	0.19	-	0.05	0.01	7.5	0.015	1478.	108.	7.70
STELLITE 20	0.93	0.35	-	0.03	0.01	7.5	0.030	610.	106.	
NITI	1.12	0.23	-	0.02	0.01	12.5	0.048	200.	35.	17.40
STELLITE 8	1.24	0.43	-	0.02	0.01	7.5	0.040	335.	78.	
STELLITE 3	0.53	0.14	-	0.02	0.01	12.5	0.022	531.	106.	1.89
STELLITE 4	1.00	0.39	-	0.03	0.02	7.5	0.031	501.	94.	
STELLITE 6	1.15	0.40	-	0.04	0.02	7.5	0.037	399.	80.	
WC/NI:8NC	0.72	0.34	-	0.11	0.03	5.0	0.021	1246.	113.	9.72
655M13.CARB.3HR	-	-	-	-	0.03	-	-	-	-	
AISI A2(210)	-	-	-	-	0.03	-	-	-	-	
817M40 (200)	-	1.17	-	0.10	0.05	7.0	0.092	604.	108.	
835M30CRCT(400)	-	-	-	-	0.06	-	-	-	-	
NYLATRON GSM	-	4.14	-	0.43	0.07	4.0	NSS	-	84.	11.60
STELLITE 2 006	1.94	0.87	-	0.17	0.08	5.0	0.054	440.	90.	
FLURUDUR	1.94	0.87	-	0.17	0.08	5.0	0.054	440.	90.	
SYNDITE	-	-	-	-	0.08	-	-	-	-	
DIN 4112 (200)	-	1.26	-	0.23	0.10	4.0	0.079	636.	103.	
AMBORITE	-	-	-	-	0.10	-	-	-	-	
817M40CRCT(400)	-	-	-	-	0.11	-	-	-	-	
AISIA2(300)	-	-	-	-	0.13	-	-	-	-	
534A99(300)	-	-	-	-	0.14	-	-	-	-	
534A99(200)	-	-	-	-	0.15	-	-	-	-	
835M30CRCT(300)	-	-	-	-	0.15	-	-	-	-	
PAX2 (150)	-	-	-	-	0.15	-	-	-	-	
534A99(100)	-	-	-	-	0.18	-	-	-	-	
TIC/WC/NI.CN02	-	1.13	-	0.30	0.18	2.0	0.064	1710.	109.	0.88
817M40CRCT(300)	-	-	-	-	0.18	-	-	-	-	
DIN 4112 (300)	-	-	-	0.35	0.19	3.0	0.086	577.	96.	
835M30CRCT(600)	-	-	-	-	0.19	-	-	-	-	
DIN 4112 (400)	-	-	-	0.38	0.21	3.0	0.068	531.	89.	
WC/CO:CG60	-	-	-	0.38	0.21	3.0	0.074	1048.	94.	2.60
817M40(600)PHT400	-	-	-	-	0.21	-	-	-	-	60.00
CAST IRON : CB24	-	-	-	0.46	0.23	3.5	0.124	873.	103.	

APPENDIX 4.1

MATERIALS - ORDER OF PERFORMANCE

MATERIAL	C . V. L. (MM^3)					INC TIME (HRS)	AVERAGE E (MM /HR)	V.H.	R.NO.	+-SCAT (%)
	40 HRS	20 HRS	10 HRS	7 HRS	5 HRS					
817M40CRCT(500)	-	-	-	-	0.26	-	-	-	-	
WC/CU:CT6S	-	-	-	0.52	0.27	3.0	0.115	933.	106.	2.88
817M40(600)PHT500	-	-	-	-	0.27	-	-	-	-	14.00
WC/CU:LAB GRD A	-	-	-	0.47	0.28	3.0	0.100	933.	88.	10.60
817M40 (300)	-	-	-	0.51	0.28	3.0	0.115	529.	98.	
835M30CRCT(600)	-	-	-	-	0.29	-	-	-	-	
905M39GASNIT60HR	-	-	-	-	0.29	-	-	-	-	
070M20NICR	-	-	-	-	0.30	-	-	-	-	
835M30CRCT(200)	-	-	-	-	0.31	-	-	-	-	38.20
AISI A2(300)	-	-	-	-	0.33	-	-	-	-	
DIN 4112 (500)	-	-	-	0.52	0.34	2.5	0.100	463.	90.	
817M40 (400)	-	-	-	0.59	0.34	3.0	0.128	469.	96.	
M40CRCT(600)	-	-	-	-	0.36	-	-	-	-	
ALLOY C	-	-	-	0.72	0.36	3.0	0.200	229.	55.	
817M40CRCT(600)	-	-	-	-	0.36	-	-	-	-	
WC/CU:LAB GRD C	-	-	-	0.62	0.38	2.5	0.122	835.	95.	8.70
CAST IRON:IB18	-	-	-	0.60	0.38	2.5	0.120	688.	93.	
817M40 (500)	-	-	-	0.78	0.38	2.0	0.163	400.	88.	
TITANIUM	-	-	-	-	0.38	-	-	-	-	
431S29 (200)	-	-	-	0.82	0.40	2.0	0.173	427.	76.	
ALLOY 3040	-	-	-	0.68	0.42	2.0	0.140	388.	79.	
835M30 (200)	-	-	-	0.69	0.42	3.0	0.131	502.	100.	
431S29 (400)	-	-	-	0.78	0.43	2.0	0.166	423.	75.	
WC/CU:CG35	-	-	-	0.66	0.45	1.0	0.101	1267.	111.	
817M40(600)PHT600	-	-	-	-	0.45	-	-	-	-	13.00
544A99(500)	-	-	-	-	0.45	-	-	-	-	
HADFIELDS	-	-	-	0.86	0.48	2.0	0.188	181.	33.	12.20
POLYACETAL	-	-	-	1.23	0.49	3.0	0.138	-	77.	14.60
817M40(600)ELNI75	-	-	-	-	0.49	-	-	-	-	
534A99(400)	-	-	-	-	0.50	-	-	-	-	
835M30 (300)	-	-	-	0.83	0.51	2.0	0.166	419.	89.	
817M40(200)ELNI25	-	-	-	-	0.54	-	-	-	-	
835M30 (400)	-	-	-	0.87	0.54	2.0	0.182	396.	91.	
DIN 4112 (600)	-	-	-	0.96	0.56	2.0	0.200	330.	68.	

APPENDIX 4.1

MATERIALS - ORDER OF PERFORMANCE

MATERIAL	C . V. L. (MM)					INC TIME (HRS)	AVERAGE $\dot{E}$ (MM /HR)	V.H.	R.NO.	+-SCAT (%)
	40 HRS	20 HRS	10 HRS	7 HRS	5 HRS					
43IS29 (300)	-	-	-	1.04	0.61	2.0	0.205	406.	80.	
WC/CO:40C	-	-	-	0.96	0.62	1.0	0.171	1033.	110.	
817M40(300)ELNI25	-	-	-	-	0.65	-	-	-	-	
817M40(600)ENI100	-	-	-	-	0.66	-	-	-	-	8.74
835M30 (500)	-	-	-	1.19	0.68	2.0	0.243	355.	84.	
AISI 304	-	-	-	1.10	0.70	2.0	0.215	194.	48.	
817M40(600)ELNI25	-	-	-	-	0.79	-	-	-	-	15.00
817M40(500)ELNI25	-	-	-	-	0.80	-	-	-	-	
534A99	-	-	-	-	0.80	-	-	-	-	
817M40(600)ELNI25	-	-	-	-	0.81	-	-	-	-	
WC/CU:C130	-	-	-	1.23	0.82	1.0	0.205	1168.	103.	
905M39IONNIT36HR	-	-	-	-	0.83	-	-	-	-	
817M40(600)ELNI50	-	-	-	-	0.93	-	-	-	-	
905M39IONNIT72HR	-	-	-	-	0.95	-	-	-	-	
817M40 (600)	-	-	-	1.55	1.03	2.0	0.280	328.	79.	7.90
43IS29 (500)	-	-	-	1.77	1.04	2.0	0.358	325.	74.	
817M40(600)PHT300	-	-	-	-	1.05	-	-	-	-	18.50
835M30 (600)	-	-	-	1.76	1.07	2.0	0.348	277.	71.	6.25
817M40(500)W2C	-	-	-	-	1.36	-	-	-	-	
43IS29 (600)	-	-	-	2.48	1.51	2.0	0.468	262.	70.	
817M40(600)ELNI10	-	-	-	-	1.69	-	-	-	-	
3CR12NI (900)	-	-	-	-	1.72	2.0	NSS	266.	70.	
GREY CAST W2C	-	-	-	-	1.87	-	-	-	-	3.87
AISI 316	-	-	-	-	1.95	2.0	0.520	194.	53.	17.90
INCALLOY 825	-	-	-	-	2.25	2.0	0.577	186.	49.	
NODULAR CAST W2C	-	-	-	-	2.31	-	-	-	-	
817M40(600)PHT200	-	-	-	-	2.36	-	-	-	-	20.70
070M20D-GUN(NS)	-	-	-	-	2.39	-	-	-	-	14.20
GREY CAST TIC	-	-	-	-	2.68	-	-	-	-	
AL BRONZ	-	-	-	-	2.80	-	-	-	-	
070M20D-GUN(S)	-	-	-	-	2.91	-	-	-	-	9.18
817M40 BORO(4HR)	-	-	-	-	3.05	-	-	-	-	1.12
817M40 BORO(5.5H)	-	-	-	-	3.06	-	-	-	-	16.20
NODULAR CAST TIC	-	-	-	-	3.06	-	-	-	-	

APPENDIX 4.1

MATERIALS - ORDER OF PERFORMANCE

MATERIAL	C . V. L. (MM)					INC TIME (HRS)	AVERAGE E (MM /HR)	V.H.	R.NO.	+-SCAT (%)
	40 HRS	20 HRS	10 HRS	7 HRS	5 HRS					
817M40 BORO(1HR)	-	-	-	-	3.19	-	-	-	-	
MONEL 400	-	-	-	-	3.41	1.0	0.185	159.	38.	
817M40 BORO(2HR)	-	-	-	-	3.44	-	-	-	-	
220M07 BORO(12H)	-	-	-	-	3.48	-	-	-	-	
220M07 BORO(2HR)	-	-	-	-	3.83	-	-	-	-	
220M07 BORO(7HR)	-	-	-	-	4.01	-	-	-	-	
3CR12NI.	-	-	-	-	4.17	2.0	NSS	167.	43.	
220M07 BORO(5.5H)	-	-	-	-	4.38	-	-	-	-	
PHOZ BRONZ	-	-	-	-	4.50	-	-	-	-	
MN BRONZ	-	-	-	-	5.10	-	-	-	-	
220M07 BORO(10H)	-	-	-	-	5.24	-	-	-	-	
CAST IRON SG80	-	-	-	-	6.79	1.0	1.820	160.	52.	
CERAMIC	-	-	-	-	10.00	-	-	-	-	
PTFE	-	-	-	-	10.60	0	2.200	-	36.	
LEADED PHOZ	-	-	-	-	11.00	-	-	-	-	
AISI 409	-	-	-	-	12.50	1.0	NSS	129.	38.	
CUPRO NI	-	-	-	-	15.50	-	-	-	-	
PTFE 15% GLASS	-	-	-	-	16.10	0	4.000	-	30.	
CAST BRONZ	-	-	-	-	17.60	-	-	-	-	
PTFE 60% BRONZ	-	-	-	-	27.20	0	7.000	-	33.	
PTFE + C + GRAPH	-	-	-	-	28.60	0	6.500	-	38.	
PTFE + 25% GLASS	-	-	-	-	36.10	0	10,000	-	28.	
AISI 430	-	-	-	-	37.20	1.0	8.300	180.	40.	
PTFE +25% CARBON	-	-	-	-	42.20	0	12.000	-	37.	

AVERAGE SCATTER +- 13. !!

* FIGURES APPROXIMATE ONLY -- SAMPLES ABSORBED WATER DURING TEST - CORRECTED AGAINST A CONTROL.

** V.H. = VICKERS HARDNESS !! +-SCAT = EXPERIMENTAL SCATTER (SEE TEXT)

! R.NO. = RESILIENCE NUMBER NSS = NO STEADY STATE ,THUS NO E.

RUNID: TONY ACCT: A0523-R001 PROJECT: RD

TONYA FIN

APPENDIX 4.2

TABLE A

POLYACETAL ABSORPTION OVER A PERIOD OF THREE WEEKS AT 70°C

Symbol	Weight before (g)	Weight after (g)	W(g)	% by weight absorbed
A	0,6257	0,6294	0,0037	0,59
B	0,6258	0,6278	0,0020	0,32
C	0,6469	0,6505	0,0036	0,56
D	0,6258	0,6253	-0,0005	-
E	0,6291	0,6275	-0,0016	-
A_5	0,6074	0,6133	0,0059	0,97
B_5	0,6267	0,6311	0,0044	0,70
C_5	0,6299	0,6358	0,0059	0,94
D_5	0,6144	0,6206	0,0062	1,01
E_5	0,5927	0,5977	0,0050	0,84
Air	0,6064	0,6055	-0,0009	-
H_2O	0,6177	0,6229	0,0052	0,84

APPENDIX 4.2

TABLE B

UHMWPE ABSORPTION OVER A PERIOD OF THREE WEEKS AT 70°C

Symbol	Weight before (g)	Weight after (g)	W(g)	% by weight absorbed
A	0,4415	0,4564	0,0149	3,4
B	0,4314	0,4596	0,0282	6,5
C	0,4455	0,4722	0,0267	5,9
D	0,4038	0,4343	0,0305	7,5
E	0,4374	0,4386	0,0012	0,3
A_5	0,4390	0,4497	0,0107	2,4
B_5	0,4353	0,4595	0,0242	5,6
C_5	0,4422	0,4655	0,0233	5,3
D_5	0,4346	0,4668	0,0322	7,4
E_5	0,4352	0,4364	0,0012	0,2
Air	0,4352	0,4351	0,0001	0,02
H_2O	0,4344	0,4344	0,0000	0,00

REFERENCES

1. S. Logan Kerr, ASME 59, 1937, p 573.

2. B.E. Protheroe, Proc. 5th Int. Conf. on Erosion by Solid and Liquid Impact, Cambridge, England, Sept. 1979, p 64-1.

3. P. Kenney et al, The Mining Engineer, Sept. 1979, p 235.

4. M.G. Talks and G. Moreton, Proc. Conf. Boulder, Colo. USA, 1981, p 139.

5. C.J. Heathcock, 'Cavitation Erosion of Materials', Ph.D. Thesis, University of Cape Town, 1980.

6. H. Rieger and H. Boche, Proc. 4th Int. Conf. on rain erosion, Meersburg, 1974, p 637.

7. C.M. Preece (Ed.), Treatise on Materials Science and Technology (Erosion), 16, Academic Press, 1979.

8. E. Webster, Ultrasonics, Jan-Mar. 1963, p 39, Mining Research and Development Establishment.

9. European Communities Commission, A Study of Erosion and Corrosion of Materials used in Hydraulic Equipment, Final Report on ECSC Research Project 6220-AE/8/803, 1979, p 60.

10. F.B. Peterson, Proc. 19th Meeting of the Mech. Failures Prevention gp., Colorado, USA, Oct. 1973, p 3.

11. T.M. Mitchell and F.G. Hammitt, Asymmetric Cavitation Bubble Collapse, Journal of Fluids Engineering, March 1973, p 29.

12. C.F. Naudé and A.T. Ellis, Journal of Basic Engineering, Trans. ASME, Series D, vol. 83, 1961, p 648-656.

13. W. Lauterborn, Proc. 5th Int. Conf. on Erosion by Liquid and Solid Impact, Cambridge, England, Sept. 1979, p 58-1.

14. N.D. Shutler and R.B. Mesler, ASME, Journal of Basic Engineering, June 1965, p 511.

15. J.H. Brunton (1970), Proc. 3rd Int. Conf. on Rain Erosion, Ed. A.A. Fyall, Royal Aircraft Establishment, Farnborough, UK, p 821.

16. J.H. Brunton, Proc. 5th Int. Conf. on Erosion by Liquid and Solid Impact, Cambridge, England, Sept.1979, p 59-1.

17. B. Vyas and C.M. Preece (1974), ASTM STP 567, p 77.

18. B. Vyas and C.M. Preece, Journal of Applied Physics, 47, No. 12, Dec. 1976, p 5133.

19. I. Hansson et al, Ultrasonic International, 1977, p 267.

20. M.S. Plesset and A.T. Ellis, Trans. ASME, 77, p 1055.

21. F. Erdmann-Jesnitzer and H. Louis, ASTM STP 567, 1974, p 171.

22. K. Steller et al, ASTM STP 567, 1974, p 152.

23. C.M. Preece et al, ASTM STP 644, 1979, p 409.

24. J.M. Mousson, Trans. ASME, 59, 1937, p 399.

25. A. Thiruvengadam, Trans. ASME, 85, Series D, 1963, p 365.

26. J.M. Hobbs (1967), ASTM STP 408, p 159.

27. R. Garcia and F.G. Hammitt, Trans. ASME, 89, Series D, 1967, p 753.

28. M. Hirotsu, ASTM STP 474, 1970, p 48.

29. G.M. Wood et al, Trans. ASME, 89, Series D, Mar. 1967, p 98.

30. B.C.S. Rao et al, Trans. ASME, 92, 1970, p 563.

31. S. Vaidya et al, Met. Trans., Vol IIA, 1980, p 1139.

32. J.Z. Lichtman, Journal of Materials, 2, No 3, Sept. 1967, p 638.

33. J.Z. Lichtman, ASTM STP 474, 1970, p 422.

34. J.Z. Lichtman et at, Corrosion, 17, No 10, Oct. 1961, p 119.

35. F.G. Hammitt et al, ASTM STP 567, 1974, p 197.

36. P. Mears, Polymers - Structure and Bulk Properties, D. van Nostrand Co., London, 1965.

37. J.A. Brydson, Plastics Materials, 2nd Ed. I Litte Books, London, 1969.

38. B. Angell et al, Proc. 5th Int. Conf. on Erosion by Liquid and Solid Impact, 3-6 Sept., 1979, Cambridge, England, Paper 75.

39. C.K. Chatten and A. Thiruvengadam, 'Testing of Polymers', (J.V. Schmid and W.E. Brown, Eds.), Vol III, Wiley Interscience, New York, 1967, p 245, cited in ref. 1, p 296.

40. R.M. Ogorkoewicz, The engineering properties of plastics, Oxford University Press, Materials Engineering Design Guides, Vol 17, 1977.

41. W.F. Alder, Proc. 5th Int. Conf. on Erosion by Liquid and Solid Impact, Cambridge, England, Sept.1979, p 9-1.

42. L. Engel, Klingele, Ehrenstein and Schaper, 'An Atlas of Polymer Damage', Wolte Publishing Ltd., 1981.

43. D.H. Kallas and J.Z. Lichtman, 'Cavitation Erosion', Environmental effects on Polymeric Materials, Vol. I, Interscience, New York, 1968, Chapt. 2.

44. J.Z. Lichtman and D.H. Kallas, Materials Protection, Vol. 6, 1967, p 40.

45. A.P. Thiruvengadam and A.A. Hockrein, Jr., Mechanical Failures Prevention Group, 23rd Meeting, Gaithersburg, Md., 1976, p 120.

46. D.A. Tuitt, Erosion Tests of Metallic Coatings, Proc. 4th Int. Conf. on Rain Erosion and Associated Phenomena, Meersburg, Germany, May 1974.

47. W.K. King, Cavitation erosion in fluid systems, Proc. Conf. Boulder Colo., USA, 1981, p 95.

48. Heathcock et al, Proc. Conf. on Wear of Materials, San Francisco, Calif., 1981, p 597.

49. H.E. Hintermann, 'Tough-Hard Composite Materials:Substrate - Interface - Coating - Coating Relationships", Annals of the CIRP vol. 31/1/1982.

50. P. de Haller (1935), Schweiz. Bauz. 101, 243, 260. Cited in ref. 1, p 154.

51. G.F. Schmitt, Jr. Proc. of 3rd Int. Conf. on rain erosion, Elvetham Hall Hants, 1976, vol 3, p 107.

52. G.F. Schmitt, Jr. Proc. 11th Symp. on Electromagnetic Windows, Aug. 1972, ed. N.E. Pouloz and J.D. Walton,Jr.

53. T.C. Wells, Surface Treatment for Protection, Series 3, No. 10, April 1978, p 1.

54. D. Yamey, University of Cape Town, Chamber of Mines Research Project, GT2-E04, 1981.

55. T.S. Eyre, Wear, vol. 34, 1975, p 385.

56. N. Dautzenberg, Boronizing of Sintered Steels, Powder Met., vol. 22, 1979, p 31.

57. K.H. Habig and R. Chatterjee-Fischer, Tribology Int., Aug. 1981, p 209.

58. M.R. St John and A.F. Sammells, Jnl. of Mat. Sci., vol. 16, 1981, LETTERS, p 2327.

59. R. Chatterjee-Fischer and R. Fischer, Powder Metallurgy, vol. 20, 1977, p 96.

60. K.H. Habig, Materials in Eng., vol. 2, Dec. 1980, p 83.

61. K.J. Cowie, Personal Communication, Bohler Steel Africa, Oct. 1982.

62. H.C. Child, Surface Hardening of Steels, Oxford University Press, Engineering Design Guides 37, 1980.

63. N.J. Archer, Phys. Tech., vol. 10, 1979, p 152.

64. H.E. Hintermann, Tribology Int., Dec 1980, p 267.

65. H.E. Hintermann, Thin Solid Films, vol. 84 (3), 1981, p 215.

66. C.B. Cameron and D. P. Ferriss, Cobalt, vol. 3, 1974, p 49.

67. R. McPherson, Thin Solid Films, vol. 83 (3), Sept.1981, p 297.

68. J.D. Reardon et al, Thin Solid Films, vol. 83 (3), 1981, p 345.

69. D.R. Gabe, Principals of Metal Surface Treatment and Protection, 2nd Ed., Int. Series on Mat. Sci.and Tech., vol 28.

70. R. Kofsky, Personal Communication, SA Electroless Nickel Plating Company, 4th Oct. 1982.

71. R. Kofsky, Properties and applications of electroless nickel deposits, SA Electroless Nickel Plating Company, SA.

72. K. Parker, Plating and Surface Finishing, Dec.1981.

73. J. Brandrup and E.H. Immergut, Polymer Handbook, John Wiley & Sons, Inc., 1966.

74. Personal communication with Borreferrum, South Africa.

75. J.M. Quets and R.C. Tucker, Jr., Thin Solid Films, Vol. 84(1), 1981, p 107.

76. T.L. Elliott, Tribology Int., April 1978, p 121.

77. J.B. Howard, In Engineering Design for Plastics, (ed. Baer), Chap. 11, p 742, Robert E. Krieger, Hunting N.Y. 1975.

78. Encylopaedia of Polymer Science, Fracture, Vol. 7, p 261.

79. J.H. Brunton, Proc. 2nd Int. Conf. on Rain Erosion, 1967, p 296; cited in ref. 7.